SUB-KILOWATT, EFFICIENT CAPACITIVE POWER AND DATA TRANSFER FOR MONITORING THE MAJOR MECHANICAL VARIABLES

A Thesis Submitted to
the Graduate School of Engineering and Sciences of
İzmir Institute of Technology
in Partial Fulfillment of the Requirements for the Degree of

MASTER OF SCIENCE

in Mechanical Engineering

by
Abtulgalip KARABULUT

December 2019
İZMİR

We approve the thesis of **Abtulgalip KARABULUT**

Examining Committee Members:

Prof. Dr. Serhan ÖZDEMİR
Department of Mechanical Engineering, İzmir Institute of Technology

Assoc. Prof. Gökhan KİPER
Department of Mechanical Engineering, İzmir Institute of Technology

Prof. Dr. İsmail BÖĞREKCİ
Department of Mechanical Engineering, Aydın Adnan MenderesUniversity

17 December 2019

Prof. Dr. Serhan ÖZDEMİR
Supervisor, Department of Mechanical Engineering, İzmir Institute of Technology

Prof. Dr. Sedat Akkurt
Head of the Department of Mechanical Engineering

Prof. Dr. Mehtap EANES
Dean of the Graduate School of Engineering and Sciences

ACKNOWLEDGMENTS

First of all, I would like to thank my supervisor Prof. Serhan ÖZDEMİR. Especially, I want to talk about his continuous assistance and a considerable amount of contribution to my thesis. During the study, he always supported and encouraged me. He was aplenty helpful and had belief in me. I would like to acknowledge Prof. İsmail BÖĞREKCİ, Assoc. Prof. Gökhan KİPER, Assoc. Prof. Pınar DEMİRCİOĞLU and Assoc. Prof. M. İ. Can DEDE for accepting my thesis defence invitation as well.

I wish to give my thanks for the efforts of Oğuzhan DOĞAN, Oğuz SEVER and Mahir TANRIYAPISI. They supported me in solving issues when I was studying my thesis in Artificial iytelligence laboratory.

Finally, I want to acknowledge my lovely parents for their invaluable efforts. They have supported me in all my experiences. I want to attribute the success of this study to them.

ABSTRACT

SUB-KILOWATT, EFFICIENT CAPACITIVE POWER AND DATA TRANSFER FOR MONITORING THE MAJOR MECHANICAL VARIABLES

The main aim of this thesis is to design and prototype a sub-kilowatt, efficient capacitive data and power transfer (CPT) system that for example, monitors the loads on an axle of a vehicle. The data and power are transmitted wirelessly. In a separate case study, the power is provided for the weight measurement system by an E class power amplifier.

In the industry, today, wireless power and data transfer methods have become quite popular. Some of those methods are inductive power transfer (IPT), capacitive power transfer, micro-wave power transfer (MCP). One of these techniques, which is the theme of this thesis, is the capacitive power and data transfer. The capacitive power system is quite compact and does not create electromagnetic interference (EMI), which is one of the strengths of the CPT. Hence, the stability of the embedded electronics system is preserved. Another attractive feature of CPT is that data and power can be transferred at the same frequency over a short distance. This thesis addresses the various facets of the CPT system. The historical development of the CPT technique has started with Nicola Tesla. Wireless power transfer methodology could safely be attributed to him.

The system consists of two main parts which are the weight measurement system and power transmitting system. The power is transferred by the copper capacitive plates with 100 cm^2 surface area. Average error of the measurement system is computed as 1.1% with high signal-to-noise ratio (SNR). Finally, the capacitive power and data transfer system has been designed with 83.8% efficiency at 1.7 MHz frequency and high SNR.

Keywords and Phrases: Capacitive power transfer, capacitive measurement system, Data acquisition system, E- class power amplifier, Wireless data and power transfer

ÖZET

TEMEL MEKANİK DEĞİŞİKENLERİ İZLEMEK İÇİN KİLOWATT ALTI, VERİMLİ KAPASİF GÜÇ VE VERİ NAKLİ

Bu tezin asıl amacı, örneğin bir aracın aksındaki yükleri izleyen bir kilovat altında, verimli kapasitif veri ve güç aktarma (CPT) sistemi tasarlamak ve prototipini yapmaktır. Veri ve güç kablosuz olarak iletilir. Ayrı bir durum çalışmasında, ağırlık ölçümü sistemi için güç, E sınıfı bir güç amplifikatörü tarafından sağlanır.

Günümüzde sanayide, kablosuz güç ve veri aktarma yöntemleri oldukça popüler hale gelmiştir. Bu yöntemlerden bazıları endüktif (IPT), kapasitif, mikrodalga güç aktarımıdır (MPT). Bu tezin konusu olan bu tekniklerden biri kapasitif güç ve veri aktarımıdır. Kapasitif güç sistemi oldukça kompakttır ve CPT'nin ana avantajlarından birisi olan elektromanyetik girişimin (EMI) noksanlığıdır. Böylece, gömülü elektronik sistemin kararlılığı korunur. CPT'nin bir başka cazip özelliği, verilerin ve gücün kısa bir mesafede aynı frekansta aktarılabilmesidir. Bu tez, CPT sisteminin çeşitli yönlerini ele almaktadır. CPT tekniğinin tarihsel gelişimi Nicola Tesla ile başlamıştır. Kablosuz güç aktarımı metodolojisini bulan ilk kişidir.

Sistem, ağırlık ölçüm sistemi ve güç aktarma sistemi olmak üzere iki ana bölümden oluşmaktadır. Güç 100 cm^2 yüzey alanına sahip bakır kapasitif plakalar tarafından aktarılır. Ölçüm sisteminin ortalama hatası yüksek sinyal gürültü oranı (SNR) ile % 1,1 olarak hesaplanmıştır. Son olarak, kapasitif güç ve veri aktarım sistemi 1,7 MHz frekansında ve yüksek sinyal gürültü oranında, % 83,8 verimlilikle tasarlanmıştır.

Anahtar Kelimeler ve İfadeler: E sınıfı güç amplifikatörü, Kablosuz veri ve güç aktarımı, Kapasitif güç aktarımı, Kapasitif ölçüm sistemi, Veri toplama sistemi

TABLE OF CONTENTS

LIST OF FIGURES

Figure **Page**

Figure **Page**

Figure **Page**

LIST OF TABLES

Table **Page**

LIST OF SYMBOLS

f	Frequency	1/s
E	Electric field	N/C
F_e	Electric force	Newton
L	Inductance	H
k_e	Coulomb constant	$N.m^2.C^{-2}$
D	Electric flux density	C/m^2
l	Magnetic circuit length	m
ρ_v	Volume charge density	C/m^3
ε_0	Permittivity of free space	F/m
H	Magnetic field	A/m
V	Potential difference	Volts
t	Time	s
B	Magnetic flux density	Wb/m^2
μ	Permeability	H/m
r	Distance	m
σ	Electrical conductivity	S/m
F_B	Magnetic Force	N
C	Capacitance	F
R	Resistance	Ω
W	Weight	N
Q	Charge	C

CHAPTER 1

INTRODUCTION

1.1. Introduction to Wireless Power Transfer

Electric energy is used to power the world. Electricity has become one of the most important element in human life. Electric power has always been transmitted through cables. Hence, cables have always been an integral part of power transmission. The same could very well be said for data transmission. Cables have many disadvantages such as transmission distance limitation, data loss, power loss, weight, cost etc. Especially for rotary mechanical systems, cable connection is not possible to mount on this system easily. Direct connections between rotary mechanical element parts and their power supply have been practically impossible in the design of many modern automation systems (Hu et al., 2008). For example, a robot's sensors and actuators are normally controlled by direct cable connections, which reduce the movement range significantly (Chabrol, 1980).

Wireless power transfer technology, on the other hand, provides a permanent and efficient solution to these problems that were addressed. Popularity of wireless power transfer (WPT) technology has been growing for its ease of usage, compact design and its respective transmission distance etc. WPT techniques have the goal of diminishing the weight of chords and batteries. Wireless transfer is an efficient method to deliver energy from one system to another when there is no physical contact between any two different systems. Basically, WPT technology is defined as a transfer of power and/or data without physically connected cables. In a wireless power transfer method, a transmitter induces electrical or magnetic field between such as coils, or to capacitive plates etc. where the receiver does supplies this power other systems it is connected to. At the same time, wireless transfer technique has many advantages:

- WPT system eliminates the cable connections, therefore it is capable of efficient power transmission.

- Cable connections could be threat risk in case of disaster. On the other hand, when the receiver and transmitter pair is separated, no harm could be expected.
- Easy connections for rotary mechanical systems.

1.2. Historical Development of WPT

The WPT system has a long historical development that dates back to Maxwell. In between 1861-1862 years fundamental equations were generated by James Clerk Maxwell which was the first practical approach to power wireless transfer (Shinohara, 2011). After these equations were generated, more than a hundred years ago Nikola Tesla had a vision of wirelessly providing all energy. At the end of 19 century, he was the first man who performed WPT experiments. First public demonstration of WPT experiment was realized by Nikola Tesla at Columbia College, New York, in 1891 which was shown in Figure 1.1 (Tesla, 1891).

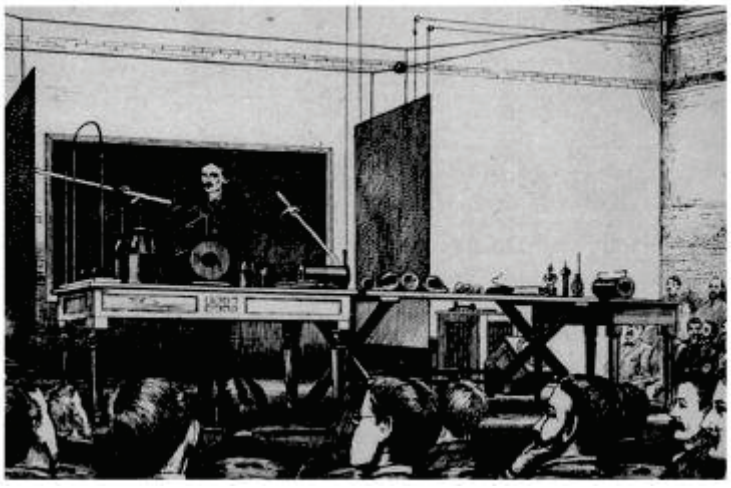

Figure 1.1. Wireless power transfer experiment of Tesla using capacitive plates (Source: Tesla, 1891)

As it can be seen from the Figure 1.1, Tesla has tried to transfer energy from one plate to the plate wirelessly. Tesla did not confine himself to capacitive power transfer method (CPT), also he has transferred energy through coils. Tesla has constructed the Wardenclyffe Tower.

The tower has been built for transferring energy without any physical link. The mechanism was basically constituted inductors. Besides, he has made a patent application to the United States Patent Office in 1902. The schematic drawing of the apparatus was given in Figure 1.2 (Tesla, 1914).

.

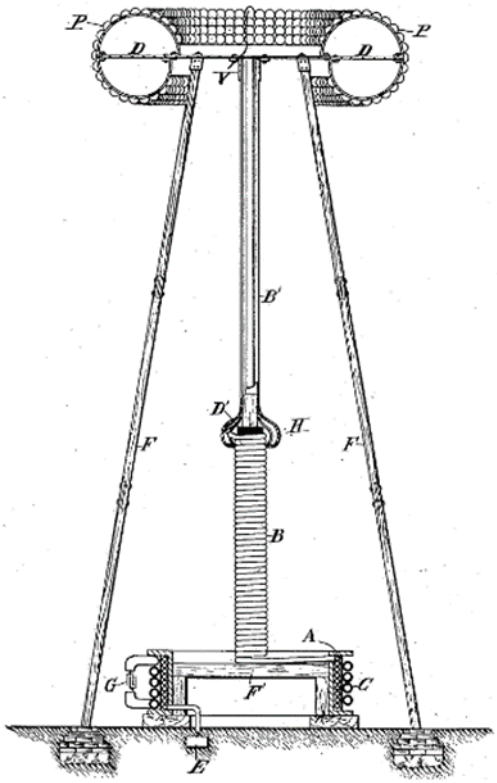

Figure 1.2. Demonstration of apparatus that was used to transmit electrical energy (Source: Tesla, 1914)

The main idea of a tower can be investigated like that the electrical energy was given to the bottom side of the invention and the supplied electrical energy goes through to the top side of the tower, finally electrical energy is delivered to the receiver from the top of the tower. He tried to realize his dream which provides the electricity worldwide wirelessly. It was aimed that Wardenclyffe Tower transmits 300kW power at 150 kHz radio wave. Unfortunately, this project could not be achieved its goal due to diffusion of the transmitting power, which correlates with the operating frequency and the dimension of antenna that used to transfer energy to the receiver (Tesla, 1914).

After the failure of Tesla, radio-wave was been top topic of the developments on wireless communication.

There was no significant improvement or invention directly related to WPT since tesla has died. However, the development of wireless communication project has been supplied to the wireless power technology secretly. With the use of microwaves, the history of WPT began again, which is called micro-wave power transfer (MPT).

During World War II, the idea of working on WPT experiment was broken out by William C. Brown. In the middle of 20 century William C. Brown has studied on WPT systems in the concept of high-efficiency wireless communication and radar remote sensing (Brown, 1980). Many different types of microwave power transfer (MPT) experiments were investigated with 2.45 GHz microwave tubes by William C. Brown. He has focused on antenna technology.

He first improved a rectifying antenna, which was called a “rectanna”. Rectanna has been used to receive and rectifier microwaves. In 1963, first efficiency rectannas have been advanced with 50% output power of 4 Watt (W) direct current (dc) and 40% output power of 7W dc (Brown, 1984). In 1964, rectanna was developed by William C. Brown. It transferred powered microwaves towards a helicopter which was hung in the air and in 1968 same experiment was performed to the free-flying helicopter. The helicopter was an unmanned aerial vehicle (UEV). The required energy of the helicopter was supplied by powered microwave signal. In this study, there was a nozzle type of microwave source. The powered microwave was transferred to the free-flying helicopter. The total dc-dc efficiency has been increased to 54% at 495 W dc power by a magnetron in the Raytheon Laboratory. MPT experiment where were realized in Raytheon Laboratory was shown in Figure 1.3 (Brown, 1973).

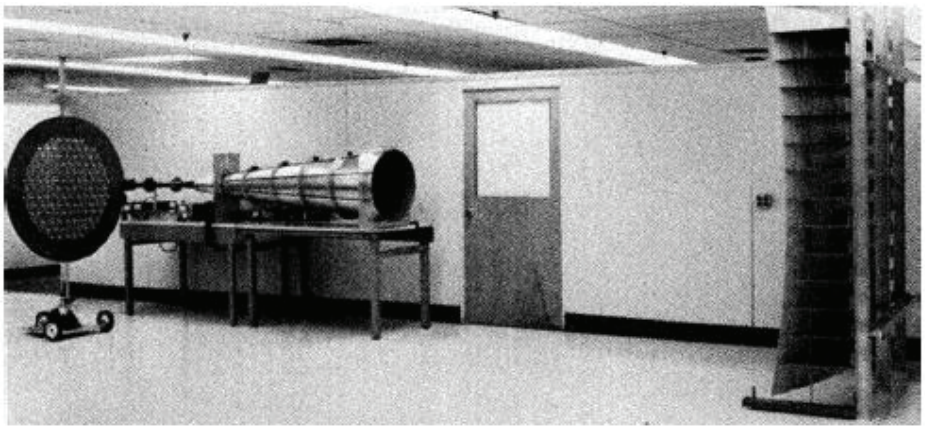

Figure 1.3. MPT experiment test set-up from Raytheon Laboratory
(Source: Brown, 1973)

Subsequent MPT study was investigated successfully by Brown and Richard Dickinson's team in 1975 that was the biggest prototype at the Venus Site of the Jet Propulsion Laboratory (JPL).

The area of receiving-converting subsystem (RXCV) was specified as 24 m^2 to provide wireless microwave power transfer system. NASA played an active role in this project in JPL for demonstration and corroborate.

The diameter of a parabolic surface of transmitter antenna was specified 26 m and the size of rectanna was designated and its array was 1.6 km. 30 kW rectified dc power with 82.5% rectifying efficiency have been obtained from 450 kW transmitter microwave klystron source at a 2.388 GHz frequency.

Despite the achievement of Brown in WPT study, the size and cost of the system were too much bigger than other empirical experiments which could be realized. For this reason, this MPT system could not be commercialized in the market. The first biggest ground-to-ground microwave power transfer study has been demonstrated in Figure 1.4 (Dickinson, 1976).

Figure 1.4. Located MPT demonstration designed by Brown and Richard Dickinson's team (Source: Dickinson, 1976)

In Figure 1.4, the receiver and transmitter have been shown that the giant size of them can be seen.

Besides, the MPT experiments have been supplied to theoretical background of WPT inwardly, due to this reason these studies can be accepted the historical development of the WPT system.

After the development of WPT method in the US, Japan which is one of the Asian countries started to move about WPT technology. In 1983, Hiroshi Matsumoto from Kyoto University and his team have succeeded MPT rocket study (Matsumoto, 2012). The rocket test set-up has been shown in Figure 1.5.

Figure 1.5. Hiroshi Matsumoto and his team MPT experiment
(Source: Matsumoto, 1976)

Solar power satellite (SPS) technology has been improved by MPT testing like the CPT system secretly.

MPT rocket study involved microwave ionosphere nonlinear interaction (MINIX). MINIX experiment was designed for the SPS. These MPT studies were being founded on modern microwave methods for wireless commination and radar technology. According to these purposes, an array of MPT experiments have been performed (Fujino et al., 1993). In 1992 university of Kyoto, Kobe University, and their group flew a fuel-free aircraft which was supplied by microwave energy at 2.411 GHz frequency. The transmitter sources included 288 antennas and 96 GaAs semiconductor amplifiers (Matsumoto et al., 1993). The aircraft was supplied by microwave energy has been shown in Figure 1.6.

(a)

(b)

Figure 1.6. Receiver aircraft (a) and Transmitter (b) MPT experiment in 1992 (Source: Matsumoto et al., 1993)

After facets of WPT were discovered by scientists, many applications have come to light. Basically, WPT technology was dived two main part radiative and non-radiative respectively (Imura and Hori, 2011) (Xie et al., 2013). Of these radiative is branched in two-part which are microwave power transfer (Shimokura et al., 1997) (Shinohara, 2007) (Shinohara et al., 2007), laser power transfer (McKinstrie, 1996).

Radiative WPT technology can be applied to large air gap distance. However, it is not suitable for high-efficiency power transfer (Imura and Hori, 2011). Electromagnetic radiation WPT system generally transfers power by way of antenna which is attached on the receiver. One of the most popular of Electromagnetic radiation WPT system is the SHARP (Stationary High Altitude Relay Platform) that was investigated by Canada's Communications Research Centre in the 1980s. The platform was unmanned aircraft and system was powered by microwave signal.

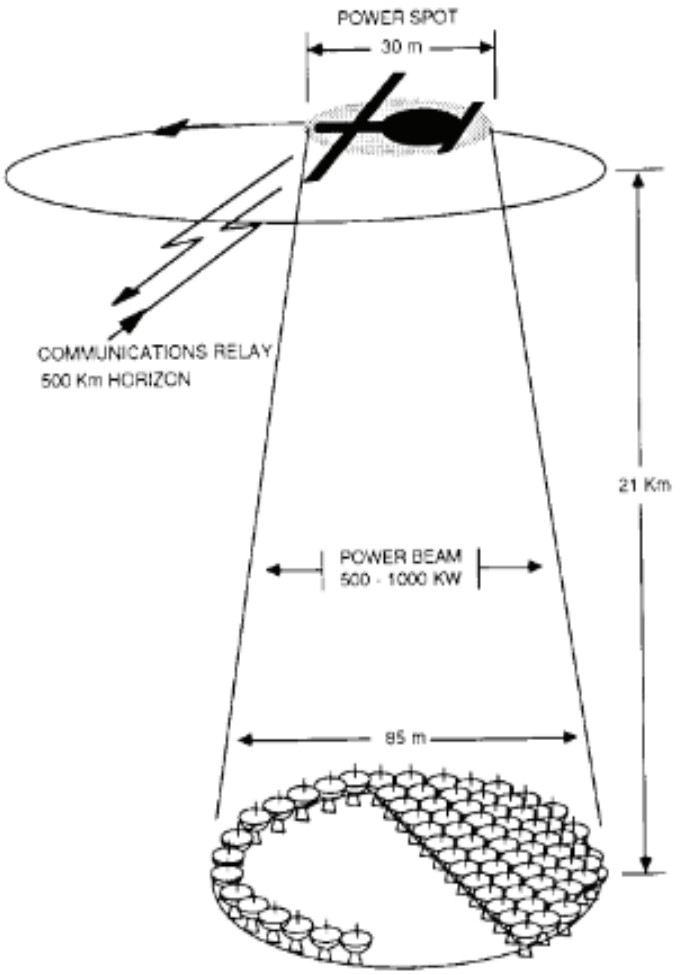

Figure 1.7. Configuration of SHARP study in 2D
(Source: Schlesak et al., 1988).

As shown in Figure 1.7, the transmitter had a large array of antennas on the ground which had 84 meters in diameter. About 500 kW microwave was tried to transfer through aircraft. However, 35 kW dc power was received by thin-film coated aircraft. 10 kW was supplied for the payload electronics and remainder part was drawn on the electronic motor system of SHARP which has been shown in Figure 1.7 (Schlesak et al., 1988).

Nevertheless, the main research topic was non-radiative WPT technology which are coupled magnetic resonance power transfer (CMRPT) (Duong and Lee, 2011), (Beh et al., 2013) inductive power transfer (IPT) (Huh et al., 2011) and capacitive power transfer (CPT) (Liu and Hu, 2009). Of these CMRP transfer, the technique consists of transmitter and receiver coils. CMRPT method has many advantages e.g. wireless power transfer with high efficiency under long distance. The schematic demonstration of the CMRPT experiment has been shown in Figure 1.8 (Kim et al., 2011).

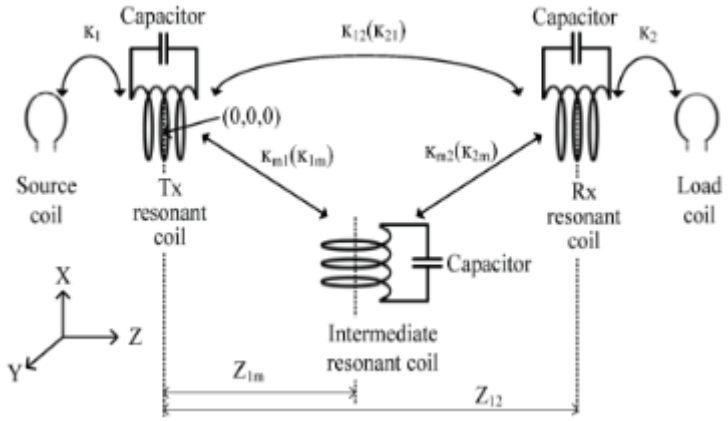

Figure 1.8. Working principle of CMRP technique
(Source: Kim et al., 2011)

As can be seen from Figure 1.8, the transmitter coil and receiver coil are called Tx and Rx respectively. During the power transfer, coils are progressed to magnetic resonance to achieve high efficiency. Although the CMRPT technique provides high efficiency, would not be commercialized by the reason of electromagnetic interference (EMI). Generally, EMI negatively affects the stability of embedded systems and human health concerns. Therefore, the CMRPT system can interfere in an embedded system where located around it and can harm the working principle of the embedded system. As well as, EMI which is created by CMRPT can damage the health of humanity.

On the contrary of electric field line, magnetic field line cannot penetrate through the metal barriers. (Kim et al., 2011).

While wireless power transfer methods are mentioned, the first things coming to mind are inductive power transfer and capacitive power transfer. Of these inductive coupling is the most popular technique to transfer power under near-field wireless power transfer. The inductive coupling method provides energy transfer where the distance between transmitter and receiver coils are restricted from millimetres to a few meters (Fnato et al., 2010). Inductive coupling technology has now reached to a $1 billion industry worldwide from the emergence of a new base (Covic and Boys, 2013). There are many application areas of the IPT system which are automation control systems (Green and Boys, 1994), robot manipulators (Kawamura et al., 1996), etc.

The above-mentioned disadvantages of IPT methods have made CPT methods more attractive. The electric flux is used to transmit power in the CPT technique. Electric field lines do not affect human health and they can penetrate through the metal barriers. Capacitive coupling does not generate EMI. Thus, CPT system does not influence the stability of embedded systems where they are located.

CPT techniques require at least two capacitive plates which are called transmitter (primary) and receiver (secondary). These plates make the transfer of current possible in the air gap. Nevertheless, capacitive coupling generally confines the distance between a transmitter and a receiver in a CPT system. The distance between the two plates should be smaller than 1 mm to provide transmission. The CPT systems can control risks with galvanic isolation. Under favour of galvanic isolation, capacitive plates do not transfer energy to the subjects or living organisms. In CPT systems, supply power should be used under the conditions of higher-voltage-lower-current in the range of 200 kHz – 1 MHz to achieve high efficiency (Dai and Ludois, 2014). From the development of CPT technology, it served many application areas which are interchip technology (Culurciello and Andreous, 2006) biosignal monitoring (Piipponen et al., 2007), biomedical implementation (Sodagar and Amiri, 2009), amplifiers (Fan et al., 2013), wireless charger circuits for robots (Hu et al., 2008), LEDs (Liu and Nair, 2009), vehicles (Kim and Bien, 2013). The comparison table has been constituted among non-radiative and techniques.

In Table 1.1, WPTs have been investigated under special topic which are distance, efficiency, EMI effect, type of field line, data and power transfer at the same frequency.

However, Table 1.1 includes more general information about facets of WPT techniques. In the next chapters, this topic was discussed more comprehensively.

Table 1.1. Comparison between non-radiative methods

Type of WPT	Distance	Efficiency	EMI effect	Type of field	Data & Power transfer at the same frequency
CMRPT	Far-field	High	Yes	Magnetic	No
IPT	Near-field	High	Yes	Magnetic	No
CPT	Near-field	Low	No	Electric	Yes

1.3. Wireless Power Transfer Experiments

30 W scale capacitive wireless power transfer was realized by Chieh-Kai Chang et al (2015). In this WPT system, 5.8 pF coupling capacitors were used to provide power transfer. There is an air gap between two parallel plates, and the gap was limited to 0.5 cm. Capacitive plates were chosen to be 5 cm x 5 cm square. Hence, a power transfer of 5.5 W per pF was obtained in the power transfer. The constructed system has been shown in Figure 1.9.

Figure 1.9. Prototype of 30 W capacitive WPT system (Source: Chang et al., 2015)

In this system, the output power was 31.82 W with 84 % efficiency. Capacitive plates have taken an active role in the WPT system in order to transfer energy.

Besides the dielectric constant of material that has been located between two parallel plates were equal to 1. A dielectric substance is a poor electricity driver, but an effective supplier of electrostatic fields. Energy transfer per square meter was calculated as 6.36 kW/m2. Results were taken from the experimental waveform of input voltage and output voltage to obtain the efficiency of the CPT system.

A composite matching network was performed to increase the efficiency of the circuit in the CPT system. The input and output voltage signals have been shown in Figure 1.10.

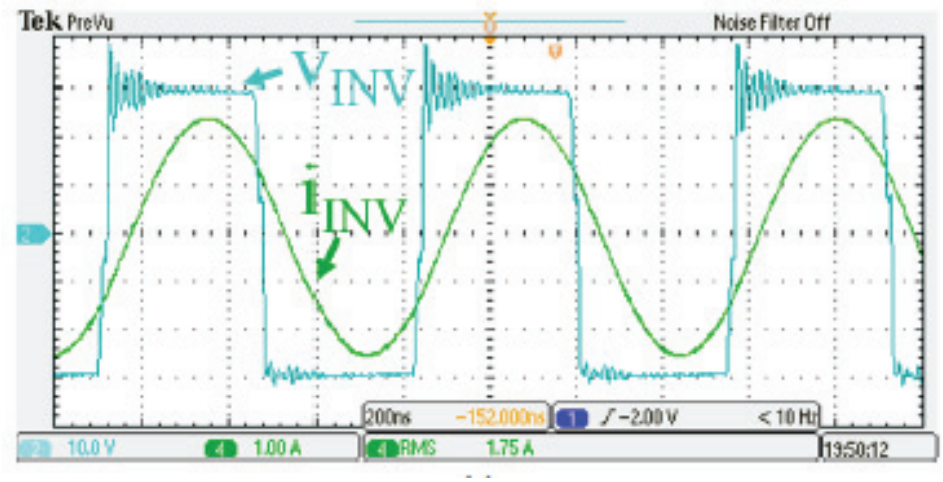

(a)

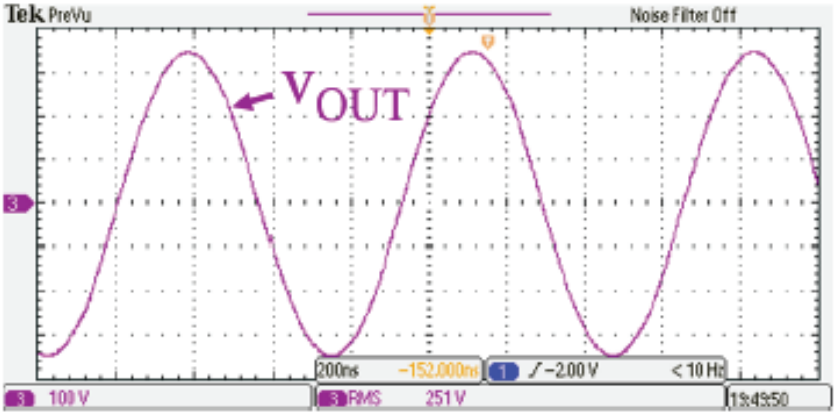

(b)

Figure 1.10. Input (a) and output (b) of voltage characteristic in capacitive power transfer (Source: Chang et al., 2015)

In Figure 1.10 (a) input voltage increased depend on input current. In this system, the input signal characteristic did not change when power was transmitted through the secondary part of the circuit. Validation can be done in Figure 1.10 (b) (Chang et al., 2015). Hua Zhang et al. (2016) have created 4 capacitive plates to provide wireless power transfer. This designed for large air gap. LCL compensation circuit has been used to generate resonate. Resonate circuit has increased the efficiency of transferred power rate. In this application, the finite-element method was performed.

Finite-elements technique has helped to the simulation of mode. Hence, the design criteria and dimension of the coupling capacitor have been investigated briefly. There was a specified area between coupling capacitors which was filled by 150mm air. The circuit topology was shown in Figure 1.11.

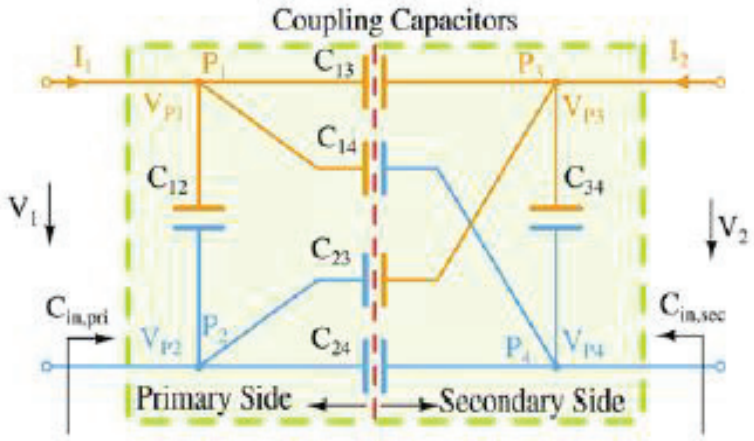

Figure 1.11. LCL compensated CPT circuit (Source: Hua Zhang et al., 2016)

The system consists of two main parts, these are primary and secondary. Energy was delivered from the primary side to the secondary side by the coupling capacitors. The operating frequency was specified as 1 MHz.

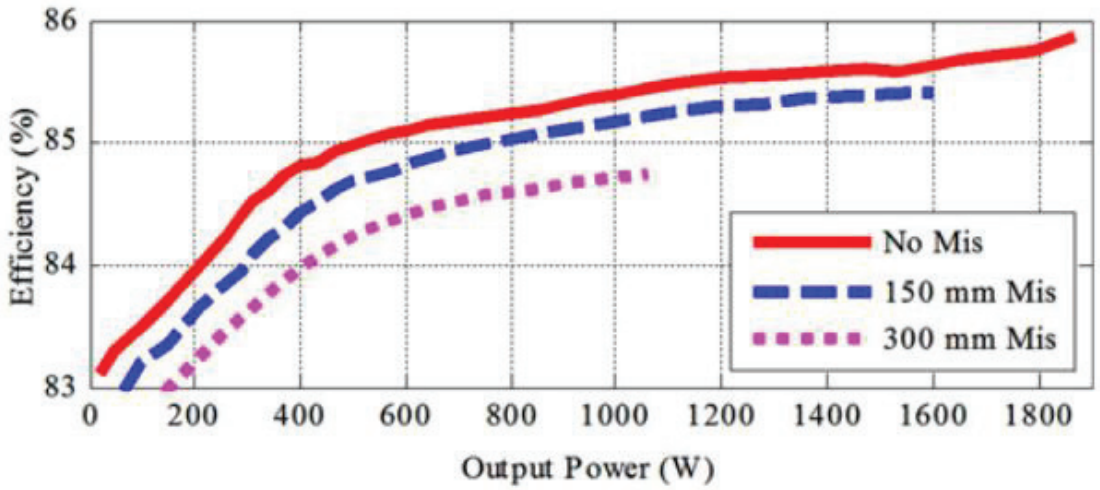

Figure 1.12. Relation between efficiency and misalignment of capacitive plates (Source: Hua Zhang et al., 2016)

Zero voltage switching was performed to increase efficiency. While the output potential differences increased, the efficiency value of the CPT system went through 86%. The relationship between output voltage and efficiency was shown in Figure 1.12. Also, this graph has shown that misalignment is very effective in WPT (Hua Zhang et al., 2016). The red line, blue line and pink lines refer no misalignment, 150 mm misalignment, 300 mm misalignment respectively. The efficiency was limited about 86% by CPT system and the output power was increased more than 1.8 kW.

According to Figure 1.12, the red line has a maximum efficiency value that means high output power with no misalignment gives the highest efficiency in the CPT system. The system has been created professionally with PCB (printed circuit board) circuits. The actual circuit has been shown in Figure 1.13.

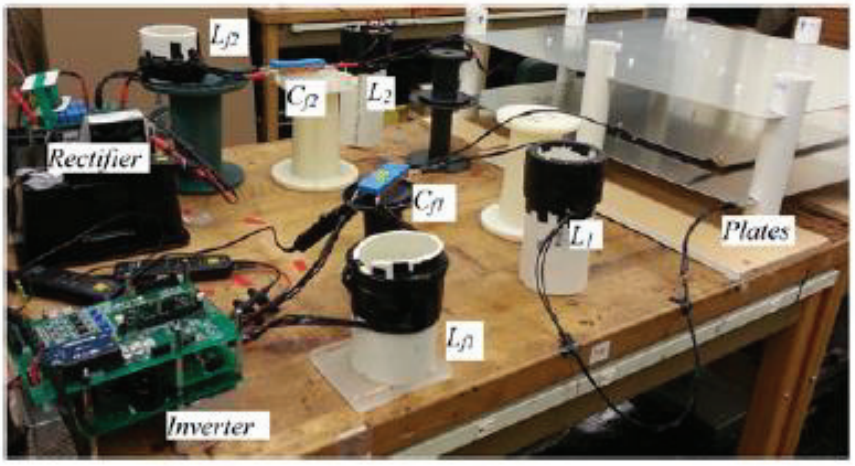

Figure 1.13. Demonstration of the actual circuit (Source: Hua Zhang et al., 2016)

Parallel plates have been carefully located with the apparatus to observe the effect of alignment on the CPT system. The CPT system efficiency has been evaluated about 85.87% with 1.87 kW transmitted throughput power from 150 mm air gap distance (Hua Zhang et al., 2016).

1.3.1. Inductive Power Transfer (IPT)

J. Huh et al. (2011) have studied the IPT system to reveal online electrical vehicles. The system is realized in a small pickup dimension and a large distance.

They have used resonant circuits to increase the inductive power transmission efficiency. A special line was divested to supply electrical vehicles. The I-type rail system has been operated as a power line. The rail system is shown in Figure 1.14.

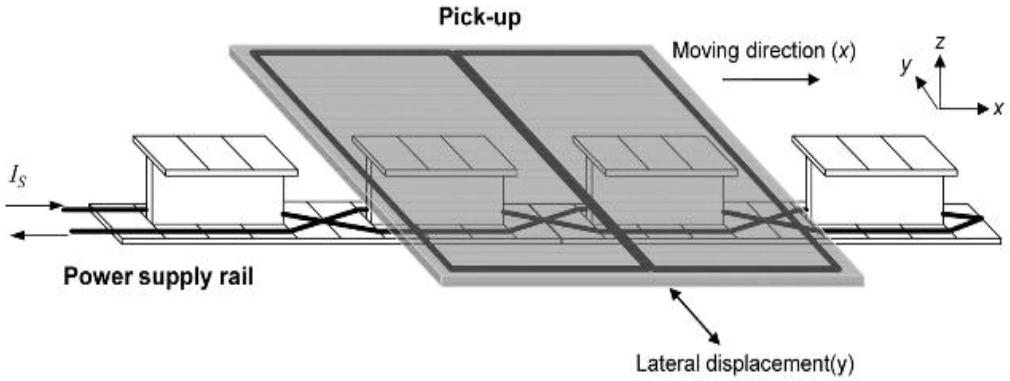

Figure 1.14. Demonstration of I-type inductive power supply rail system (Source: J. Huh et al., 2011)

Lateral displacement at y-axis and width approximately were 24 cm and 10 cm, respectively. Power supplied system was used as a transmitter. The pick-up vehicle was selected as the receiver. IPT system was investigated by simulations and experiments to make validation. Maximum efficiency has been obtained about 77%at 27 kW throughput power. IPT system transfers energy by magnetic field lines which generate the magnetic flux. Magnetic flux could be dangerous for human health and the stability of the embedded system. The distribution of magnetic flux density is given in Figure 1.15.

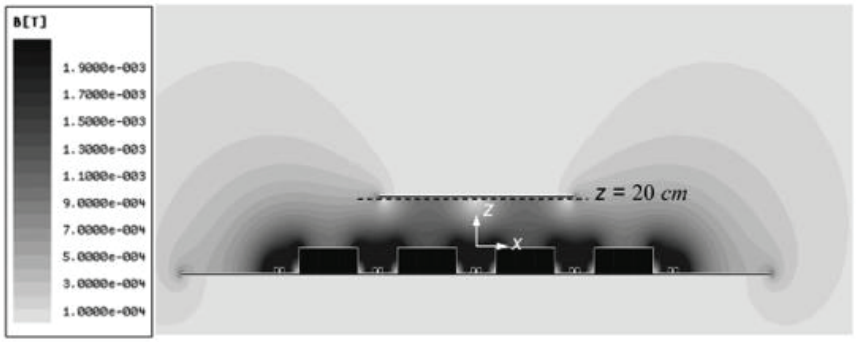

Figure 1.15. Magnetic flux density distribution between transmitter and receiver (Source: J. Huh et al., 2011)

Magnetic flux distribution has been observed by a simulation program. Input current and operating frequency were selected 200 A and 200 kHz, respectively. J. Huh et.al have realized the project as seen in Figure 1.16. In the system, Litz wires were implemented.

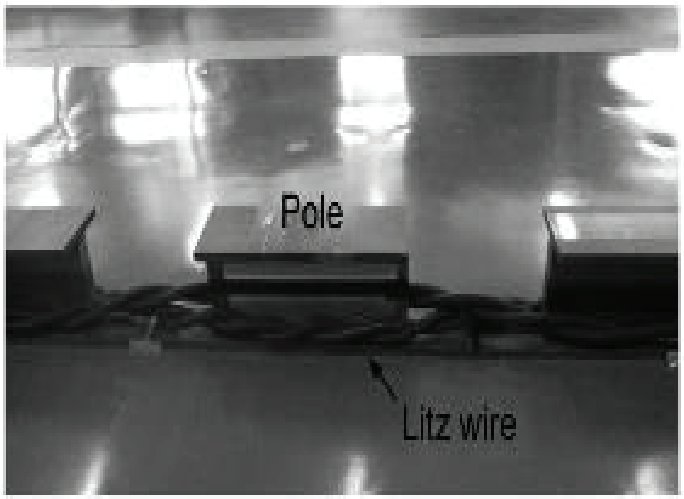

(a)

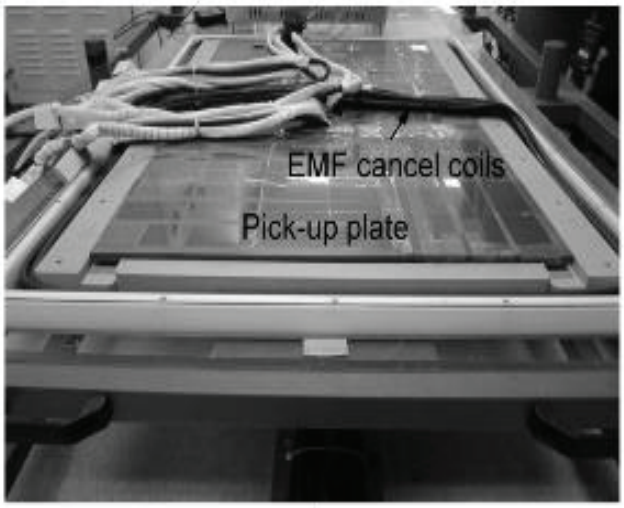

(b)

Figure 1.16. Primary side (a) and secondary side (b) of system
(Source: J. Huh et al., 2011)

27 kW output power was obtained from the 35 kW input power. The efficiency was calculated as 77 %. The project has been performed to decrease the ratio of CO_2 and other harmful gases.

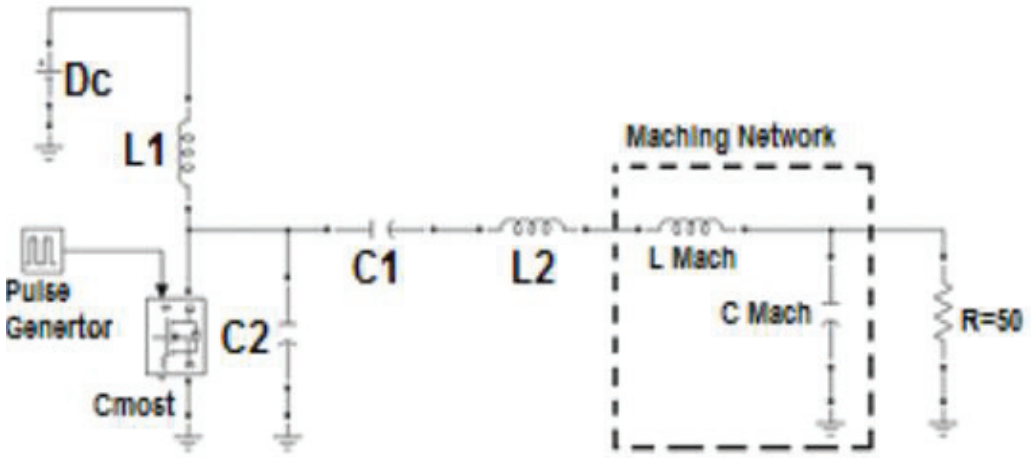

Figure 1.17. Circuit diagram of the class-E amplifier system in biotelemetry (Source: Abbas et al., 2012)

The inductive power transfer has been tested with efficient Class-E power amplifier for biodata transfer by Abbas et al. (2012). Circuit topology has been demonstrated in Figure 1.17.

The Class-E circuit (Figure 1.17) has been used to increase the transmitted power ratio with respect to the input. The system frequency was selected as 13.56 MHz. This frequency was proposed carefully due to provide high data transfer rate. In order to decrease the switching losses on the MOSFET, zero voltage switching (ZVS) method has been applied.

A matching network was composed of a resistor and a capacitor. Class-E power amplifier topology has two states which are “ON” and “OFF” depending on MOSFET. While MOSFET is in “ON” state, the current from the DC source is directed to the ground.

In other states, the current flows through the matching network. L1 and C2 refer to the choke coil and the shunt capacitor, respectively. Switch was operated under 50 % duty cycle with 3.3 DC voltage. The system has been designed for monitoring the biodata transfer. Hence, operating frequency and electromagnetic flux have been kept in compliance with international standards.

The most important aspect of the biodata transfer is that it does not damage the living organism. Achieved efficiency values and, the detail of the components have been given in Table 1.2.

Table 1.2. Operated electronic materials and efficiency values of system (Source: Abbas et al., 2012)

F MHz	L_1 (µH) opti. Resis.	L_1 (µH) small Resis.	C_2 (PF)	L_2 (µH)	C_1 (PF)	η_1 %	η_2 %
13.56	12	30	51.5	4.92	33.11	87.2	≥80
27	1.2	0.65	82	2.7	14	73	88
0.135	-	85	23 nF	150	2.8 nF	-	94.8

η_1 efficiency for optimum resistor,
η_2 efficiency for small resistor

Two resistors were tested to reach the highest efficiency value. The purpose of this experiment to specify the optimum resistance that was determined from the theoretical background earlier. Obtained efficiency values were distinguished on two-part according to optimal and small resistive values. When Table 1.2 is considered, decreasing in frequency causes increasing efficiency that means there is an inverse proportion between frequency and efficiency valid for the small resistor. However, there is a direct proportion between efficiency on optimum resistor and frequency (Abbas et al., 2012).

1.3.2. Capacitive Power Transfer

CPT system has also been used for monitoring the health care measure system. ECG (electrocardiography) vital values were observed with coupling capacitors. The system has been shown in Figure 1.18.

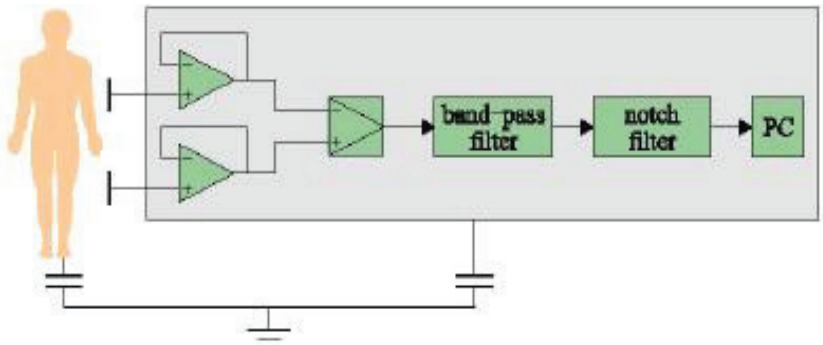

Figure 1.18. ECG measurement system by capacitive coupling method (Source: Maruyama et al., 2007)

Coupling capacitors transfer data or energy without any interference on the embedded system. Also, the capacitive coupling system uses the electric field to transmit power and data at the same frequency. These features make CPT technology attractive. In 2007, one or two coupling capacitors were implemented to ECG measurement by Maruyama et al (2007).

Capacitive coupling plates have been used as electrodes. Electrodes have been connected to the body of subjects in order to monitor virtual values and no ground electrode was placed on the skin of the subjects. Two coupling capacitor was attached to the body. They have been designed with the same type and method to investigate the voltage difference in the body. This voltage difference was acquired with a voltage follower op-amp circuit. The circuit topology has been shown in Figure 1.19. C_E, C_G, C_K represent capacitance values between body and electrode, capacitive between ground (world) and body, the capacitance between the ground and follower circuit respectively. C_{in} and R_{in} denote the amplifier's input capacitance and input resistance, respectively. V_{out} is the throughput voltage.

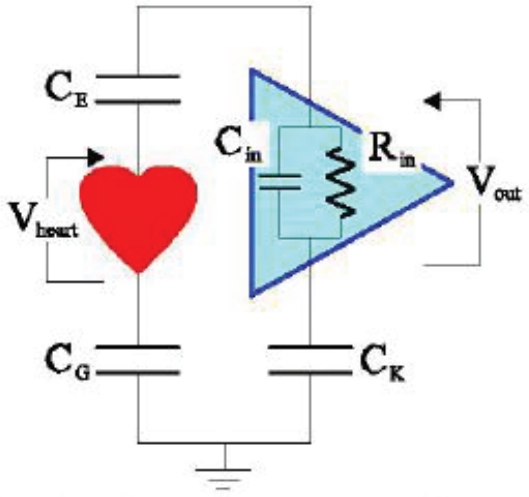

Figure 1.19. ECG measurement by CPT circuit (Source: Maruyama et al., 2007)

After the circuit has been designed by the help of theoretical background, the EGC experiment has been realized on a subject's body (Figure 1.20). As mentioned before, two main electrodes were attached to the test subject. The recorded two main signals were connected to the comparative op-amp circuit. The output signal was amplified by the op-amp depending on its gain.

However, some noise could be seen in the output signal. ECG signal was retrieved with the help of bandpass and notch filters. Finally, this data has been transferred to the PC.

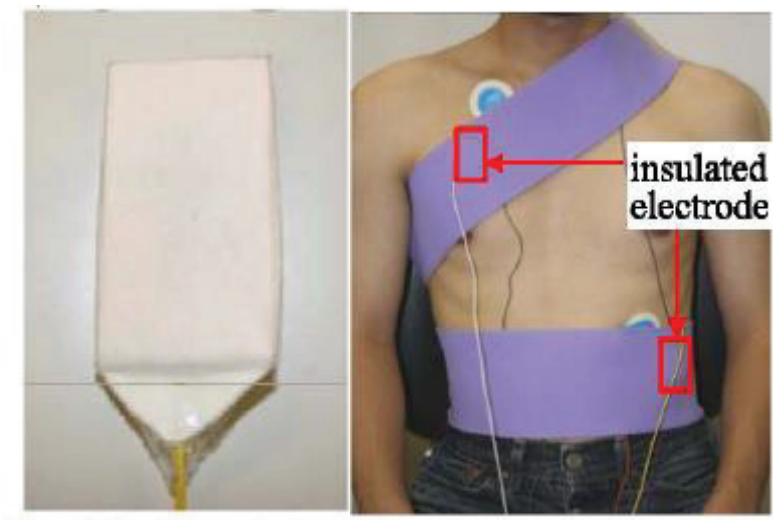

(a) (b)

Figure 1.20. Capacitive coupling (a) electrode (b) on subject
(Source: Maruyama et al., 2007)

Height, width and thickness of isolated electrode size were 50 x 20 x 0.1 mm. These electrodes were attached to the body by an elastic band.

The frequencies of sampling and bandpass filters were 1 kHz and 5-100 Hz, respectively. Although experiments were realized in many different environments, SNR was large in the presence of environmental noise as expected.

Three types of experiments have been performed depending on electrode locations. However, the cleaned signal has been obtained by two coupling capacitors electrodes without any insulation applied.

In this experiment, one of the most important issues of ECG measurement by capacitive coupling method was the noise at 60 Hz which was caused by mains frequency. Gathered results were compared with row ECG signals which have been shown in Figure 1.21. As a result, the study has shown that the capacitive coupling (CPT) method can be performed for ECG measurements without any harmful effect on the living organism (Maruyama et al., 2007).

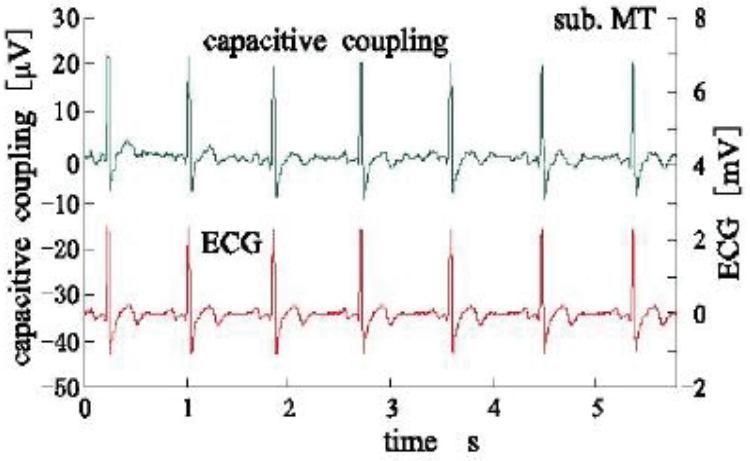

(a)

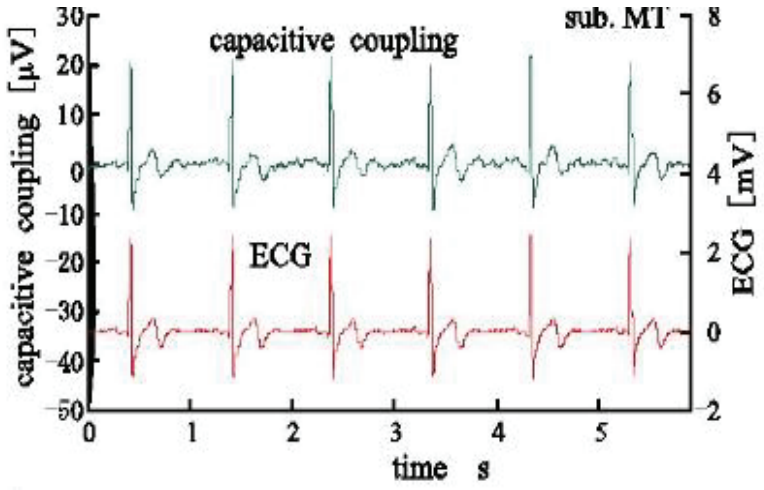

(b)

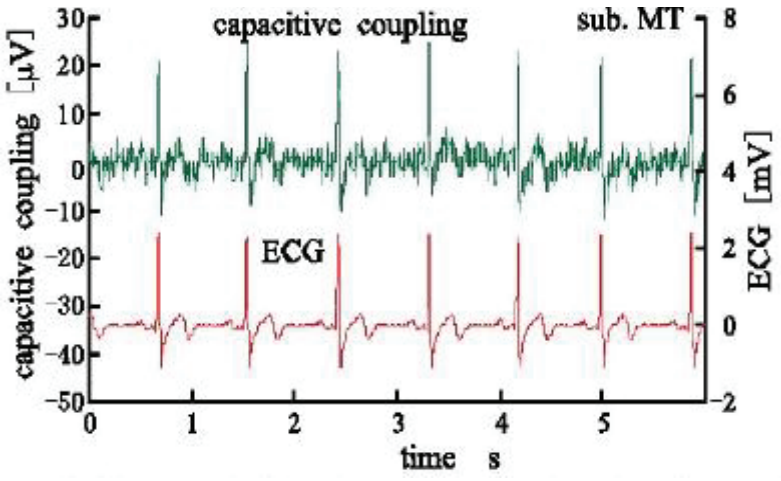

(c)

Figure 1.21. Comparison between ECG measurement results by (a) No isolated coupling capacitors (b) Two isolated electrodes with ground (c) Two isolated electrodes for ground (Source: Maruyama et al., 2007)

Besides, capacitive power transfer has been performed on a vehicle charging system by a conformal bumper (Dai and Ludois, 2007). The gap between receiver and transmitter has been kept as small as possible to obtain high efficiency. Therefore, the charging system was mounted on the backside (bumper) of the car instead of the bottom side. The bumper has been designed flexible and compressible to make the air gap minimum. Additionally, the size of the bumper maximizes the surface area which was used for power transfer. Conformal bumper idea has been suggested for these reasons. The EV (electric vehicle) includes two main topics which are the power electronics and the CPT design. The charge station (dock) and EV car have been shown in Figure 1.22a and Figure 1.22b.

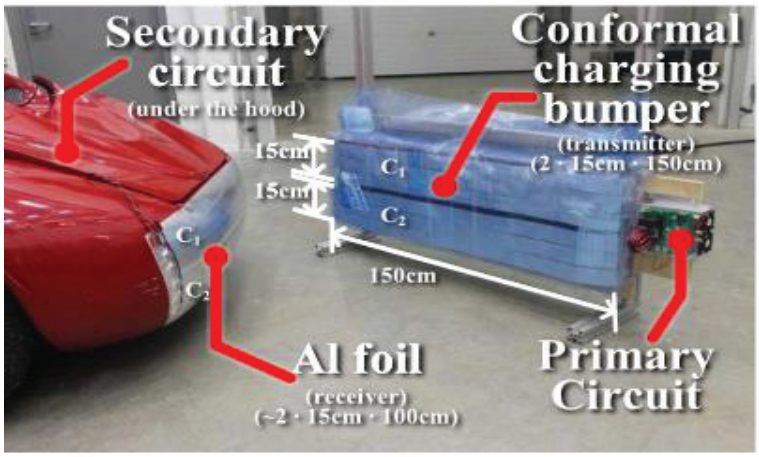

(a)

(b)

Figure 1.22. Demonstration of EV car approaching the charging station. EV charging CPT system (a) The charging process (b) (Source: Dai and Ludois, 2007)

A kilowatt scale CPT system was designed in order to satisfy the high charge per second rate of the car. In Figure 1.22 (a), two coupling capacitor (C1 and C2) have been performed for charging. Height, length and width of them. Pairs of the coupling capacitors were placed on the EV car. Coupling capacitor on the EV car was called secondary part and other coupling capacitors were called primary. Coupling capacitor on the secondary side was made by aluminium foils. The charging process has been summarized in Figure 1. 22 (b).

C1 and C2 capacitance values have been measured 10.5 and 9.5 nF, respectively during the charging process. The EV car has a 156 V battery pack. The output power was measured more than 1 kW with 90% efficiency at 530 kHz frequency (Dai and Ludois, 2007).

1.4. Thesis Objectives

The aim of the thesis is transferring data and power for monitoring mechanical variable by efficient coupling capacitor. The scale of power should be chosen sub-kilowatt. Sub-kilowatt power is suitable for the required energy of the data measurement system. In this thesis, the weight of a load on the axle has been selected as a mechanical variable. In order to actualize wireless data and power transfer efficiently, a small prototype design was aimed.

Data and power transfer experiments have been carried out by capacitive coupling plates. CPT method has been chosen for investigation. CPT method has many advantages that are as follows:

1. Data and power transfer at the same frequency
2. It does not generate electromagnetic interference (EMI) due to the usage of electric field lines
3. Electric field lines are not harmful to human beings or living organisms
4. Compact design and attachable connection on rotary mechanical systems
5. Suitability for under skin applications and biomedical implementation
6. Galvanic isolation minimises the risks to humans while data and power transmission are on.

This thesis addresses the various facets of CPT. Objectives of the thesis are as follows:

1. To design an efficient Class – E circuit that corresponds to CPT technology.
2. To minimize the noise of the circuit
3. To design efficient full-bridge rectifier circuit
4. To calibrate the weight sensor
5. To provide continuous information without any interrupt
6. To perform experiments under static load with the whole system (data and power transfer).

However, there are design criteria while CPT technology is performed to data and power transfer. The restrictions of the thesis are;

1. The constricted distance between receiver and transmitter
2. To achieve maximum power, one-to-one oriented coupling surface is needed
3. The limited power transfer rather than other near-field WPT systems

1.5. Overview of the Thesis

In this thesis, there are 6 Chapters; Introduction, Theoretical Background of Wireless Power Transfer and Class- E Circuit Topology, Capacitive Power And Data Telemetry, Prototype of the CPT System, Testing of Prototype and Conclusions. The outline of the thesis is as follows;

In the next Chapter "Theoretical background of capacitive power transfer and Class- E circuit topology";

1. The theory of WPT technology has been investigated,
2. Electromagnetism and electric field theories have been analysed with the fundamental formulas (Maxwell equations).
3. Class –E power amplifier circuit topology has been described briefly,

In the third Chapter "Capacitive power and data telemetry";

1. Design criteria of CPT experiments and case studies were presented,
2. Selection criteria, specification of the electronic component, details of the circuit analysis and brief description of the weight sensor are explained,

3. Circuit configuration and components are described,
4. Data acquisition and power transfer circuit design process is clarified,
5. Data and power transfer system schematic and technicality are expressed,

In the fourth Chapter “Prototype of the sub-kilowatt and efficient CPT system”;

1. The small prototype is explained and tested for data and power transfer,
2. Calibration of the weight sensor is studied,
3. The working principle of the prototype is explained briefly,
4. The results of the performed prototype are presented,

In the fifth Chapter “Tests”;

1. The efficiency of the prototype has been researched.
2. The validation of the weight measurement system is analysed.

In the sixth chapter, the gathered experimental results are discussed in detail.

CHAPTER 2

THEORETICAL BACKGROUND OF WIRELESS POWER TRANSFER and CLASS –E CIRCUIT TOPOLOGY

This chapter includes a literature survey on theoretical explanations for especially capacitive power transfer and Class-E circuit topology. In addition, the fundamental theory of electric filed has investigated from the beginning of the first experiments. Finally, an available prototype of efficient CPT system has been explained briefly.

2.1. The Theory of Capacitive Power Transfer Systems

The story of capacitive power transfer has started with Charles Coulomb. He is the first man who measured the magnitude of the electric force between charged particles by special test set-up. This test apparatus was called the torsion balance. During the experiments, he has discovered the corroborated electric force which is called electrostatic force as well. The magnitude of the electrostatic force has been found from the experimental investigation. Hence, Coulomb's law has been established. The formula has been given in Equation 2.1.

$$F_e = k_e \frac{|q_1||q_2|}{r^2} \tag{2.1}$$

Where F_e indicates the electric force between charged particles and the unit is Newton (N). k_e represents the Coulomb constant. Its unit is $N \cdot m^2/C$. The magnitudes of charged particles have been shown by q_1 and q_2.

The distance between two charged particles has been presented by r. Coulomb's constant is $8.987 \times 10^9 N \cdot m^2 / C^2$. It can be written as Equation 2.2.

$$k_e = \frac{1}{4\pi\varepsilon_0} \tag{2.2}$$

Where the ε_0 (epsilon) is known as permittivity of free space and its theoretical values is;

$$\varepsilon_0 = 8.8542 \times 10^{-12} C^2 / N \cdot m^2 \tag{2.3}$$

Besides, the electric field theory has to be known in order to understand the concept of this thesis. The electric field lines are located between source charge and test charge depending on the electric force. Electric field is defined as the electric force acting per test charge. The electric field formula has been given in Equation 2.4.

$$\vec{E} \equiv \frac{\vec{F}_e}{q_0} \tag{2.4}$$

The electric field can be described mathematically as newton per coulomb (N/C). The test charge (q_0) has been given in Equation 4. Electric field tangent at each point to electric field lines. The electric fields lines are perpendicular to the surface and proportional to the electric field. The magnitude of the electric field is inversely proportional to the distance between charges. Hence, where electric fields are intensity the electric fields line are close to each other. Electric field lines always go through from positive charge to negative charge. The frequent electric lines leave from a negative or a positive charge. Electric field is responsible for the attractive force or repel force in atomic-scale that helps to atoms to hold together that causes chemical bonding. Electric field has a monopole structure. The CPT has the advantage that the electric field lines terminate on charge and do not need a closed return path (monopole). The unit charge can be positive or negative. However, the magnitude of the electric field is approximately zero for real life when charges are far adequate from each other.

The electric field is a vector quantity and can be shown with arrows that go through the charged particles. The SI unit of electric field strength is known as potential difference per meter (V/m).

After the basic concept has been investigated, the Maxwell equations were included in the theoretical background of this thesis.

Basically, Maxwell equations are Gauss's law, Gauss's law for magnetism, Faraday's law and Ampere's law respectively (Serway and Jewetty, 2010).

2.1.1. Gauss's Law for Electricity

The first equation of the Maxwell equation is Gauss's law that identifies the relation between electrically charged particles and the electric field. Gauss's law can be described as in the equivalent form of Coulomb's law. Gauss's law postulates the nature of electric charges. Gauss's law has been given in Equation 2.5.

$$\nabla \cdot D = \rho_V \tag{2.5}$$

The Equation 2.5 is valid for anywhere in space. ∇ operator (divergence) is used to show the vector flows where is located out of the surface at a point (x, y, z). While electric field vectors flow through the outside surrounding, the magnitude of divergence becomes a positive number. While electric field vectors flow through the inside on the surface, the magnitude of divergence becomes a negative number. If V value is accepted as an input vector function, the magnitude of the electric vector field has been identified as Equation 6.

$$V = \begin{bmatrix} V_x \\ V_y \\ V_z \end{bmatrix} = V_x \hat{x} + V_y \hat{y} + V_z \hat{z} = V_x \begin{bmatrix} 1 \\ 0 \\ 0 \end{bmatrix} + V_y \begin{bmatrix} 0 \\ 1 \\ 0 \end{bmatrix} + V_z \begin{bmatrix} 0 \\ 0 \\ 1 \end{bmatrix} \tag{2.6}$$

The sum of the vectors at the specified axis can be expressed with the partial derivative form depending on the axis. The form has been shown in Equation 2.7 with the input vector function of V.

$$\nabla \cdot V = \frac{\delta V_x}{\delta x} + \frac{\delta V_y}{\delta y} + \frac{\delta V_z}{\delta z} \tag{2.7}$$

If somewhere in space there is no electric charge, the divergence of D equals to zero. In equation 2.5, D refers to the electric flux density that is related to the electric field. This relation has been shown in Equation 2.8.

$$D = \varepsilon E \tag{2.8}$$

ε is the permittivity of material where measure is realized (isotropic linear dielectric). In Equation 2.8, the electric field formula is substituted which shown in Equation 2.9.

$$D = \varepsilon E = \frac{q}{4\pi r^2} \tag{2.9}$$

According to Equation 2.9, the electric flux density is proportional to the electric field that does not depend on the material. Besides, D is the vector quantity and the SI unit is C / m^2 that means charge per meter square. As can be seen from Figure 2.1, the electric flux density depends on cosine theta ($\cos\theta$) angle. While the angle between the surface vector and the electric field line is 90° the electric flux through the area equals to zero (Serway and Jewetty, 2010).

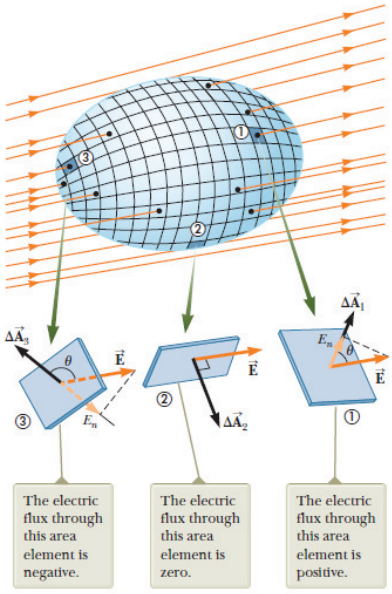

Figure 2.1. Electric flux characteristics on the surface
(Source: Serway and Jewetty, 2010)

In order to increase the vision of Gauss's law, the integral form has been given in Equation 2.10. In this formula, the act of electric flux on per area equals the charge per permittivity of free space. The electric flux is directly related to charge due to constant permittivity of free space.

$$\int_V (\nabla \cdot D) \cdot \mathrm{dv} = \int_V \rho_V dv \tag{2.10}$$

According to Equation 2.10, the electric charge is shown with ρ and volume charge density is defined by subscript V. The ρ_v shows the charge per volume (C/m^3). The electric charge density can be positive, negative or zero.

2.1.2. Gauss's Law for Magnetism

The second law of Maxwell is the Gauss's law for magnetism. The first law of Maxwell should be known thoroughly in order to understand Gauss's law for magnetism. The second law has been given in Equation 2.11.

$$\nabla \cdot B = 0 \tag{2.11}$$

While the second law is investigated, the divergence has been used in the equation. The divergence of electric field density is equivalent to the volumetric electric charge density. However, it is not valid for the magnetic field. The divergence of magnetic flux density is equal to zero.

In this equation, B refers to magnetic flux density. It is vector quantity as electric flux density. A magnet or other object used for creating magnetic field has dipole topography.

Similar to the electric charges, magnetic poles repel or attract each other. Nevertheless, the magnets always have a positive side and a negative side, the total magnetic flux on the object equal to zero. No matter the magnet always has two poles which is called dipole. Monopole magnets cannot exist in the universe. This expression is formulated by Gauss's magnetism law. This formula expresses that every element volumes have same the same number of magnetic field or flux in-universe.

The SI unit of magnetic flux is Wb/m^2. This unit also same with the Tesla (T). The differential form of Gauss's magnetism law can be written as Equation 2.12 and Equation 2.14.

$$B = \mu \cdot H \tag{2.12}$$

Where, μ, H represent the permeability and magnetic field. Of these, permeability depends on the material or medium type.

The unit of permeability is Henries per meter (H/m). This unit shows the inductance per length. In basic term, the permeability is a function that measures how easily magnetic field can pass through inside of an object or a medium. For example, the permeability of vacuum air has been measured $4\pi \cdot 10^{-7} H/m$ (μ_0). The permeability of a medium is often described by its relative permeability The permeability value of a medium is the ratio of the relative permeability value of the medium to the vacuum air permeability. The formula of relative permeability has been given in Equation 2.13.

$$\mu_r = \frac{\mu}{\mu_0} \tag{2.13}$$

Where, μ_r and μ indicate the relative permeability and medium permeability, respectively. If a medium's relative permeability is equal to the 1, it is known as diamagnetism. In this case, a material generates an inner magnetic field at the opposite of the magnetic field externally applied. While relative permeability value of a medium or a material is greater than 1, this is called paramagnetic. Magnetic field and magnetic flux vector are linearly related to these type of materials.

The permeability does not depend on changes in the magnetic field intensity for these materials. However, ferromagnetic is a form of permanent magnet that shows hysteresis behaviours in materials. Generally, these type of materials have very high permeability values that can repel or attract other magnets.

In differential form of Gauss's magnetism law has been given in Equation 2.14. H represents the magnetic field strength on the surface and dA shows the surface area vector.

$$\oiint H.dA = 0 \tag{2.14}$$

The SI unit of magnetic field in Amps/meter. This means the current per meter. The current passing through a wire creates a magnetic field around itself at distance r. The magnetic field is a vector quantity just as the electric field. The magnitude of the magnetic field diminishes when distance r is increased. It is inversely proportional to the distance r. However, the magnetic field is directly proportional to the current. The magnetic flux density has been shown in Figure 2.2.

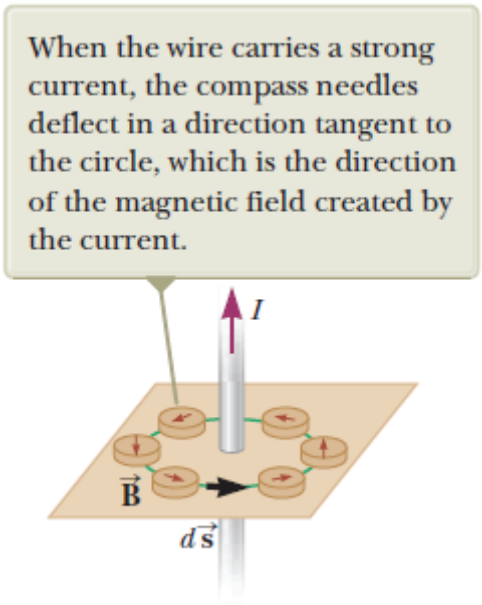

Figure 2.2. Created a magnetic field by current passing through the wire
(Source: Serway and Jewett, 2010)

The existence of a magnetic field has been corroborated by compasses where were placed around the wire in Figure 2.2. According to Figure 2.2, the magnetic field can be calculated with Equation 2.15

$$H = \frac{I}{2\pi r} \tag{2.15}$$

H and r represent the magnetic field vector and distance r, respectively. The notation has been arranged depending on Figure 2.2. The magnetic force has been obtained due to the magnetic field. The direction of compasses show the direction of magnetic force. It is also a vector quantity like the magnetic field. The magnetic force has magnitude and direction.

In order to express the potential of magnetic force, the charges where are located in the magnetic field have been investigated. While the charged particle has v velocity in B magnetic field, the magnetic force formula can be written as:

$$F_H = qv \times H \tag{2.16}$$

Where F shows the magnetic force quantity and H present the magnetic field strength. The x is the cross product. In Equation 2.116, all quantities are vector quantity except q value.

The magnetic force is directly proportional to the magnitude of the magnetic field strength and velocity of the charged particle. While the external electric field is applied to the system the Lorentz Force comes to light. The Lorentz Force is given in Equation 2.17.

$$F = q(\mathrm{E} + v \times H) \tag{2.17}$$

Where E symbolizes the magnitude of electric field strength and B resents the magnetic field flux (Serway and Jewetty, 2010).

2.1.3. Faraday's Law of Induction

The third law of Maxwell is Faraday's law of induction. The law is given in Equation 2.18, mathematically.

$$\nabla \times E = -\frac{\partial H}{\partial t} \tag{2.18}$$

Where t presents the time in second. The formula has been found with experiments that were performed by Faraday. The experiment has been demonstrated in Figure 2.3.

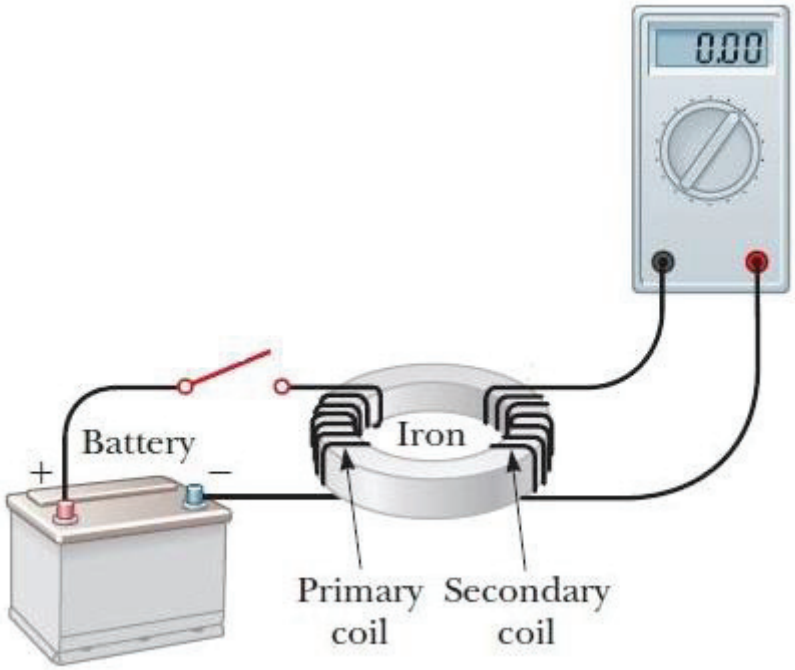

Figure 2.3. Faraday's experimental set-up (Source: Serway and Jewetty, 2010)

Experiment has been performed by Faraday. In the experiment, the 3 main elements have been used which are the battery, ammeter and iron core, respectively. According to the experiment, two states have been considered that depend on the switch state. They are "ON" state and "OFF" state.

Before the starting experiment, he has expected two ideas for two states. First one of is "ON" state. While the switch is open, there is no current flow through the wires.

Therefore, the monitoring value on the ammeter should be zero.

For "OFF" state, the current flows through the wire and ammeter should show the value higher than zero. While Faraday has launched into the experiments, he has first applied "ON" state. The observation of Faraday was the same as the "ON" state expectation.

There was no current flow through the iron coil or wire and the value of ammeter was equal to zero. After then, Faraday has carried out the second state which is "OFF" state. At the beginning of the experiment, everything that happened was the same as the expectations. The ammeter has reached the maximum value. However, after a while later, the observed value in ammeter has gone back to zero.

After Faraday has changed state from “OFF” to “ON”, the ammeter value first has gone through the negative maximum value and subsequently has reached zero. These results are not the same as the second expectation.

After a while, Faraday has figured out that after the switch state is altered from “ON” to “OFF” state, the magnetic flux inside the magnetic core (iron) raises from zero to maximum number with respect to time. While magnetic flux increases, the current has induced on the opposite side. In a similar way, after the “OFF” state is changed, the magnetic flux inside the core goes back to zero. Therefore, the opposite current induces on the right side depending on decreasing magnetic flux.

Faraday has discovered the EMF (Electromotive Force) that was given in Equation 2.19.

$$EMF = -\frac{d\Phi}{dt} \tag{2.19}$$

According to formula, the EMF depends on the changing in magnetic flux with respect to time. The negative symbol represents the induced current at the opposite side. The magnetic flux has been shown with Φ and t shows the time in seconds.

$$\Phi(t) = \int_S H(t)\, dS \tag{2.20}$$

Equation 2.20 expresses the magnetic flux on the sum of magnetic field B enclosed S surface. The total EMF over the enclosed area can be written as:

$$EMF_{total} = \oint d(EMF) \tag{2.21}$$

Now, remember that the electric field is directly proportional to the electric charge force from Equation 2.4. The SI unit of electric field on the wire is V/m. The integration form has been given in Equation 2.22.

$$V = \int E \cdot dl \tag{2.22}$$

The total voltage between the head to the tail of the wire has been written as Equation 2.23. The integration part has been given in Equation 2.23.

$$E = \frac{dV}{dt} \tag{2.23}$$

The potential difference with respect to time is equal to the electric field. Equation 2.21 and 2.23 explain that the integral of the electric field at any location over the area is equal to the total EMF. This expression has been formulated in Equation 2.24.

$$EMF_{total} = \oint E.dl \tag{2.24}$$

Stokes theorem is getting involved at this state to combine two equations which are Equation 2.24 and 2.18, respectively. Stokes explains that integrating a field around a loop (averaging) is exactly like integrating a field curl into the loop. Therefore, the new equation has been constructed.

$$\oint E.dl = \int \nabla \times E.ds \tag{2.25}$$

If Faraday's law is integrated, Equation 2.26 is obtained.

$$\begin{aligned} \int_S \nabla \times E \cdot dS &= -\frac{d}{dt}\int_S \mathrm{H(t).dS} = \int_S -\frac{dH(\mathrm{t})}{dt} \cdot ds \\ \nabla \times E &= \frac{-\partial H(\mathrm{t})}{\partial t} \end{aligned} \tag{2.26}$$

According to Equation 2.26, some interpretations can be done. Faraday found that (Serway and Jewetty, 2010);

- Magnet fields originate from Electric Current. The electric current is caused by magnetic fields around a circuit.
- Unit change of magnet field in time leads to rising of an electric field.
- An electric field circulating in time leads to a time increasing in the magnetic field.

2.1.4. Ampere's Law

Ampere is a scientist who has studied on the magnetic force of wires carrying current. While he was working on the experiment, faraday was dealing with faraday equation.

Ampere's law-related with the magnetic field which was generated by a current-carrying wire. The magnetic field surrounds the wire with r radius. The current flows can be calculated by Equation 2.27.

$$\oint H.dl = I_{enc} \tag{2.27}$$

dL and I represent an imaginary path of the wire and the current that is encircled by this path, respectively. The SI unit of current is ampere (A). The magnetic field around the wire has been shown in Figure 2.2. If the radius of the circle is accepted as r, the calculation of the magnetic field can be calculated as:

$$H = \frac{I_{enc}}{2\pi r} \tag{2.28}$$

According to formula, the magnetic field from the specified distance can be calculated changing in radius r. If encircled current keeps constant, increasing of distance, decreases the magnetic field around the wire.

In this case, stoke equation again used to obtain the Ampere's law and Equation 2.29 was achieved.

$$I_{enc} = \oint H.dL = \int (\nabla \times H) \cdot dS \tag{2.29}$$

The stoke theorem has been applied to the right side of the equation. The total current flows through the wire can be written as Equation 2.30.

$$I_{enc} = \int_S J \cdot dS \tag{2.30}$$

Where J shows the current density. The SI unit of electric current is Ampere, however, the flowing charge per second is the same expression.

The SI unit of electric current density is the amount of current per meter square (A/m^2). Because, while current flows through the wire, the cross-sectional area of the wire is considered. The Equation 2.29 expresses that total electric current density on the area where current flows through the wire. The current density is related to σ electrical conductivity.

The unit of electrical conductivity is Siemens/meter. Electrical conductivity is proportional to the electric field. The current density formula has given in Equation 2.31.

$$J = \sigma E \tag{2.31}$$

The electrical conductivity is inversely proportional to resistance. The fundamental ohm law comes from Equation 2.31. Maxwell has observed the change in the Electrical Field in the capacitor. He realized the increase in the magnetic field. However, there was a question inside of his head. Why would increase in the electric field not increase the magnetic field? He has obtained the relation between the changing in the electric flux density and the displacement current density. The formula has been given in Equation 2.32.

$$\frac{\partial D}{\partial t} = J_d \tag{2.32}$$

J_d presents the displacement current density. Ampere's law is the symmetric of Faraday's Law. The final equation has given in Equation 2.33.

$$\begin{aligned} \nabla \times H &= J + J_d \\ \nabla \times H &= J + \frac{\partial D}{\partial t} \end{aligned} \tag{2.33}$$

According to Equation 2.33, increasing electric current density increases the magnitude of the magnetic field. Fluctuation of electric flux density (D) with respect to time, acts on the magnetic field (H). According to Maxwell equations and the coulomb law, the theoretical background of the capacitor has been constructed.

Capacitor is a combination of two conductive plates. A time-varying potential between the plates generates a current through them. The charge is shown with Q. The surface area of the conductor is shown with S and the distance between them shown by d. The structure of the capacitor has been given in Figure 2.4.

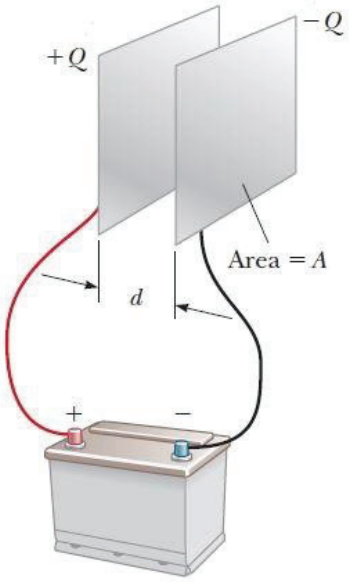

Figure 2.4. The basic demonstration of capacitor
(Source: Serway and Jewetty, 2010)

The current that comes from the source is carried by capacitive parallel plates. The SI unit of capacitance value of the capacitors is Farad (F). The fundamental relation between charge and voltage has been given in Equation 2.34.

$$Q = C\Delta V \tag{2.34}$$

The potential difference value between capacitive plates (ΔV) is directly proportional to charge value. For parallel plates, it is easy to calculate the magnitudes of voltage or charge values. If the cylindrical capacitor has been chosen, Equation 2.35 can be used.

$$C = \frac{Q}{\Delta V} = \frac{Q}{k_e Q / a} = \frac{a}{k_e} = 4\pi\varepsilon_0 a \tag{2.35}$$

The ε_0, k_e and α present the permittivity of free space, the coulomb constant and the radius of cylinder or sphere, respectively. The SI unit of permittivity of free space is the F/m. The SI unit of coulomb constant is henry (H).m^{-1} or $N.m^2.C^{-2}$.

If two parallel plates have surface area A, the surface charge density can be expressed as:

$$\sigma = \frac{Q}{A} \tag{2.36}$$

The electric field between two parallel plates can be expressed by Equation 2.37.

$$E = \frac{\sigma}{\varepsilon_0} = \frac{Q}{\varepsilon_0 A} \tag{2.37}$$

The electric field between capacitor plates is uniform and the voltage can be computed with the help of the Equation 2.38.

$$\Delta V = Ed = \frac{Qd}{\varepsilon_0 A} \tag{2.38}$$

If the electric field formula is substituted in Equation 2.38, the capacitance value can be determined by Equation 2.39.

$$C = \frac{Q}{\Delta V} = \frac{Q}{Qd / \varepsilon_0 A} = \frac{\varepsilon_0 A}{d} \tag{2.39}$$

The permittivity of free space value is constant in Equation 2.39. The capacitance value is directly proportional to the surface area A and inversely proportional to the distance between two parallel plates. Parallel capacitors have two types of combination in the circuit which are series and parallel, respectively. The circuit design of the series capacitor has been shown in Figure 2.5.

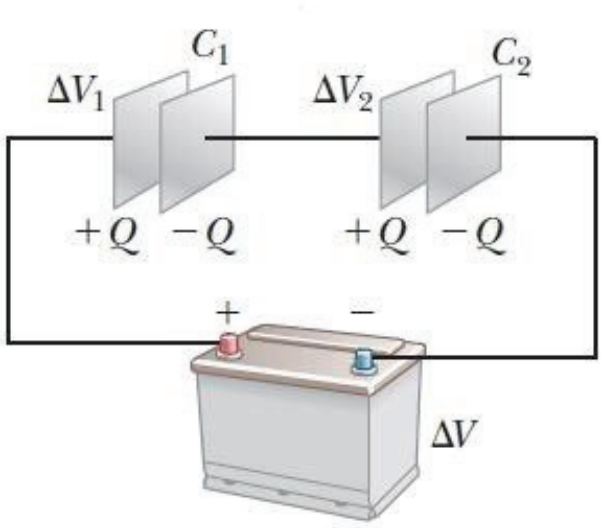

Figure 2.5. The series combination of parallel plates
(Source: Serway and Jewetty, 2010)

C_1 and C_2 capacitors were connected to the circuit serially with potential differences which are ΔV_1 and ΔV_2 respectively. For serial connection, Equation 2.40 and Equation 2.41 are used.

$$\frac{1}{C_{eq}} = \frac{1}{C_1} + \frac{1}{C_2} \tag{2.40}$$

$$\Delta V_{tot} = \Delta V_1 + \Delta V_2 \tag{2.41}$$

The equivalent capacitance value and the total voltage value can be calculated by those equations. On the other hand, the formulas are not suitable for parallel capacitive plates. They are located on a different branch in the circuit. However, branches have the same voltage values. Equivalent capacitance value can be calculated with the addition process. The equivalent capacitance value can be evaluated with Equation 2.42 (Serway and Jewetty, 2010).

$$C_{eq} = C_1 + C_2 \tag{2.42}$$

The total charge is calculated by Equation 2.43.

$$Q_{tot} = Q_1 + Q_2 \tag{2.43}$$

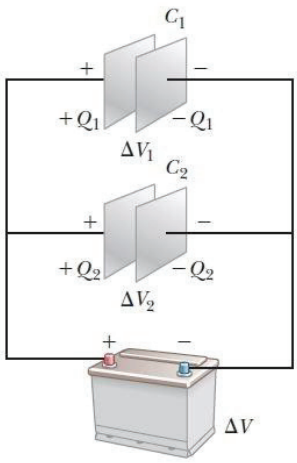

Figure 2.6. The parallel combination of parallel plates
(Source: Serway and Jewetty, 2010)

According to Equation 2.42 and 2.43, the general formula is reconditioned by Equation 2.44.

$$Q_{total} = C_{eq}\Delta V \tag{2.44}$$

2.2. Class-E Circuit Topology

Class-E tuned power amplifier (PA) allows exceedingly high efficiency in dc to ac conversion at high frequencies, as the loss of switching is reduced substantially. The fundamental consideration behind the techniques of the switch-mode power amplifier is to run transistor at its saturation level. Therefore, current and voltage can be controlled with respect to switch states which are "ON" and "OFF", respectively. The transistor influences on a large scale while the driver is used. However, there are parasitic losses due to capacitors and inductors. In the class-E circuit, they are ignored when the circuit is analysed. There are many power amplifiers A, B, AB, D, E etc. They have many advantages and disadvantages. When the power amplifier circuit is designed, these conditions have to be considered. For example, the class-D amplifiers have been widely used in audios. However, the efficiency of the Class D power amplifier reduces at high frequencies due to parasitic reactance. The class-F power amplifier has harmonic components that decrease efficiency. The class-E circuit has been discovered by Sokal (Sokal & Sokal, 1975). The efficiency of the class-E circuit is %100 theoretically. The function of the linear shunt capacitor and MOSFET practical use absolutely differs from the theory. In order to understand the circuit logic, the circuit topology should be investigated.

2.2.1. The Analysis of Class – E circuit

The class- E circuit primarily composes of choke coil, shunt capacitor, MOSFET and R_{load}. Generally, the PWM pulse is connected to the gate of MOSFET with %50 duty cycle. Actually, the gate pin of the MOSFET behaves like a small capacitor. However, it reduces efficiency while the MOSFET is driven at high frequencies. Therefore, a MOSFET driver should be implemented to pomp charge.

To increase efficiency, zero voltage switching (ZVS) method should be applied. While the MOSET is driven, two cases are considered which are “ON” and “OFF” states. While the MOSFET state is changed, there is energy loss due to heating on the MOSFET. ZVS makes the minimum this energy loss on the MOSFET. The working frequency has to be the resonant frequencies for obtaining ZVS condition. The general configuration of the class-E power amplifier (PA) circuit is given in Figure 2.7.

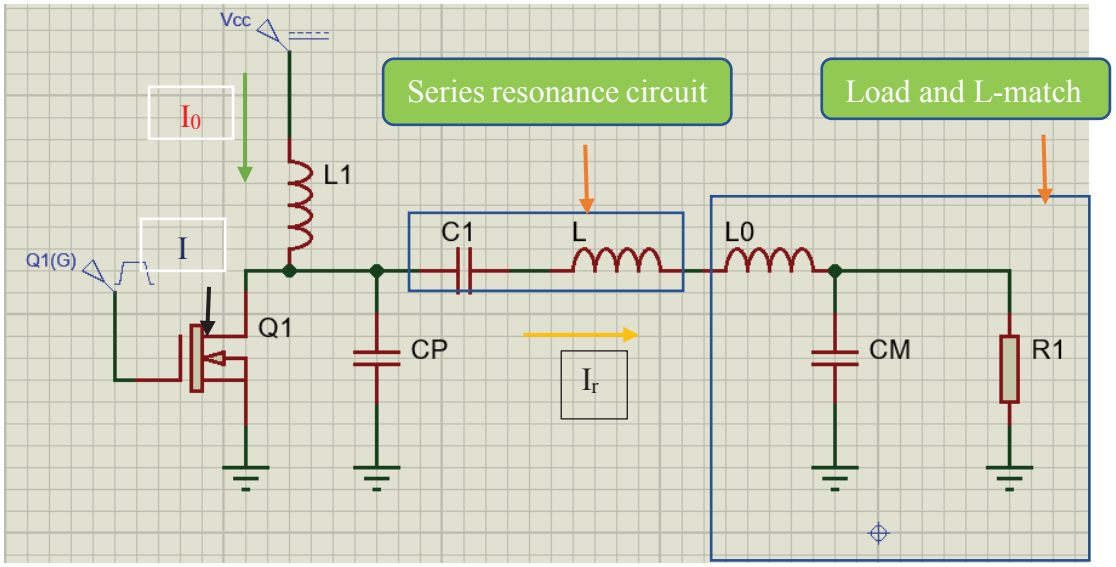

Figure 2.7. The class-E power amplifier circuit demonstration

Before the analysis, some assumptions have been accepted in order to simplify the calculations which are;

- ✓ The switch on the MOSFET is perfect.
- ✓ At the frequency of operation, the choke coil on DC supply operates as an optimally open circuit.
- ✓ The duty cycle of switch is 50 % (optimal value).
- ✓ Harmonic signals have been neglected.
- ✓ The class-E circuit is supplied while the “OFF” state of the switch at $\omega t = 2\pi n$

$$V(\omega t)|_{\omega t=2\pi n} = 0 \tag{2.44}$$

$$\frac{d}{d(\omega t)} V(\omega t)|_{\omega t=2\pi n} = 0 \tag{2.45}$$

According to Figure 2.7, the variables have given on Table 2.1.

Table 2.1. The description of the electronic component on the class-E circuit

Description of Variable	Symbol of variable	Definition
DC supply voltage	V_{cc}	
DC supply current	I_0	
Current on the load	$I_r(\omega t)$	Sine wave
Current on the shunt capacitor	$I_c(\omega t)$	Active at "ON" state
Switch current	$I(\omega t)$	Active at "ON" state
Shunt capacitor	C_P	
Series capacitor	C_L	
Series inductor	L	$L = L_{res} + L_{ext}$
Series resonance inductor	L_{res}	
Series loading inductor	L_{ext}	Extra inductance
L-match inductor	L_0	Load impedance
L-match capacitor value	C_m	
Optimal load resistor	R_l	Generally 50 Ω
Load resistor	R	Before L match

The potential difference over the switch is defined as $V(\omega t)$ with the $I(\omega t)$ current at any moment in normalised time ωt. Instantly after the switch is closed, the current on the capacitor has to be zero with respect to Equation 2.45.

$$I_c(\omega t) = \omega C \frac{d}{d(\omega t)} V(\omega t) = 0 \tag{2.46}$$

Equation 2.46 shows the initial conditions for the MOSFET switch between $2\pi n$ and $(2n+1)\pi$. Therefore Equation 2.47 can be generated.

$$I = I_0 + I_r \tag{2.47}$$

At the "ON" state, current on the load can be written as;

$$I_r(\omega t) = I_{ro} \sin(\omega t + \phi) \tag{2.48}$$

$$I_0 = -I_{ro} \sin(\phi) \tag{2.49}$$

While $\omega t = 2\pi n$ the phase angle (ϕ) cannot be determined yet. This enables to write the current on the switch during "ON" state ($(2n+1)\pi < \omega t$ ($(2n+2)\pi$)).

$$I(\omega t) = I_0 + I_{r0} \sin(\omega t + \phi) \tag{2.50}$$

If Equation 2.50 is substituted in Equation 2.47, Equation 2.51 is obtained.

$$I(\omega t) = I_{r0}(\sin(\omega t + \phi) - \sin\phi) \tag{2.51}$$

The potential difference on the shunt capacitor can be determined by Equation 2.52.

$$V(\omega t) = -\frac{1}{\omega C} \int_{\pi}^{\omega t} I(\omega t) d(\omega t) = -\frac{I_{r0}}{\omega C} (\cos(\omega t + \phi) + \cos\phi + (\omega t - \pi)\sin\phi) \tag{2.52}$$

Class-E initial conditions are V (0) =0 at $\omega t = 2\pi n$.

$$2\cos\phi - \pi\sin\phi = 0 \tag{2.53}$$

Equation 2.53 can be written as 2.54.

$$\tan(\phi) = \frac{2}{\pi} \tag{2.54}$$

These equations are needed for the calculating phase shift angle. The voltage waveform is belated by the current when ϕ angle equals to the -32.48˚. Equation 2.55 and 2.56 are very beneficial to define the phase angle in the type of sine and cosine.

$$\sin\phi = \frac{2}{\sqrt{\pi^2 + 4}} \tag{2.55}$$

$$\cos\phi = \frac{\pi}{\sqrt{\pi^2 + 4}} \tag{2.56}$$

These equations are taken from the trigonometric calculations. If these equations are substituted in Equation 2.52, Equation 2.57 is acquired.

$$V(\omega t) = \frac{I_{r0}}{\omega C}(\pi\cos(\omega t) + 2\sin(\omega t) + \pi - 2(\omega t - \pi))\frac{1}{\sqrt{\pi^2 + 4}} \tag{2.57}$$

If these trigonometric equalities are used in Equation 2.49, Equation 2.58 is obtained.

$$I_0 = \frac{2I_{ro}}{\sqrt{\pi^2 + 4}} \tag{2.58}$$

The final function form of voltage across the MOSFET can be calculated by Equation 2.59.

$$V(\omega t) = \frac{I_0}{\omega C}(\omega t - \frac{3\pi}{2} - \frac{\pi}{2}\cos\omega t - \sin\omega t) \tag{2.60}$$

The choke coil is assumed as an ideal (without no resistance). The supply voltage (V_{cc}) should be equal to the average voltage across the switch/shunt capacitor when ω is between or equal to the π and 2π .

$$V_{cc} = \frac{1}{2\pi}\int_{\pi}^{2\pi} V(\omega t)d(\omega t) = \frac{I_0}{\pi\omega C} \tag{2.61}$$

According to the assumptions, there are no switching losses. Therefore the power across the load resistor has to be equal to the power of DC source (Conservation of energy).

$$I_0 V_{cc} = \frac{1}{2} {I_{r0}}^2 R \tag{2.62}$$

If Equation 2.58 is substituted into Equation 2.62, the new equality is obtained.

$$\frac{2I_{r0}}{\sqrt{\pi^2+4}} V_{cc} = \frac{1}{2} {I_{r0}}^2 R \tag{2.63}$$

If Equation 2.63 is rearranged, the obtained equation as follows;

$$\frac{4}{\sqrt{\pi^2+4}} V_{cc} = I_{r0} R = V_{r0} \tag{2.64}$$

While the I_0 is substituted into Equation 2.64, Equation 2.65 is obtained.

$$I_{r0} = \frac{V_{r0}}{R}\sin\phi = \frac{8V_{cc}}{(\pi^2+4)\mathrm{R}} \tag{2.65}$$

If Equation 2.65 is rearranged, the delivered power can be calculated by Equation 2.66.

$$P_{load} = \frac{8{V_{cc}}^2}{(\pi^2+4)\mathrm{R}} \tag{2.66}$$

Depending on the evaluations up till now, the delivered power across the load was specified. The I_0 value also can be calculated by Equation 2.66.

However, the shunt capacitor C_P contains a parasitic drain. Therefore, it has to be taken into consideration that the choice of switching transistor is acted by the parasitic drain. In the process of design involves finding a good combination of Vcc, R and C to make an efficient amplifier. Predominantly, load resistance R should not be chosen too high otherwise, the series coils have to be high.

At this moment, addition inductor is needed. The current flows through the load has been expressed. The load and L_{ext} are attached on the same branch. Hence, the voltage of the extra inductance can be calculated by derived Equation 2.67.

$$V_R = \frac{1}{\pi}\int_{\pi}^{2\pi} V(\omega t)\sin(\omega t+\phi)\,d(\omega t) \tag{2.67}$$

$$V_{Lext} = \frac{1}{\pi}\int_{\pi}^{2\pi} V(\omega t)\cos(\omega t+\phi)\,d(\omega t) \tag{2.68}$$

If Kirchhoff's law is applied to Equation 2.65 with the -32.43˚ phase angle, Equation 2.69 and 2.70 are obtained.

$$\frac{V_{Lext}}{V_R} = \frac{\omega L_{ext}}{R} = \frac{\pi + 2\sin 2\phi - (\pi/2)\cos 2\phi}{(\pi/2)\sin 2\phi + 2\cos 2\phi} \tag{2.69}$$

$$\frac{\omega L_{ext}}{R} = 1.153 \tag{2.70}$$

The next process is the constituting of equations for the series resonant part of class-E circuit. The frequency of the circuit and the load résistance of R have been designated. However, the quality factor Q has to be specified to go further in the design. From the analysis of series RLC resonant circuit, Equation 2.71 and 2.72 have been obtained.

$$C_l = \frac{1}{\omega QR} \tag{2.71}$$

$$L_{res} = \frac{QR}{\omega} \tag{2.72}$$

At the end of the calculation part, the L-match network is needed to increase the efficiency depending on circuitry. Basically, the load resistance is chosen about 50 or 75 ohms. The C_m and L_0 can be calculated with Equation 2.73 and 2.74, respectively.

$$C_m = \frac{1}{\omega R_l}\sqrt{\frac{R_l}{R} - 1} \tag{2.73}$$

$$L_0 = C_m R R_1 \tag{2.74}$$

The total inductance value can be evaluated as;

$$L_{total} = L_{ext} + L_{res} + L_0 \tag{2.75}$$

Therefore, all required component values can be specified with respect to these equations. However, in the experiments, these values are not be perfectly matched. The harmonic losses and the omics losses have been ignored before starting the calculation. The class-E circuit efficiency is 100% theoretically. In the experiment these losses are included and the efficiency value is calculated under the limit of expected. The quality values of inductor and capacitor can be calculated perfectly (Slade, 2010).

CHAPTER 3

CAPACITIVE POWER & DATA TELEMETRY

In this Chapter, capacitive data and power transfer experiments have been presented. The experiments have been divided into 2 parts which are capacitive power transfer and capacitive data transfer, respectively. To design an efficient power transfer, the different types of class–E power amplifier circuits have been implemented and tested. These experiments are the resonant class-E, the series LC compensated and the parallel LC compensated experiments. The efficiency values of these circuits have been studied to design an optimal, sub-kilowatt power amplifier. Modulation topic has been investigated to provide data and power transfer at the same frequency without any loss. The modulation experiment parts consist of AM (amplitude modulation), FM (frequency modulation) and multiplexer chip. According to the experiment results, the efficient, sub-kilowatt capacitive data and power transfer circuit has been established for monitoring mechanical variables.

3.1. Wireless Data and Power Transfer Experiments

Power or data can be transferred under limited distance by the coupling capacitor wirelessly. However, the power signal is dominant that cannot lose in nature easily with the help of its high-frequency characteristic. Thereby, it is very simple to transfer power when compared with data telemetry. In this section, experiments were started from the fundamental concept of the capacitor. Theoretical approximations were specified as the starting point for transferring data and power. This part of the thesis was divided into three parts. They are power transfer, data transfer, power and data transfer. The basic design was created for transferring power without wire. For understanding the concept behind the capacitive power transfer and data transfer, the structure of the basic capacitor should be investigated according to circuit theory knowledge. Fundamental analysis was carried out with using basic equations in Chapter 3.

3.1.1. Wireless Energy transfer with Coupling Capacitors

In the experiment, the two-rail system was performed to provide power transfer wirelessly. This system consists of two rails. The performed two rails are in the form of ”I” profile. One of the two rails was connected to one branch of AC generator and the other branch was fixed to the other rail. A rectangular, electrically, non-conductive, dielectric material having a wall thickness of mm scale was fixed under each rail. Therefore two capacitors were created. Alternating current flows between two plates. The schematic demonstration of the coupling capacitor in the rail system was given in Figure 3.1.

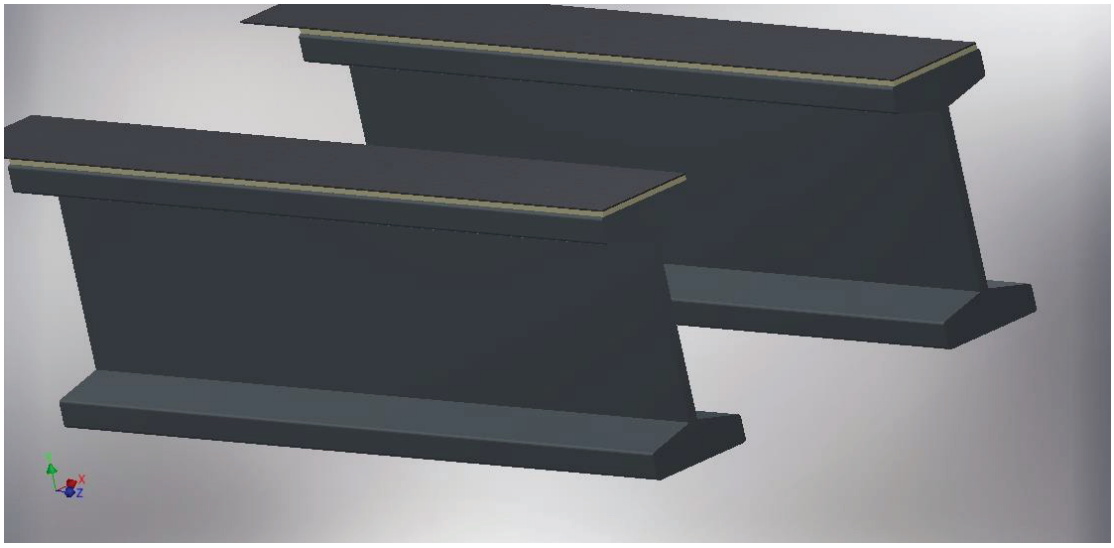

Figure 3.1. 3D demonstration of the coupling capacitor in the rail system

In this system, AC was used due to provide current flow between capacitive plates. The coupling capacitors block the direct current. Therefore, energy cannot be transferred through coupling capacitor.

AC fluctuates in between its peak-to-peak value. Herewith, the potential difference occurs and the circuit is energized by coupling capacitors. This study was realized with iron “I” profile capacitive plates which have been demonstrated in Figure 3.2.

Figure 3.2. Coupling capacitors in the rail system

In this study, carton sealing tape was operated as a dielectric material. Therefore, the short circuit probability has been annihilated and capacitor system was established. The system was supplied under 20 V alternating current which is equal to 7.25 True RMS value.

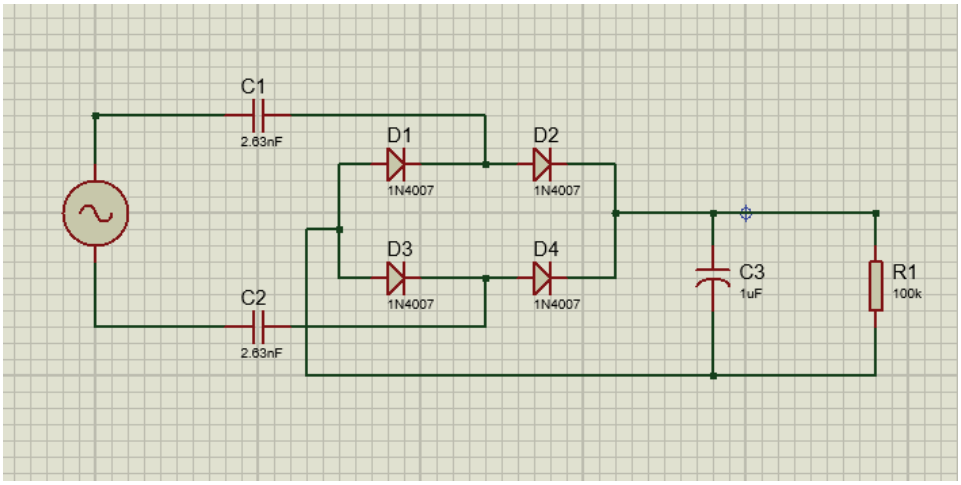

Figure 3.3. Capacitive power transmission on iron I profile

Capacitance values were measured 8 times and the average was taken into consideration which was specified as 2.63 nF. The rectifier circuit was used in the secondary side with a load resistor which is about 100Ω.

20-volt pick-to-pick AC was rectified at the secondary side of the circuit. Potential differences on load were measured. The experimental design of the circuit has been given in Figure 3.3.

At the beginning of the test, 100 Ω resistor was operated at the 50 Hz frequency level with 1uF polarized capacitor. By means of the polarized capacitor, the rectified alternating current will be direct current. The obtained results were given on Table 3.1.

Table 3.1. Capacitive rail experiment results

Exp	f(Hz)	V_{supply} (V)	I_{supply} (A)	V_{load} (V)	I_{load} (A)	R1 (Ω)	C3 (uF)	Efficiency
1	50	20	0.000002	5.6	0.000002	100	1	20 %
2	500	20	0.000017	8.27	0.00001	100	1	14.1 %
3	500	20	0.000017	8.15	0.00001	100	43	14.4 %
4	5000	20	0.0004	8.74	0.0001	100	1	64.6 %

As can be seen from Table 3.1, the efficiency changed according to fluctuation in the frequency. The farad value of polarized capacitor does not have considerable significance on efficiency. The farad value of C3 capacitor generally, influence on voltage ripple which can be seen in rectified signals. The capacitor is operated as charge store member in the circuit. By this means, it is able to fill in the gap between signal characteristic in order to achieve pure direct current. The most effective parameter of the circuit is the frequency.

At the resonance frequency, the total impedance of the circuit strikes out for zero. Thereby, the whole resistance of the circuit is equal to the resistance of the resistor. For this “I” profile iron coupling capacitor, the resonance frequency approximately 5 kHz. The maximum efficiency is succeeded at the resonance frequency of the system which about 64.6 %.

3.1.2. Data Transfer via Capacitive Plates

After succeeded capacitive wireless power transfer, the wireless data transfer was selected as the second step of this thesis.

In this level, the most significant duty was specified as sending data without any loss. In order to see how capacitive plates successful to send data wirelessly, the infrared test set up was operated.

In this experiment two microcontroller, infrared data transfer sensor pair, and capacitive coupling plates were used. Arduino Uno was preferred as microcontroller and the data was specified as "Galip_Karabulut Follows Tesla ". Serial port screen was used for communication. The experimental set setup has been demonstrated in Figure 3.4.

In this study, the basic infrared circuit was created. Data is coded by an integrated infrared couple. The electronic component sends data at 38 kHz. The capacitive coupling plates take an active role in the data-carrying system.

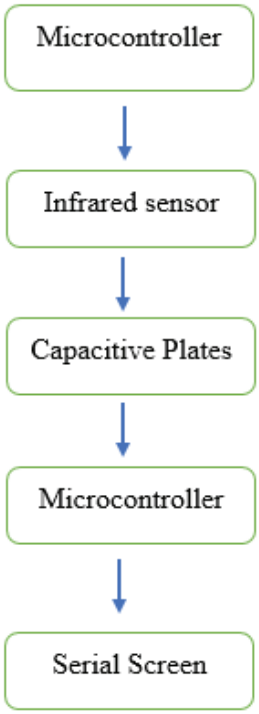

Figure 3.4. Wireless data transfer circuit description blog diagram model

The data transmission system could be successful using a cable connection instead of capacitive coupling plates as well. Nevertheless, this system was configured to investigate data carriage potential of capacitive plates.

Arduino Uno was performed as a microcontroller. Because Arduino Uno has many options to choose about integrated sensor technology.

3.2. Modulation Experiments

The waves can be collected under two headings. Electromagnetic waves and mechanical waves. The data to be transmitted are" low Frequency" (Mechanical Waves) signals in modulation. It is impossible for these signals to complete their journey mentioned above by themselves. High Frequency (Electromagnetic Waves) signals are used for this purpose. Low-Frequency signals (which we want to transmit) cannot reach too long distances due to their low energy.

Low frequency in the electromagnetic spectrum, in other words, large wavelength signals are not passed to the upper layers by the atmosphere, instead, they continue their journey between earth and atmosphere. Modulated Signal is able to carry the data signal over long distances by overlapping a high frequency. This operation is called Modulation. High-Frequency Radio Signals provide ideal transmission paths for Satellite Communication Systems by eliminating all the disadvantages of Low-Frequency Radio Signals. In the literature, there are 3 types of widespread modulation processes which are respectively amplitude modulation, frequency modulation and phase modulation etc. In order to send data and power at the same time with wireless, the modulations techniques are widely used.

3.2.1. Amplitude Modulation

In this type of modulation, only the amplitude of the carrier signal is changed depending on the frequency and amplitude of the information signal. The information in the form of low-frequency sound or music, which is intended to be sent over long distances, is first converted to electrical energy.

Then the carrier is superimposed on the signal and transmitted to the distances as electromagnetic waves. There are two important signals for modulation. These are the information signal and the carrier signal.

Of these, the signal sent to be long-distance with low frequency is the data signal. High frequency is the carrier signal which acts as a transport. First experiment was realized with the function generator in order to observe the pure modulated signal.

Therefore, the sine signal was used as a data signal and the PWM signal was selected as a carrier signal. Low-frequency data signal can be carried by a high-frequency carrier signal. General useful formula for sine – sine amplitude modulation formula is given in Equation 3.1.

$$[1+\sin(2\pi F_m \, x)]*\sin(2\pi F_c \, x) \tag{3.1}$$

Where, F_m, F_c and x are modulator signal frequency, carrier signal frequency and time respectively. In MATLAB software, 10 Hz data signal was tried to carry with 100 Hz carrier signal (Vidkjær, 2012).

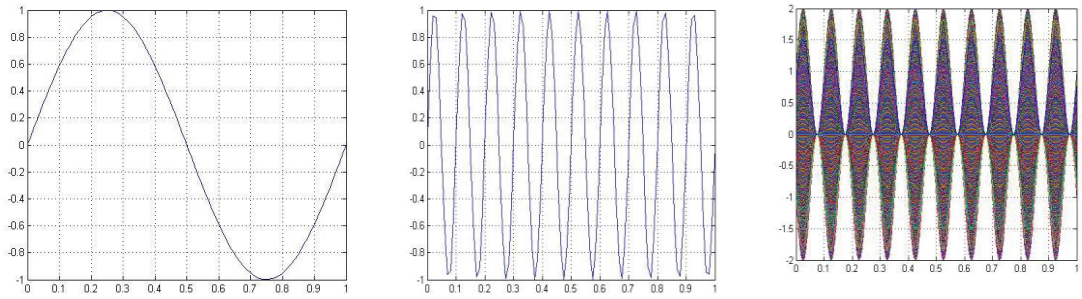

(a) (b) (c)

Figure 3.5. AM modulation steps, data signal (a), carrier signal (b) modulated signal (c)

The simulation was implemented by MATLAB software to achieve Figure 3.5. Previous equation is divided into two parts, the first part belongs to the calculation of data signal and the second component of the equation belong to carrier signal calculation (after the multiplication). Modulated signal was constructed result of this equation. In this experiment, the Amplitude modulation is provided by a transistor BC547 NPN. In the first experiment, the data signals were given in pulse-width-modulation type (PWM) and the carrier signal form was given in sine.

Data signal was connected to the base of NPN transistor. The carrier signal input was attached to the collector of the transistor. The oscillator probe was connected to the emitter of BC547.

However, the absence of the message signal, the transistor cannot be activated. According to the working principle of the transistor, without any trigger power through the base of the transistor, the sensible result could not be achieved at the emitter of the transistor. The circuit was constructed by Proteus computer program and observed results are given below.

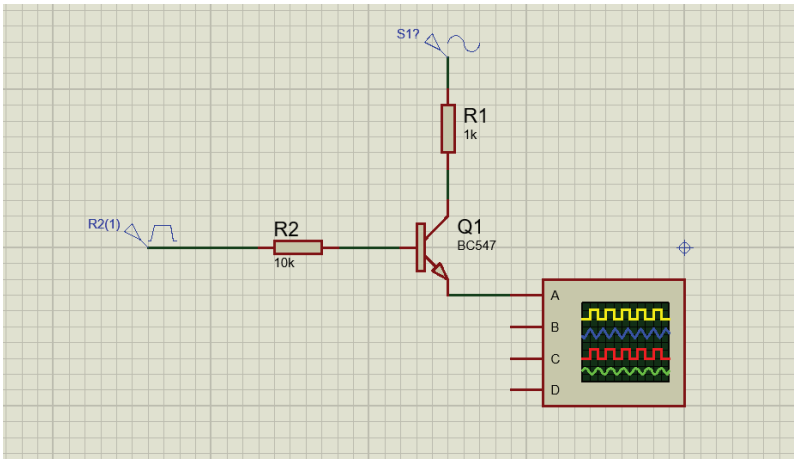

Figure 3.6. Amplitude modulation experiment in Proteus software

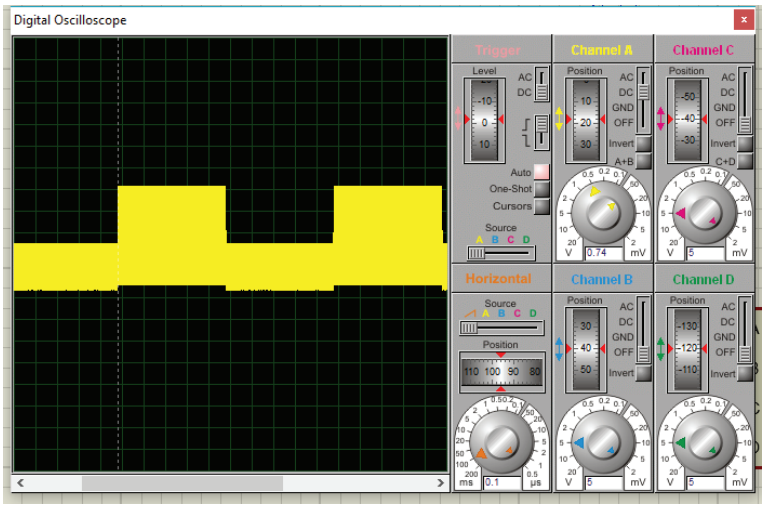

Figure 3.7. Observed result according to constructed circuit

3.2.2. Frequency Modulation

Frequency modulation is one of the most used modulation types especially in the field of communication and signal processing. It is the method of encoding the

information by changing the frequency of a high-frequency wave according to the information signal to be sent. Nowadays, it can be said that radio transmitters work mainly with this method.

To provide the frequency modulation (FM), CD4046 chip was operated. Simulation was carried out by Proteus. The circuit was given in Figure 3.8.

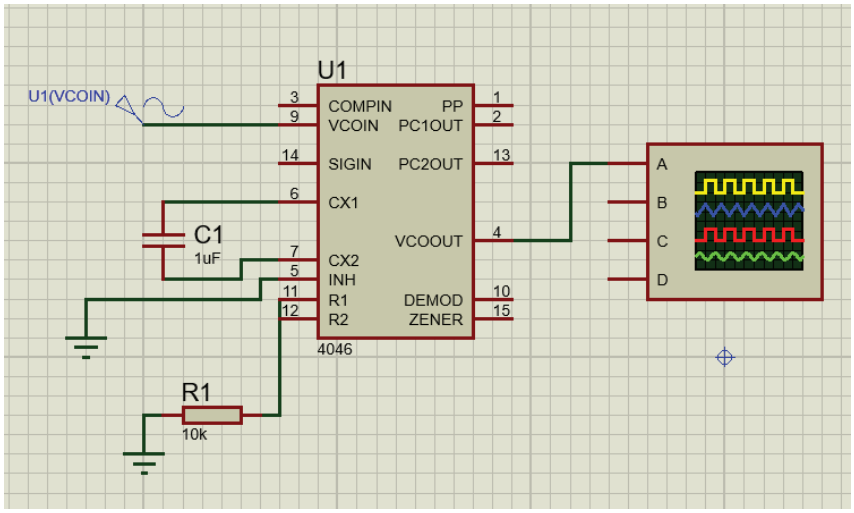

Figure 3.8. Frequency modulator circuit

In the simulation, the PWM signal was tried to modulate with carrier sine signal. Carrier sine signal has 50 Hz frequency and 3 V peak-to-peak value.

However, the voltage supply of the CD4046 chip was characterized automatically. Acquired result was demonstrated in Figure 3.9.

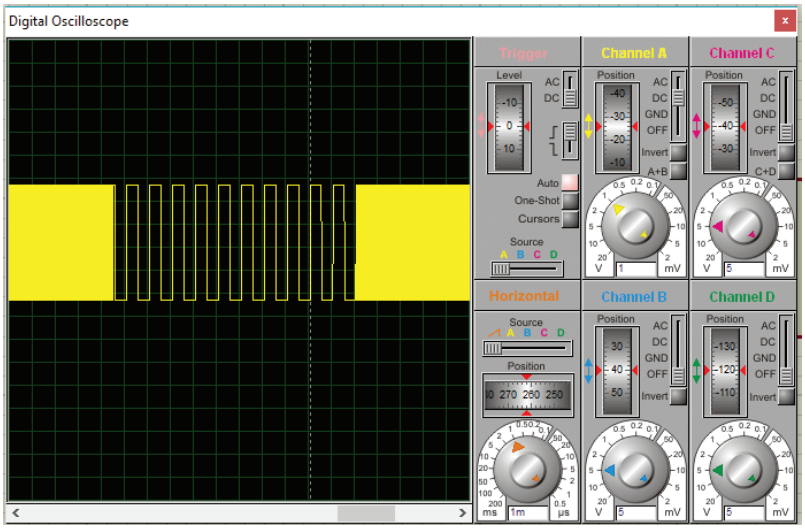

Figure 3.9. The observed result from the circuit

3.2.3. Modulation with Multiplexer Chip

Most common basic an analogue multiplier has three terminals. Analog multiplier operates mathematical operations like multiplication and division, by appropriate terminal connections. In this thesis, AD633JN analogue multiplier was performed to observe the multiplied signal. Division and square-rooting operations can be implemented by replacing the path of an operational amplifier multiplier in the feedback. The characteristic structure of AD633JN microchip given below.

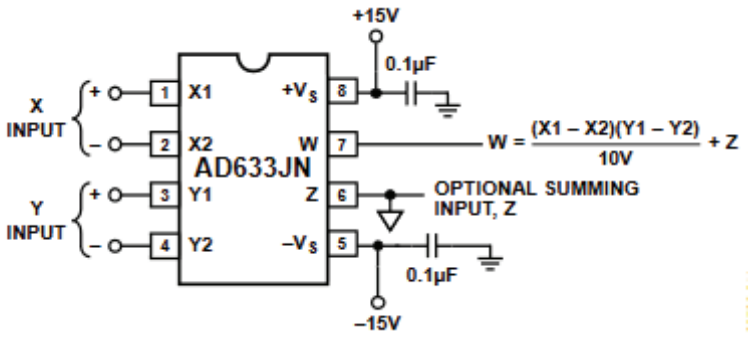

Figure 3.10. Simple multiplexer circuit of AD633JN microchip (Anonymous, 2015)

According to Figure 3.10, required connections were done to provide modulation with multiplexer method.

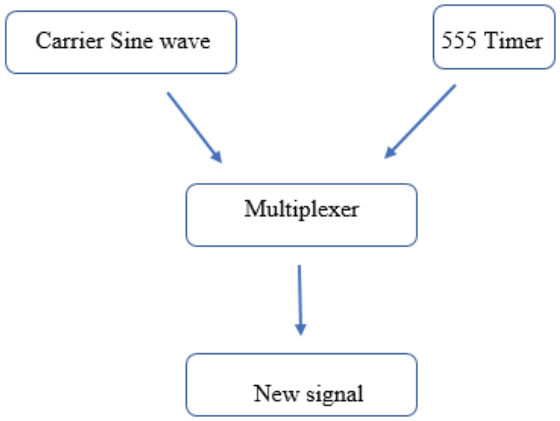

Figure 3.11. 555 pulse generator circuit and multiplexer circuit blog diagrams

Output signal was recorded from optimal summing terminal of the chip. This technique is very useful when the message signal and carrier signals have a different frequency. To test the multiplexer modulation, the message signal was connected to the terminal 1 and 2 which called “X input”. Carrier signal was attached “Y input”. Multiplexer chip was supplied 15 V from dc supply. The modulated signal was observed from terminal 6. Message signal was selected as the PWM signal. PWM signal was created from the 555 timer circuit. Sine signal was selected to carry PWM message signal. The circuit was demonstrated in Figure 3.11. To supply +15 volt and -15 volt, the extra circuit was designed with resistors and capacitors which has been shown in Figure 3.12.

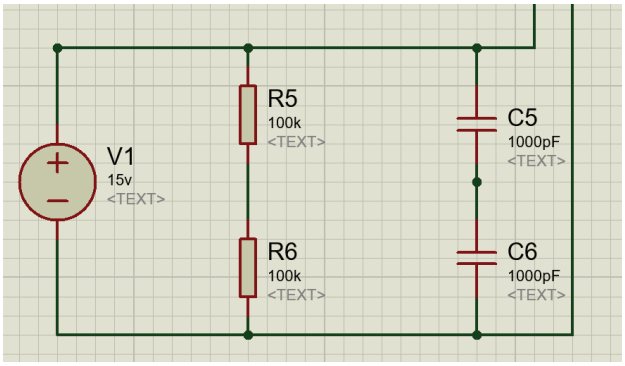

Figure 3.12. Negative voltage generator circuit

Negative voltage was needed due to obtain, the precision of the message signal. Otherwise, the oscilloscope cannot detect negative value of sensor information. It means that the carried message signal will not include certain data. In order to preserve data from that type of issue, demonstrated circuit was constituted.

The -15V was supplied from point 2. Point 1 was chosen as a ground of circuit. While ground of PWM generated circuit connects to the ground of multiplexer, this statement was considered. Therefore, +15 volt was received from point 3. 5V peak-to-peak carrier sine signal was connected to Y terminal of multiplexer with 5 kHz frequency.

The 555 timer circuit was supplied from dc source to generate message signal which is pulse-width modulation (PWM). 5V DC voltage and 0.02 A current was used. Multiplexer chip utilized from 15 V dc voltage as supply voltage. Oscilloscope probe was connected to the terminal 6 of AD633JN multiplexer for observing the output signal. The circuits were soldered on the circuit board professionally because of observed results was successful. The soldered circuits were shown in Figure 3.14.

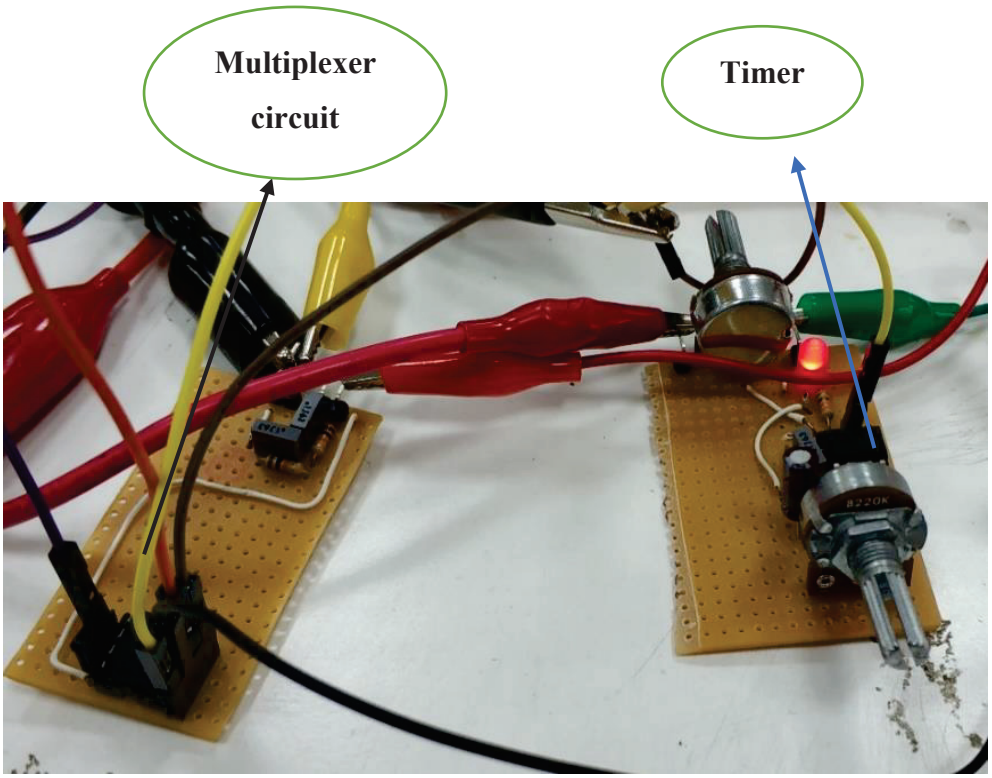

Figure 3.13. The Circuits printed on perforated stripboard

3.3. Basic Class-E Power Amplifier Experiment

In this experiment, the efficiency of pure Class-E power amplifier has been studied. Class-E circuit has been designed for antennas. Therefore a smaller sine wave is presented to the antenna load. This design also requires careful selection of the typical shunt-resonant circuit to reduce the high harmonic levels. Voltage and current phase adjustments are used to maximize efficiency. L and C are series-resonant part uses to block unwanted harmonics from reaching the load. L and C are modelled as an ideal component in this thesis. However, there are parasitic losses due to capacitors and inductors. Also, the choke inductance filter the harmonics signals. The choke is selected as being sufficiently high so that the ac component is much lower than the DC component of the input current.

The quality factor Q of the LC series resonant circuit is selected sufficiently high such that the current passing through the resonant circuit is sinusoidal. 12-volt direct current was connected to the choke inductor. The operating duty cycle of the MOSFET is specified as 50 %. The pick-to-pick voltage of this signal is 6V.

In order to drive the MOSFET, the MOSFET driver was implemented. The MOSFET driver was supplied with 8V direct current. Diodes were used to form a full-wave rectifier. According to derivated formulas on class-E power amplifier theory, a circuit layout was designed. The consumed power from the DC source has been calculated by Equation 3.1.

$$P_d = 12V \times 0.4A = 4.8W \tag{3.1}$$

The R_{load} is computed by Equation 3.2.

$$R_1 = \frac{8 \times {V_{cc}}^2}{(\pi^2 + 4) \times \mathrm{P}_d} = \frac{8 \times (12v)^2}{(\pi^2 + 4) \times 4.8W} = 17.30\Omega \tag{3.2}$$

The resonance frequency of the class-E power amplifier is selected as 5 MHz.

$$f_{resonance} = \frac{1}{2\pi\sqrt{LC}} = 5 \times 10^6 Hz = \frac{1}{2\pi\sqrt{0.17 \times 10^{-9} F \times 5.9 \times 10^{-6} H}} \tag{3.3}$$

The series inductor value of the circuit has been specified with help of the Equation 3.4. Quality factor of the inductance is taken 10, which is customary in the literature.

$$L_2 = \frac{QR_1}{\omega} = \frac{17.30 \times 10}{2\pi f_{resonance}} = 5.506\mu H \tag{3.4}$$

The shunt capacitance value is evaluated as 0.844 nF.

$$C_1 = \frac{I_{dc}}{\omega\pi P_d} = \frac{0.4A}{(2\pi f_{resonance})\pi \times (12\,\mathrm{v} \times 0.4A)} = 0.844nF \tag{3.5}$$

According to Equation 3.6, L_{min} minimum choke inductance was specified about 24 μH.

$$L_{1,\min} = 2 \times (\frac{\pi^2}{4} + 1) \times \frac{R}{f_{resonance}} = 24\mu H \tag{3.6}$$

The calculated and theoretical values have been tabulated.

Table 3.2. The theoretical and operated values of circuit elements

Circuit members	Theoretical Value	Operated value
L_1 (μH)	24	100
L(μH)	5.506	13.6
C_P (nF)	0.844	0.362
R_1 (ohm)	17.30	21.9
$f_{resonance}$ (MHz)	5	1.7

According to Table 3.2, there are differences between calculated values and experimental values of circuit members. There were no suitable appropriate capacitors and inductors. Thus, the closer circuit members were operated instead of original acquired results. 12 DC voltage was applied to the choke inductance. MOSFET driver was supplied with 8v dc voltage. 6V peak-to-peak PWM signal was connected to the gate of MOSFET in order to use the soft switch model. Diodes were operated to converting ac to dc, this diodes construction also called full-wave rectifier. The basic class-E power amplifier has been shown below.

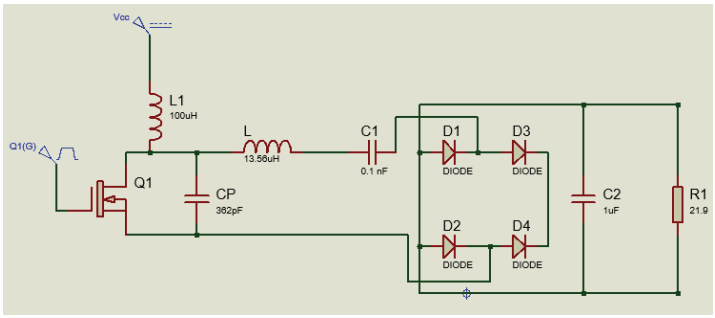

(a)

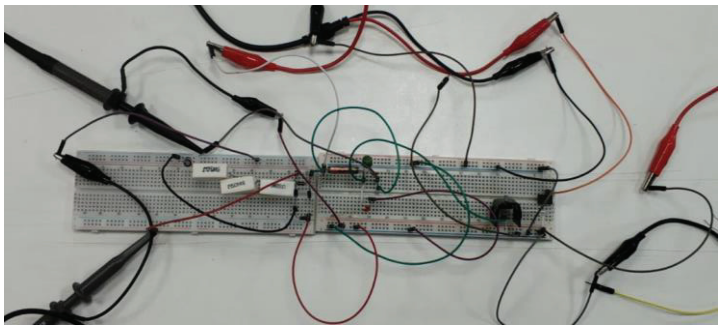

(b)

Figure 3.14. Class-E circuit demonstration (a) Experimental setup of class-E circuit (b)

Two breadboards were used. One of them is responsible for Class-E circuit with a MOSFET driver, other is responsible for the rectifier circuit. The class-E power amplifier circuit parameters have been tabulated.

Table 3.3. The Class-E circuit parameters

V_{in} (V)	V_{supply} (V)	I_{in} (A)	I_{supply} (A)	V_{pwm} (V_{pp})	f_{pwm} (MHz)	Crest factor
12	8	0.44	0.02	6	1.7	1.23

V_{in}, V_{supply}, I_{in}, I_{supply}, V_{pwm} (V_{pp}), f_{pwm} (MHz) show input voltage through the choke inductor, supply voltage for the MOSFET driver, current input on choke inductor, supply current for MOSFET driver, peak-to-peak voltage of PWM pulse and frequency of the circuit, respectively. The gate of a MOSFET behaves like a small capacitor. At the high frequencies, the capacitor cannot be charged sufficiently, in this case, MOSFET cannot be triggered.

The MOSFET drivers worked as a charge pump to provide the current to the capacitor. Therefore, MOSFET has been become appropriate to operate under high frequency. This scheme turns an inefficient MOSFET into a capable high-frequency switching device. The throughput of class-E signal characteristic is given in 3.17. The MOSFET gate signal form is presented in Figure 3.18.

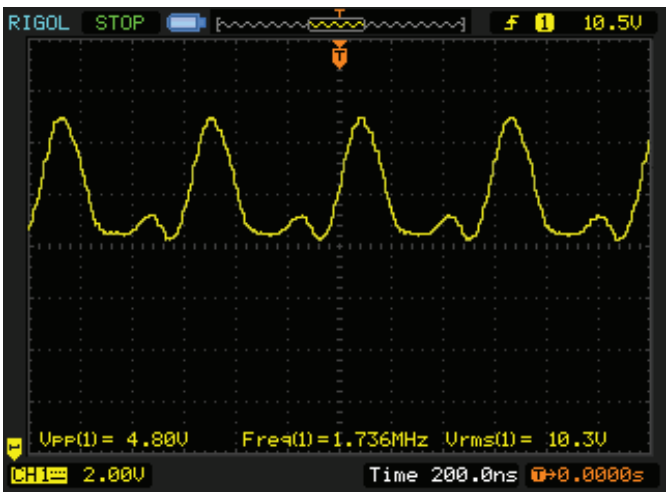

Figure 3.15. The output signal characteristic of the class-E circuit

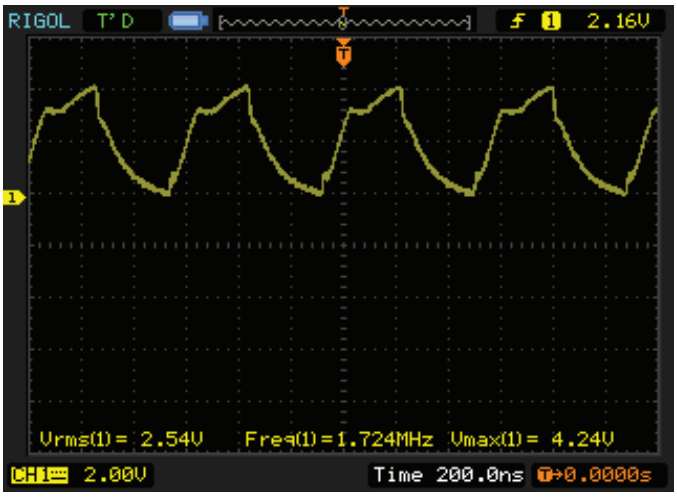

Figure 3.16. Gate-source voltage form of the class-E circuit

According to the obtained signals characteristics from Figure 3.16 and 3.17, the efficiency calculation can be applied as the following Equations.

$$P_{dc,\text{in}} = 0.44A \times 12v = 5.28W \tag{3.7}$$

$$P_{driver} = 8V \times 0.02A = 0.16W \tag{3.8}$$

$$P_{driver,pulse} = V_p \times I_{driver,pulse} = 3\text{V} \times 0.01A = 0.03W \tag{3.9}$$

$$P_{total,in} = P_{dc,in} + P_{driver} + P_{driver,pulse} = 5.47W \tag{3.10}$$

$$P_{out} = \frac{(10.3V)^2}{21.9\Omega} = 4.84W \tag{3.11}$$

$$\eta = \frac{P_{out}}{P_{total,in}} \tag{3.12}$$

$$\eta = \frac{4.84W}{5.47W} = 88.48\% \tag{3.13}$$

3.4. Class-E Amplifier Experiment With Capacitive Coupling Plates

The capacitive wireless power transfer circuit was promoted with Class-E topology in order to acquire high efficiency. This circuit consists of a choke inductor, a shunt capacitance, capacitors, an inductor, a capacitive plate (made by cupper) and a resistance with high watts, diode, MOSFET driver and field-effect transistor (FET). 12 dc voltage was applied to the choke inductance. MOSFET driver was supplied with 8v dc voltage. 6V peak-to-peak PWM signal was connected to the gate of MOSFET in order to use the soft switch model. Diodes were operated to converting ac to dc, this diodes construction also called full-wave rectifier.

C_2 and C_3 are pair capacitors. Consumed power is about 4.8 W with 0.4 A current. Calculations were begun from the coupling capacitors. The capacitances of coupling capacitors are 0.17 nF at the rest position. The capacitance values of coupling capacitors have been measured by capacitance meter and is shown in Figure 3.17. According to obtained formulas from the class-E power amplifier theory, the circuit design was created.

Equations were implemented step by step to obtained high efficiency as much as possible. Characteristic of the output signal was converted to the dc voltage by full-wave Rectifier Bridge.

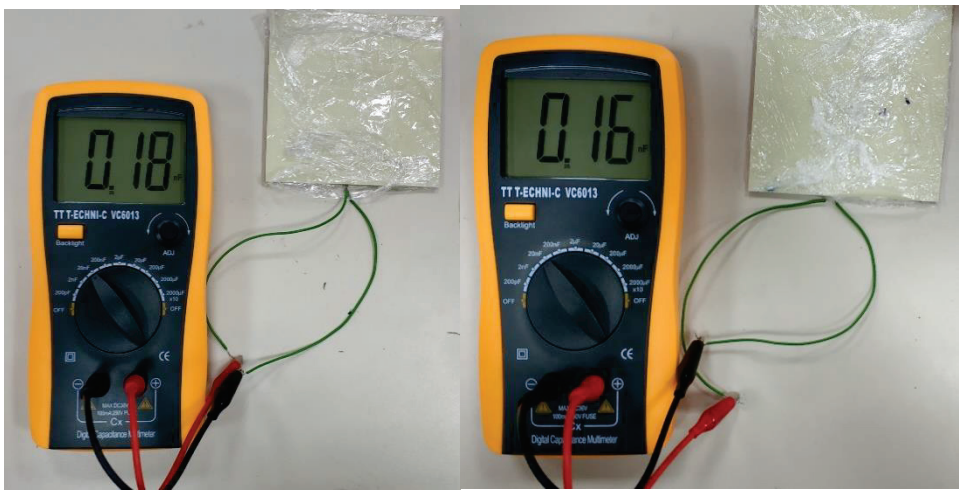

Figure 3.17. The capacitance value of coupling capacitors

$$P_d = 12V \times 0.4A = 4.8W \tag{3.14}$$

P_d is consumed power. The circuit was supplied by 12 V direct current. The optimal resistance was computed as;

$$R_1 = \frac{8 \times V_{cc}^{\ 2}}{(\pi^2 + 4) \times P_d} = \frac{8 \times (12v)^2}{(\pi^2 + 4) \times 4.8W} = 17.30\Omega \tag{3.15}$$

5 MHz was selected as an operating frequency.

$$f_{resonance} = \frac{1}{2\pi\sqrt{LC}} = 5 \times 10^6 Hz = \frac{1}{2\pi\sqrt{0.17 \times 10^{-9} F \times 5.9 \times 10^{-6} H}} \tag{3.16}$$

Therefore, the inductance value was calculated with the help of Equation 3.17. Q is a quality factor, it was selected 10 by academic background.

$$L_2 = \frac{QR_1}{\omega} = \frac{17.30 \times 10}{2\pi f_{resonance}} = 5.506\mu H \tag{3.17}$$

$$C_1 = \frac{I_{dc}}{\omega\pi P_d} = \frac{0.4A}{(2\pi f_{resonance})\pi \times (12\,\mathrm{v} \times 0.4A)} = 0.844nF \tag{3.18}$$

The shunt capacitance was computed by Equation 3.18.

$$L_{1,\min} = 2 \times (\frac{\pi^2}{4} + 1) \times \frac{R}{f_{resonance}} = 24\mu H \tag{3.19}$$

According to Equation 3.19, L_{min} minimum choke inductance was specified about 24 μH. There were no suitable appropriate capacitors and inductors. Thus, the closer circuit members were operated instead of original acquired results. The required information was tabulated on Table 3.4.

Table 3.4. The calculated values and operated values of class-E circuit members

Circuit members	Calculated Value	Operated value
L_1 (μH)	24	100
L_2(μH)	5.506	13.6
C_1 (nF)	0.844	0.362
R_1 (ohm)	17.30	21.9
$f_{resonance}$ (MHz)	5	1 - 5

The Class-E amplifier capacitive coupling circuit was demonstrated in Figure 3.16a and shamanic demonstration was given in Figure 3.16b. In this Figure, C2, C3 represents coupling capacitors that two channels were used.

Two breadboards were operated when the circuit was installed. One of them is Class-E circuit with MOSFET driver, other is responsible for rectifier circuit. Capacitive parallel plates were used as artificial capacitor in this scheme.

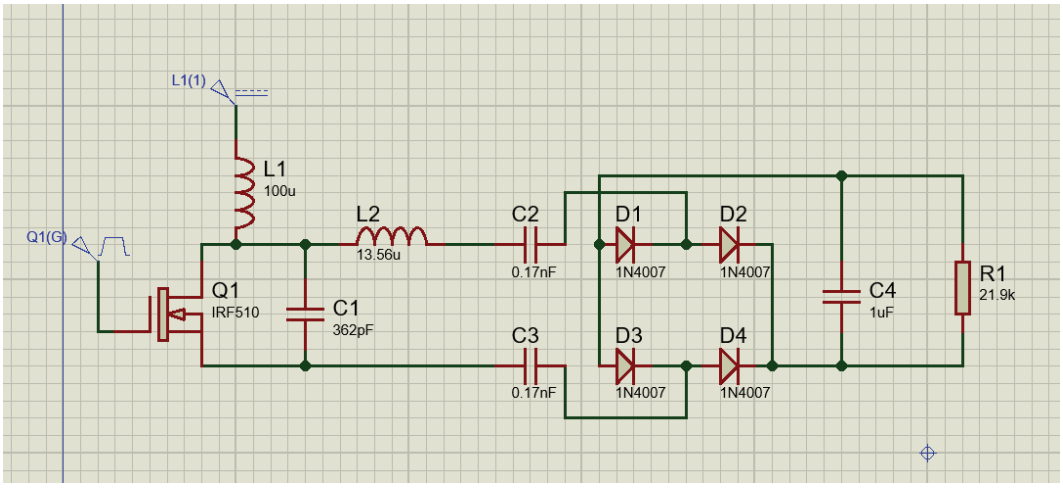

(a)

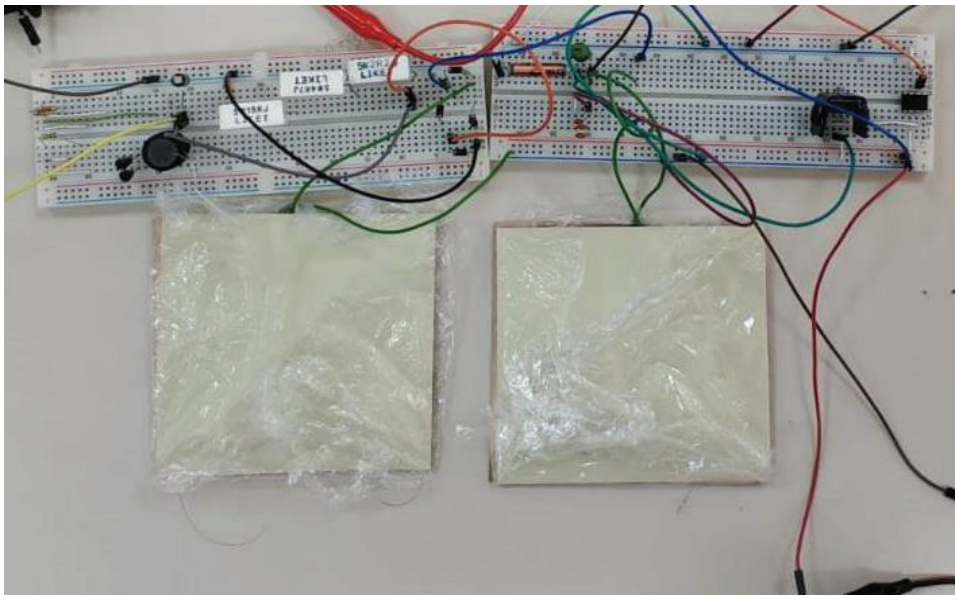

(b)

Figure 3.18. The schematic demonstration of class- E amplifier circuit (a) The demonstration of class –E circuit (b)

V_{in}, V_{supply}, I_{in}, I_{supply}, V_{pwm} (V_{pp}), f_{pwm} (MHz) represent voltage input through choke inductor, the supply voltage for MOSFET driver, current input on choke inductor, supply current for MOSFET driver, peak-to-peak voltage of PWM pulse and frequency of the circuit, respectively. The magnitudes of these parameters were given on Table 3.5.

Table 3.5. Numerical value of circuit voltage, ampere and frequency

V_{in} (V)	V_{supply} (V)	I_{in} (A)	I_{supply} (A)	V_{pwm} (V_{pp})	f_{pwm} (MHz)	Crest factor
12	8	0.4	0.02	6	1.739	1.23

The MOSFET driver was supplied with 8V and 0.02 A which are named as V_{supply} (V) and I_{supply} (A) respectively. There is a capacitor inside the gate of MOSFET which must be charged for activating the MOSFET. The circuit was supplied with 12 V dc and 0.32 A which refers to V_{in} (V) and I_{in} (A) respectively. 6 V peak-to-peak voltage with 50% duty cycle PWM signal was attached to the gate of MOSFET at 1.7 MHz frequency.

According to the results, the global efficiency was investigated. When the efficiency was calculated, the input current of MOSFET driver and throughput current of signal generator taken about 0.02 A and 0.01 A respectively. The throughput of class-E signal characteristic is given in 3.19. The MOSFET gate signal form is presented in Figure 3.20.

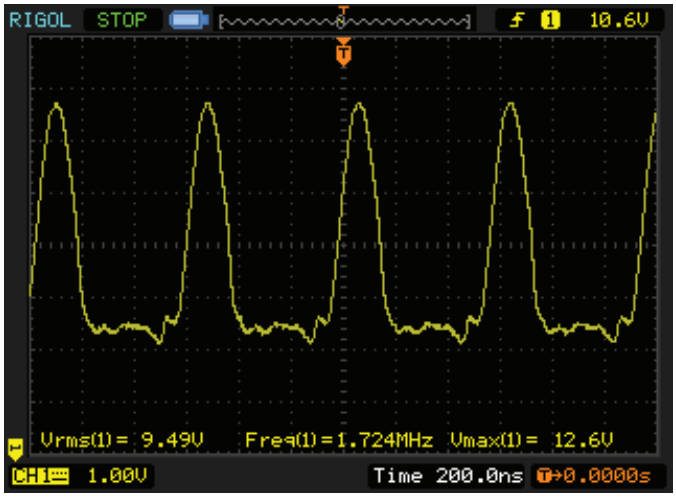

Figure 3.19. The output of class-E signal form

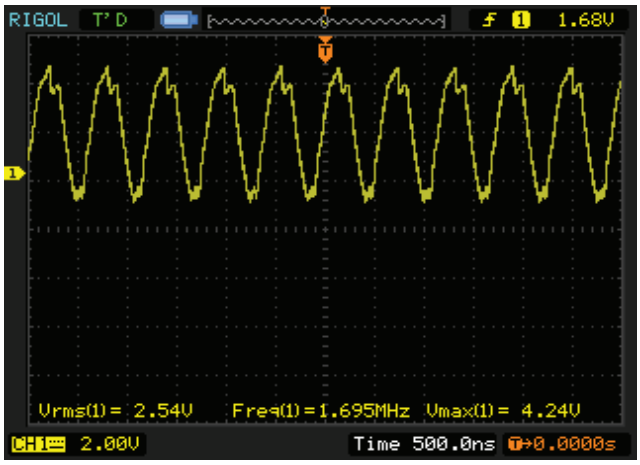

Figure 3.20. The gate-source voltage waveform of MOSFET

According to the obtained signals characteristics from Figure 3.19 and 3.20, the efficiency calculation can be carried out by the following Equations.

$$P_{dc,\text{in}} = 0.40A \times 12v = 4.8W \tag{3.20}$$

$$P_{driver} = 8V \times 0.02A = 0.16W \tag{3.21}$$

$$P_{driver,pulse} = V_p \times I_{driver,pulse} = 3\text{V} \times 0.01A = 0.03W \tag{3.22}$$

$$P_{total,in} = P_{dc,in} + P_{driver} + P_{driver,pulse} = 4.99W \tag{3.23}$$

$$P_{out} = \frac{(9.48V)^2}{21.9\Omega} = 4.1W \tag{3.24}$$

$$\eta = \frac{P_{out}}{P_{total,in}} \tag{3.25}$$

$$\eta = \frac{4.1W}{4.99W} = 82.1\% \tag{3.26}$$

The rectified signal is presented in Figure 3.21. The efficiency value is calculated from the RMS of alternating current and the diodes losses are neglected.

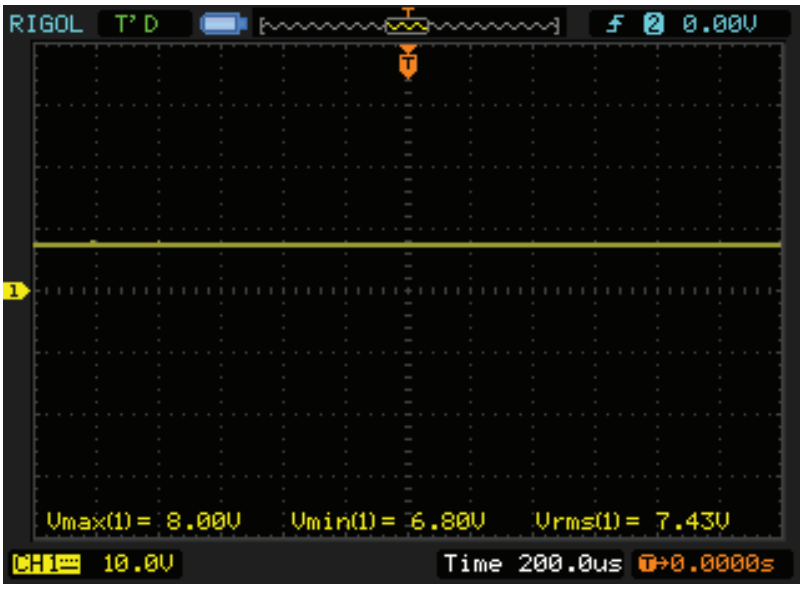

Figure 3.21. The characteristic of the rectified signal on the R1

In order to present the power of throughput signal from the class-E, a led bar was activated. The electrical characteristic of the led bar has 12 V DC and 1 Ampere.

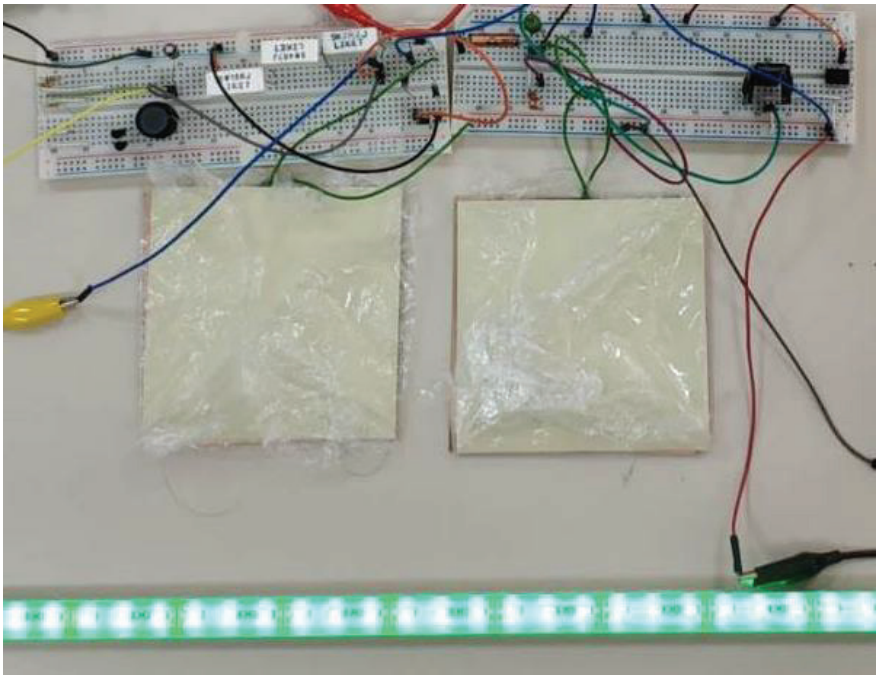

Figure 3.22. Demonstration of the powered led bar

Nevertheless, the supplied current has increased from 0.40 A to 0.51A. The frequency scanning method was used in order to investigate the throughput power of the Class-E amplifier circuit. Therefore, the frequency was changed from 1 MHz to 5MHz scale.

3.5. LC Compensated Class-E Amplifier Experiment

The Class-E amplifier circuit is very effective for wireless power transmission topology. As it is known that the LC circuit could have zero impedance at the resonance frequency. According to this experiment, zero impedance feature of the LC circuit in resonance was tried to be used. In order to understand this methodology, the structure of the RLC circuit should be investigated. This type of circuits are widely used in telecommunication systems. The general RLC circuit operates in two states for each member; charging and discharging case. In theory, these charging and discharging states realize infinite loop. This feature makes RLC compensated circuit very useful. RLC circuit also called tank circuit as well. The total reactance of this circuit called impedance.

$$Z = X_L + X_C + R \tag{3.27}$$

Where Z, X_L, X_C, R represent total impedance, the reactance of coil, reactance of capacitor and resistance of resistor, respectively.

$$\omega = 2\pi f \tag{3.28}$$

Where ω represent natural frequency. The reactance of the coil could be calculated by a formula which is given in Equation 3.29.

$$X_L = 2\pi fL = 2\omega L \tag{3.29}$$

Besides, the reactance of the capacitor can be calculated by Equation 3.30.

$$X_C = \frac{1}{2\pi fC} = \frac{1}{2\omega C} \tag{3.30}$$

In addition to this, the resistance should be taken into consideration. V represents the potential difference across the resistor and I symbolizes the current which flows through the resistance.

$$R = \frac{V}{I} \tag{3.31}$$

In this experiment, the serial RLC circuit was used. However, to analyse the RLC circuit, the graphical model is widely used. Therefore probable phase shift could be realized with the help of this methodology. The phase difference was occurred by capacitor and inductor which can store the electrical energy. While the parallel circuit investigated, the titles of arrows have to change in order to acquire the phase difference properly. The phase diagrams of RLC circuits have been given in Figure 3.23.

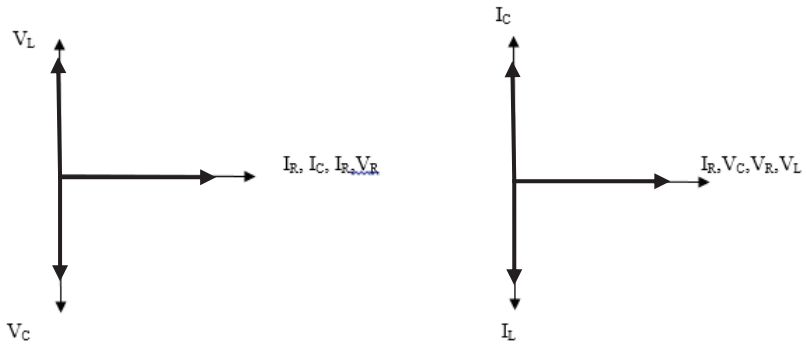

Figure 3.23. The phase differences of inductance capacitor according to a series circuit (a), parallel circuit (b)

The schematic of the circuit and real circuit were given in Figure 3.24.

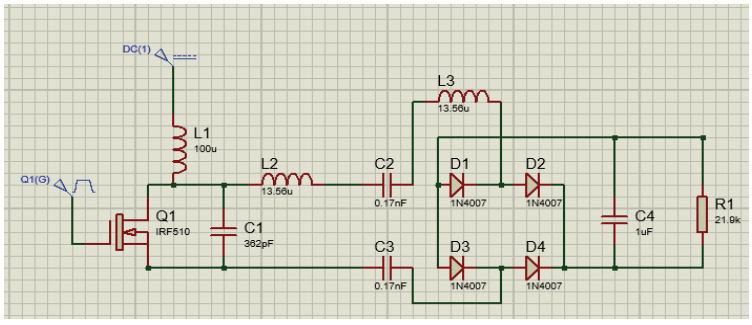

(a)

Figure 3.24. (Cont on next page)

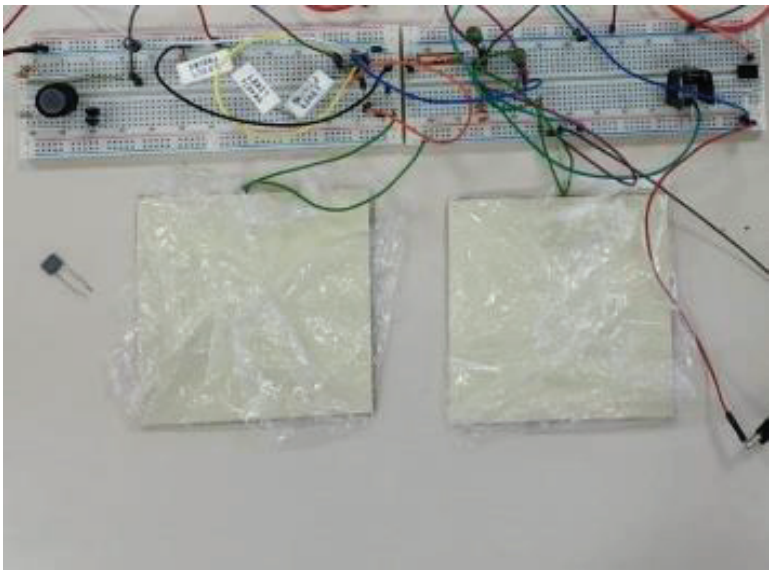

(b)

Figure 3.24. LC compensated circuit Class-E with capacitive coupling plates (a) and LC compensated circuit Class-E with capacitive coupling plates in real life (b)

In this experiment, L3 inductor was connected in series to the class-E circuit. The henry value of the inductor is the same as the primary inductor which is L2. Therefore LC compensated circuit was constructed with respect to coupling capacitors. At the resonance frequency, the impedance of the circuit reaches zero theoretically. This circuit was constructed by using extra inductor. The operated and calculated values of the circuit members were given on Table 3.6.

Table 3.6. Demonstration of evaluated and operated values in LC compensated circuit

Circuit Members	Calculated Value	Operated Value
L_1 (μH)	24	100
L_2 (μH)	5.506	13.6
C_1 (nF)	0.844	0.362
R_1 (Ω)	17.30	21.9
$f_{resonance}$ (MHz)	4.7	1-5
L_3 (μH)	5.506	13.6

In this experiment, 12 V dc was given to the system with 0.31 Ampere. MOSFET driver was operated with 8 V dc and 0.02 A. With help of frequency scanning method, the most efficient values for frequency was obtained about 1.342 MHz. The potential difference of PWM value was 6 V. The DC source values and AC source values were given on Table 3.7.

Table 3.7. Operated AC voltage and its frequency values for Class-E LC compensated circuit

V_{in} (V)	V_{supply} (V)	I_{in} (A)	I_{supply} (A)	V_{pwm} (V_{pp})	F_{pwm} (MHz)	Crest factor
12	8	0.31	0.02	6	1.322	1.23

Investigation on less time range was caused the clearness of the signal was damaged. According to the results, efficiency was calculated.

$$P_{dc,\text{in}} = 0.31A \times 12v = 3.72W \tag{3.32}$$

$$P_{driver} = 8V \times 0.02A = 0.16W \tag{3.33}$$

$$P_{driver,pulse} = V_p \times I_{driver,pulse} = 3\,\text{V} \times 0.01A = 0.03 \tag{3.34}$$

$$P_{total,in} = P_{dc,in} + P_{driver} + P_{driver,pulse} = 3.91W \tag{3.35}$$

$$P_{out} = \frac{(7.98V)^2}{21.9\Omega} = 2.907W \tag{3.36}$$

$$\eta = \frac{P_{out}}{P_{total,in}} = 74.36\% \tag{3.37}$$

Additionally, voltage ripple values were taken out from 7.98 RMS voltage output value. Also, these results have taken without any compression on the coupling capacitor. It is observed that the efficiency value of the Class-E circuit is very sufficient for capacitive power transfer system. To see the real power of compensated Class-E circuit, the led bar was connected to the output of the system. The electrical characteristic of led bar is 12 V and 1 A.

However, if the pressure is applied to the coupling capacitor, some of the unexpected states have occurred under the same conditions. It was observed that the characteristic of the output signal has changed under static load. The iron was used to provide the static load on the coupling capacitors.

If an external force is applied to the coupling capacitors, the response of the Class-E circuit is a distorted sine wave. However, with respect to frequency, a minute change occurs to provide resonance frequency.

While Class-E experiments are compared, they generally use the same current values approximately. With respect to these input parameters, the efficiency of the Class-E circuit can be increased by coupling capacitors under static load. However, the characteristics of primary and secondary capacitors corrupted.

3.6. LC Parallel Compensated Class-E Amplifier Experiment

The lower- current higher-voltage nature of CPT also aids to keep omic losses low. Parallel LC circuit is also called as an inductor-capacitor circuit, a resonator circuit. Parallel LC circuit is a simple or tuned circuit that provides magnetic resonance to store an electrical charge or produce electromagnetic frequency. As the electrical charge flows through the coil, the capacitor loses electromagnetic energy and the inductor is charged electromagnetically.

However, when the inductor is charged more than the capacitor, the electromagnetic cloud around the coil begins to dissipate and the energy flows through the capacitor. This procedure begins to repeat until the entire original energy is lost in the resistance of the circuit. When the coil is first supplied with electrical energy, the coil voltage comes to the fore and creates a phase difference between the current and the voltage.

In this experiment, inductance and capacitor were connected to the circuit in parallel to each other. Therefore a classic LC compensation circuit was created. The impedance of the parallel LC circuit is lower than the series. To achieve higher efficiency, the experiment was realized with the class-E amplifier.

In this experiment, an inductor was connected to a capacitor in parallel. The henry value of the inductor is the same as the primary inductor. Therefore LC compensated circuit was constructed with respect to coupling capacitors.

At the resonance frequency, the impedance of circuit decreases due combination of inductor and coupling capacitor. The circuit has been demonstrated in Figure 3.23a by Proteus computer program. The test setup is presented in Figure 3.23b. Operated components were given on Table 3.8.

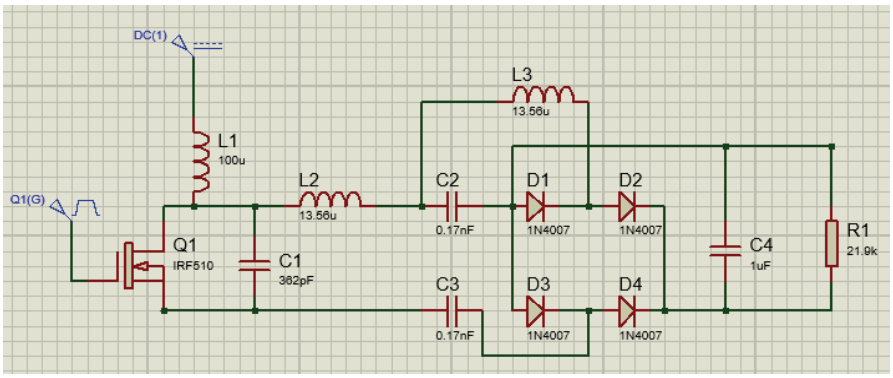

(a)

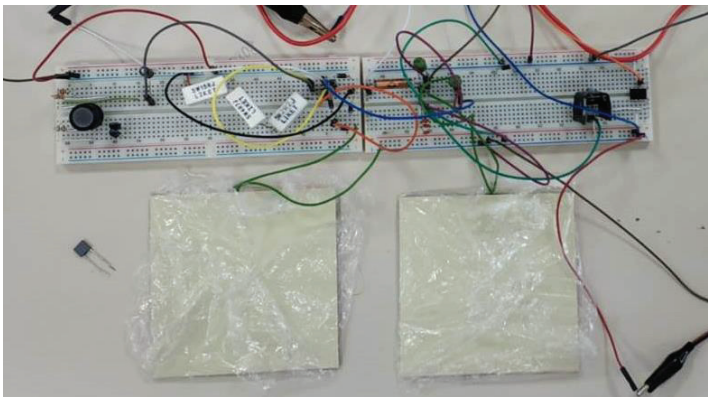

(b)

Figure 3.25. Circuit demonstration in Proteus (a) and the realized experimental setup for LC parallel compensator (b)

Table 3.8. Demonstration of theoretical and operating values in the LC parallel compensated circuit

Circuit Members	Calculated Value	Operated Value
L_1 (µH)	24	100
L_2 (µH)	5.506	13.6
C_1 (nF)	0.844	0.362
R_1 (Ω)	17.30	21.9
$f_{resonance}$ (MHz)	4.7	1-5
L_3 (µH)	5.506	13.6

12 V DC current was given through the system with 0.30 A. MOSFET driver was operated with 8 V DC and 0.01 A.

With the help of the frequency scanning process, the most efficient values for frequency was obtained at about 1.309 MHz. The potential difference of PWM value was 6 V. The DC source values and AC source values were given on Table 3.9.

Table 3.9. Operated AC voltage and its frequency values for Class-E LC compensated circuit

V_{in} (V)	V_{supply} (V)	I_{in} (A)	I_{supply} (A)	V_{pwm} (V_{pp})	F_{pwm} (MHz)	Crest factor
12	8	0.30	0.01	6	1.309	1.25

6 V peak-to-peak PWM voltage was used to drive for MOSFET at 1.309 Mhz frequency. The PWM pulse is operated with 50 % duty cycle. According to results, efficiency calculation was carried out.

$$P_{dc,\text{in}} = 0.30A \times 12v = 3.6W \tag{3.38}$$

$$P_{driver} = 8.1V \times 0.01A = 0.081W \tag{3.39}$$

$$P_{driver,pulse} = V_p \times I_{driver,pulse} = 3\text{V} \times 0.01A = 0.03 \tag{3.40}$$

$$P_{total,in} = P_{dc,in} + P_{driver} + P_{driver,pulse} = 3.7W \tag{3.41}$$

$$P_{out} = \frac{(7.70V)^2}{21.9\Omega} = 2.707W \tag{3.42}$$

$$\eta = \frac{P_{out}}{P_{total,in}} = 73.1\% \tag{3.43}$$

As a result of Class-E experiments, the three efficiency values were recorded. In this thesis, the most efficient system is operated as mentioned topic before.

In daily life, these systems can be damaged by environmental factors. Therefore the most efficient circuit was specified with using a table which was given on Table 3.10.

Table 3.10. The efficiency comparison of the Class-E circuits

Type of circuit	Efficiency
Class-E with fundamental topology	82.1%
LC series compensated Class-E circuit	74.36%
LC parallel compensated Class-E circuit	71.3 %

According to Table 3.10, the most efficient circuit was obtained at Class-E fundamental topology. To procure efficient capacitive power transfer circuit, the fundamental Class-E circuit has been used in the prototype.

While the alternating current is converted to the direct current, the losses can be seen. While the parallel plates are operated in the circuit the capacitance value of parallel plates are not stable.

This circumstance can cause the error in theoretical calculation and the resonance frequency cannot be calculated perfectly. If the circuit is not operated at its resonance frequency, the resistance of inductor and conductor decrease the efficiency of the circuit.

CHAPTER 4

PROTOTYPE OF THE SUB-KILOWATT, EFFICIENT CPT SYSTEM FOR DATA AND POWER TRANSFER

As mentioned in the introduction part of the thesis, the main idea is the designing a sub-kilowatt, efficient capacitive coupling system for mechanical variable. The mechanical variable to be monitor is a force that acting on the axle of a vehicle. The force acting the vehicle axle should be under limited range. Otherwise, the overload force could cause irreversible damages on the axis of the vehicle. The axle is a fundamental part of the vehicle.

The axle consists of two parts, fixed and movable. Fixed part is a very important element for balancing a vehicle. The majority of the weight is carried by the axle of the vehicle. The movable part provides the motion for the vehicles. The broken or damaged axle can cause the car crash that interiors loss of life and property.

To provide an early diagnosis of vehicle axle, the wireless weight measurement system is aimed to design. It is proposed that designing a wireless weight measurement system capacitively with high efficiency. However, the capacitive system has many disadvantages which are limited distance, low power transfer etc. To overcome those disadvantages, the optimal capacitive power and data transfer were constructed by the copper parallel plates. The copper is selected because of its high electrical permittivity value while compared with other materials in nature. The electrical conductivities of some metals have been given on Table 4.1 (Tsakiris et.al., 2011).

Table 4.1. The electrical conductivity of metals

Number	Material	Electrical Conductivity ($\Omega^{-1}.cm^{-1}$)
1	Cu	29×10^5
2	Fe	0.031×10^5
3	Ag	2.8×10^5
4	Ni	21.7×10^5

4.1. Capacitive Data Transfer System

In this thesis, a small prototype was established. For measuring the weight of the axle, the load cell was used. The load cell consists of a mechanic part and an electronic part. Of these, the mechanic part is a rectangular metal that has a hollow in the middle. The load cell has been presented in Figure 4.1.

Figure 4.1. Demonstration of load cell to measure the weight

Electronic part of load cell is strain gauges. As can be seen in Figure 4.1 the one strain gauge has been placed on every side of the load cell. Strain gauge is a sensitive resistance that can sense the changing in, temperature, pressure etc. The strain gauge was shown in Figure 4.2.

Figure 4.2. Demonstration of strain gauge

Generally, strain gauges are used for force measurement, strain measurement and pressure measurement etc. These processes depend on the number of strain gauge and position of strain gauge. The strain gauges are operated with respect to the Wheatstone bridge principle.

According to the Wheatstone bridge, two resistor sets are connected to the circuit in parallel and the voltage difference (V_a - V_b) between them is equal to zero while the resistance values of resistors are equal to each other. The Wheatstone bridge has been shown in Figure 4.3.

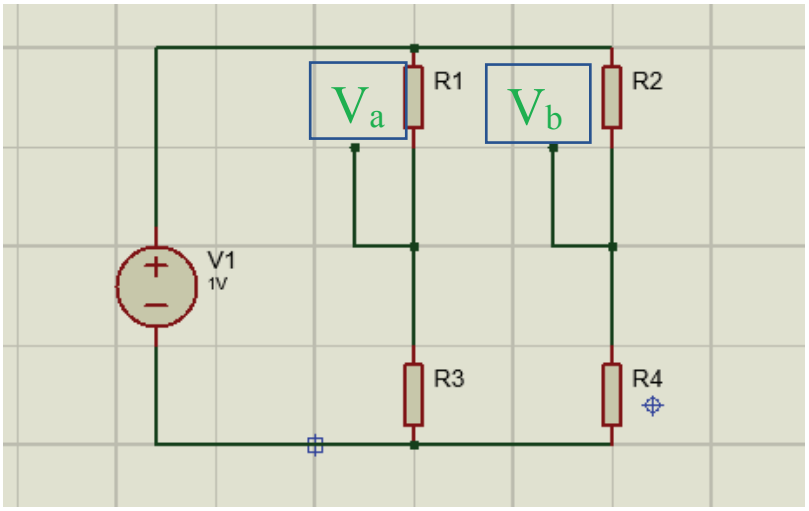

Figure 4.3. Wheatstone bridge circuit topology

The potential difference between V_a and V_b is equal to zero while the resistance values of R1, R2, R3 and R4 are equal to each other. This potential difference is called V_{out}. In order to understand the analogy, the circuit should be analysed briefly.

At the equilibrium condition, the relation between the resistances can be calculated as Equation 4.1.

$$\frac{R1}{R3} = \frac{R2}{R4} = 1 \tag{4.1}$$

The V_{out} can be calculated with the help of Equation 4.2.

$$V_{out} = V_a - V_b = V_{R3} - V_{R4} = 0 \tag{4.2}$$

The V_{out} value is equal to zero at the equilibrium condition. The equivalent resistance value on the left side was shown R_a and the right side was demonstrated R_b.

$$R_a = \frac{R3}{R1 + R3} \tag{4.3}$$

$$R_b = \frac{R4}{R2 + R4} \tag{4.4}$$

At the equilibrium condition, V_{R3} and V_{R4} are equal to each other. The currents on the branches are equal to each other as well. Therefore R_a and R_b are equal to each other. The relation between also can be written as Equation 4.5 (Bird, 1997).

$$\frac{R3}{R1 + R3} = \frac{R4}{R2 + R4} \tag{4.5}$$

$$R4 = \frac{R2 \cdot R3}{R1} \tag{4.6}$$

If the one resistor is changed with the strain gauge, this circuit is called Quarter Bridge. In this study, the four strain gauges were implemented. The voltage difference (V_a - V_b) gives the change in a system. However, the resistance change of strain gauge is low that cannot be seen by microcontroller distinguishably.

Therefore, the amplifier should be used in order to increase the voltage difference. In this case, the non-inverting type of op-amp should be operated in order to save the waveform. For this reason, a precision 24 bit ADC (analogue-to-digital) HX711 chip was operated.

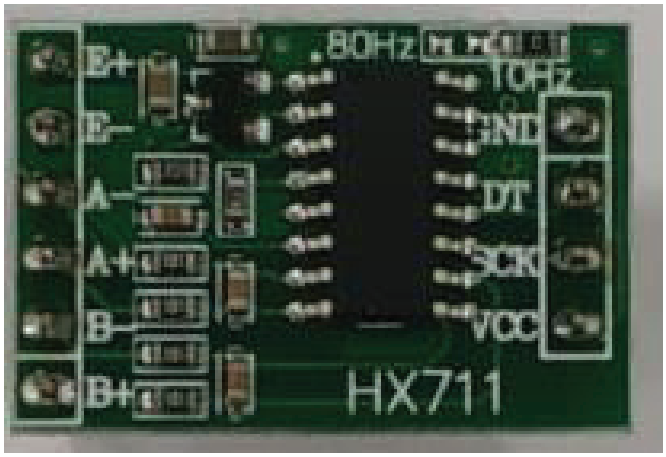

Figure 4.4. 24 bit ADC HX711 chip with preamplifier

This chip is appropriate for the weight measurement by load cell. The HX711 24 bit ADC is displayed in Figure 4.4. The HX711 chip interiors 24 bit ADC and preamplifier. The chip runs in synchronism with the help of the serial clock pinout (SCK).

The potential difference which data is transmitted on the DT pin. In this study, the weight measuring system was designed to monitor a load on the axle of the vehicle. The mini prototype has been constituted instead of a real prototype. 5 kg load cell was implemented to measure the weight.

The maximum carrying capacity of the load cell is 5 kg. In the near future, it is supposed that the wireless weight measurement system will be used on the axle of the car. As mentioned before, the axle is a very substantial component of a vehicle.

The mechanic health of axle should be always controlled by a special measurement system. Especially, the moving parts in the vehicles cannot be wired. One of the wireless power and data transfer technology model, the capacitive coupling method comes to light for solving this problem. In this thesis, it is suggested that the data coming from the axle of the vehicles can be transferred wirelessly and smoothly to the microcontroller by capacitive coupling method.

The measured weights are data that is wanted to transfer. In this prototype, the weight is measured by the load cell as given in Figure 4.1. The voltage difference between the Va and Vb provides the data with the help of the Wheatstone bridge circuit. However, the data signals are so feeble not to be detected by the microcontroller.

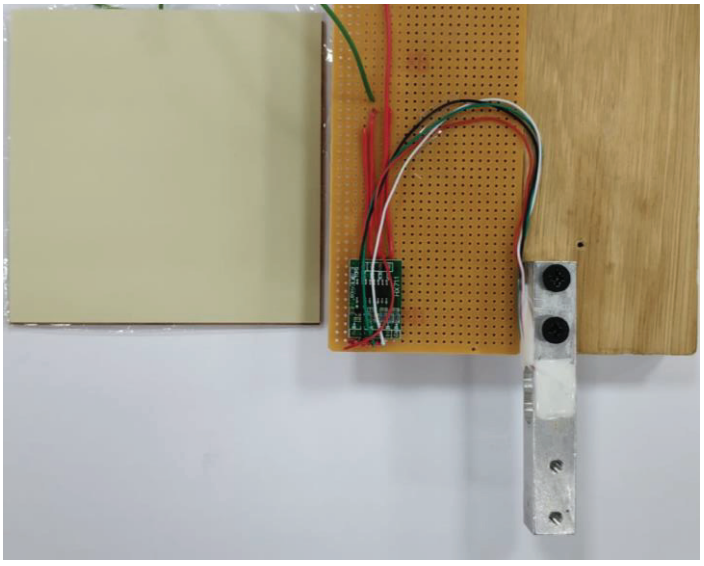

Figure 4.5. The capacitive weight measurement part of the prototype

The signal should be amplified by a special circuit such as the non-inverting op-amp circuitries. In order to provide this amplification process, the preamplifier 24 bit ADC HX711 chip is implemented.

At the end of the capacitive data transfer section, it is planned that the collected data is transferred the microcontroller to monitor the mechanical variable. The capacitive data transfer section of the prototype is indicated in Figure 4.5.

.As can be seen from Figure 4.5, it is purposed that the measured data are transferred to the microcontroller by capacitive coupling method. The required energy for supplying HX711 chip is procured by the rectified output of the Class-E amplifier circuit. The capacitive power transfer part is mentioned next section.

4.2. Capacitive Power Transfer System

In this part, the power transfer system of the capacitive coupling method is discussed. The power of the capacitive data transfer system is supplied by Class-E amplifier. In order to provide an efficient system, the Class-E power amplifier circuit is implemented. As mentioned before, the theoretical efficiency of the Class-E power amplifier circuit is 100 %. There are many types of power amplifiers. They have advantages and disadvantages. The efficiency and phase difference values are presented in Figure 4.6.

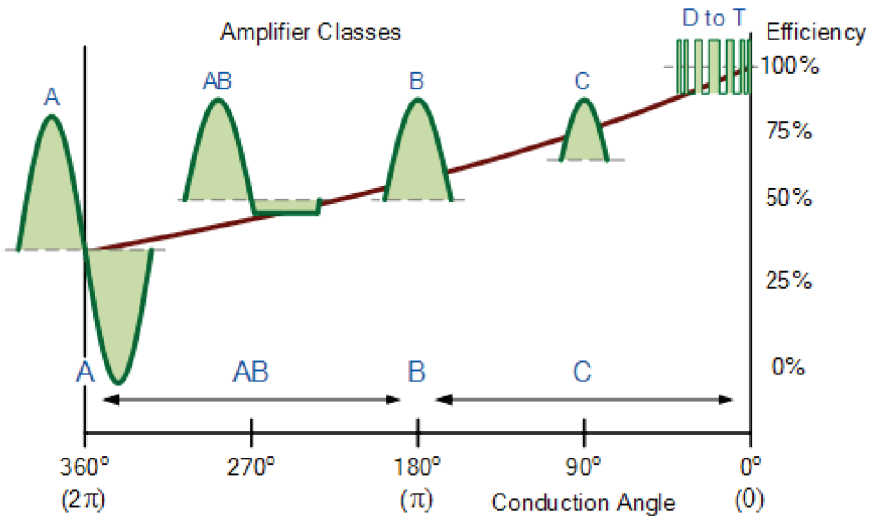

Figure 4.6. Conduction angles and Efficiency percentages of power amplifiers (Source: Cripps, Steve C., 2006)

The efficiency of A, AB, B and C power amplifier are lower than other amplifier classes. However, as mentioned in chapter 3, the class F amplifier has harmonic signals. The harmonic signals decrease efficiency.

Thus Class-E power amplifier is implemented to acquire high efficiency. The schematic of the Class-E amplifier circuit is designed by Proteus computer software and shown in Figure 4.7.

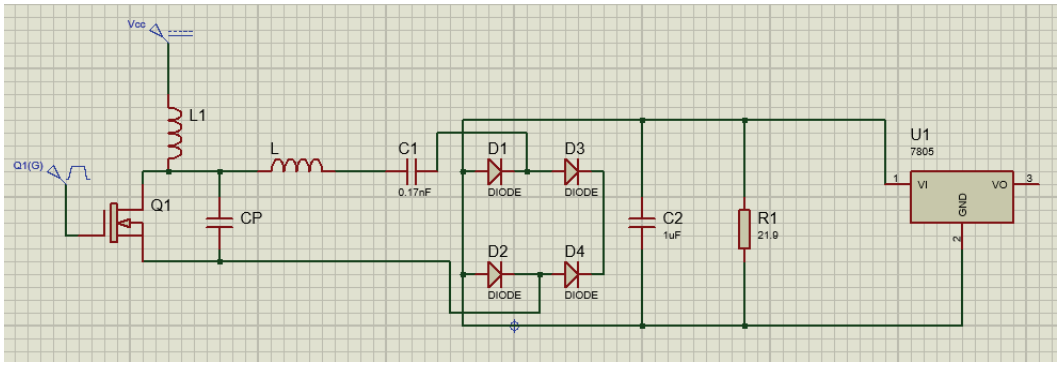

Figure 4.7. The schematic configuration of the Class-E amplifier circuit

V_{cc} is 12 V direct current that is given to the L1 choke coil. The Q1 is the MOSFET. The MOSFET is supplied by the MOSFET driver. The driver is energized with 6 V peak-to-peak PWM with 50% duty cycle.

The MOSFET cannot be driven by only PWM pulse at the high frequency. There is a micro-scale capacitor inside the gate of MOSFET. The sufficient charges have to be pumped to the gate of MOSFET.

The MOSFET driver TC4427 takes on the task. CP is the shunt capacitor. The shunt capacitor acts as a filter in the Class-E circuit. C1 is the capacitive plates. The power signal is transferred by the coupling capacitor C1. Obtained signal form is converted to the direct current by full-wave rectifier circuit. The 1N4007 diodes are implemented in the Class-E circuit. The rectified signal form is used to energize the measurement system that is shown in Figure 4.5.

The theoretical calculation of the Class-E circuit is started with the obtained formulas from Chapter 3. First of all the Vcc is 12 volt and the drawn current is accepted as 0.4 A. Therefore, the supplied power is equal to 4.8 W as given in Equation 4.7.

$$P_d = 12V \times 0.4A = 4.8W \tag{4.7}$$

In order to calculate the optimal resistance R1, Equation 4.8 is implemented.

$$R_1 = \frac{8 \times V_{cc}{}^2}{(\pi^2 + 4) \times \mathrm{P}_d} = \frac{8 \times (12v)^2}{(\pi^2 + 4) \times 4.8W} = 17.30\Omega \tag{4.8}$$

5 MHz is selected as an operating frequency at the gate of MOSFET. The magnitude of coil L is evaluated with the help of the operating frequency value and the capacitance value of the coupling capacitor. The operating frequency is adjusted according to the resonance frequency. At the resonance frequency, the total impedance of the circuit is equal to zero theoretically. The selection of inductor can be calculated in Equation 4.9.

$$f_{resonance} = \frac{1}{2\pi\sqrt{LC}} = 5 \times 10^6 Hz = \frac{1}{2\pi\sqrt{0.17 \times 10^{-9} F \times 5.9 \times 10^{-6} H}} \tag{4.9}$$

According to the resonance frequency, the magnitude of L is evaluated by Equation 4.9. The inductance value of L is calculated from the following equations for the Class-E circuit analogy. In Equation 4.10, the series resonant value is evaluated. The extra inductance value for Class-E circuit is calculated by Equation 4.11. The total of extra inductance value and the series resonant value of inductance gives the inductance value of L.

$$L_{res} = \frac{QR_1}{\omega} = \frac{17.30 \times 10}{2\pi f_{resonance}} = 5.506\mu H \tag{4.10}$$

$$L_{ext} = \frac{(1.153)\mathrm{R}}{\omega} = \frac{(1.153)(21.9)}{2 \cdot \pi \cdot 1 \times 10^6} = 3.17\mu H \tag{4.11}$$

$$L = L_{ext} + L_{res} = 8.676\mu H \tag{4.12}$$

If the formulas of Class-E circuit are implemented, L inductance value, the result is equal to 9.5 μH. However, there is not much difference between calculated inductance values. The capacitance value of the shunt capacitor is computed by Equation 4.13.

$$C_p = \frac{I_{dc}}{\omega \pi P_d} = \frac{0.4A}{(2\pi f_{resonance})\pi \times (12\,\mathrm{v} \times 0.4A)} = 0.844nF \tag{4.13}$$

The minimum required inductance value of the choke coil is computed by Equation 4.14. However, at the beginning of the calculation process, the choke inductance value has been known.

In order to see how much bigger theoretical value than practical values, this calculation is done. The operated inductance value of the choke coil is bigger than the theoretical value L_{min}. To provide this, some mathematical operations are implemented. The used values are arranged with respect to this logic.

$$L_{1,\min} = 2 \times (\frac{\pi^2}{4} + 1) \times \frac{R}{f_{resonance}} = 24\mu H \tag{4.14}$$

However, obtained theoretical values are not used exactly. In practice, the closer values are implemented. The difference between has been shown on Table 4.1. During the experiment, the capacitance value of the coupling capacitor is not stable. Thus, the frequency scanning method is applied to obtain the resonance frequency. The frequency is scanned between 1 MHz to 5 MHz. Besides, the close to theoretical calculations, the inductance, the capacitance and the resistance values are implemented. After the frequency scanning, the maximum efficiency of the signal is obtained at 1.7 MHz frequency without signal distortion. Thus the theory of Class-E circuit topology is not broken. As can be seen in Figure 4.8, the true-RMS (root mean square) value of the output signal is 10.1 Voltage at 1.724 MHz frequency

Table 4.2. The difference table between computed and operated circuit elements values

Circuit members	Calculated Value	Operated value
L_1 (µH)	24	100
L(µH)	8.676	13.6
Cp (nF)	0.844	0.362
R_1 (ohm)	17.30	21.9
$f_{resonance}$ (MHz)	5	1 .7

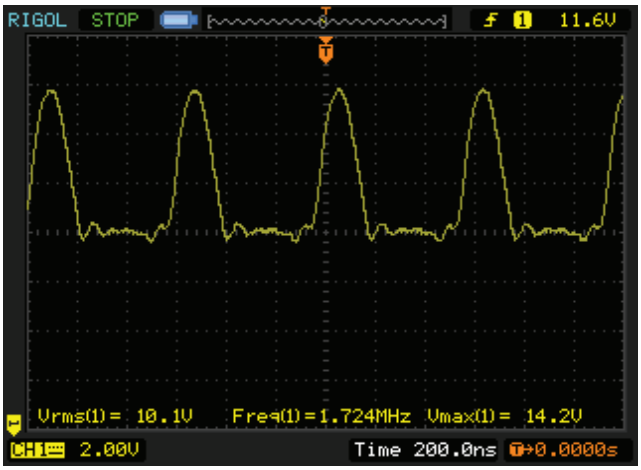

Figure 4.8. The signal form of Class-E throughput

. The maximum voltage of the signal is 14.2 V. The signal characteristic has a noise that can be rejected and SNR (signal-to-noise-ratio) ratio of signal is very high. The signal on the secondary capacitive plate that is transferred is given in Figure 4.9.

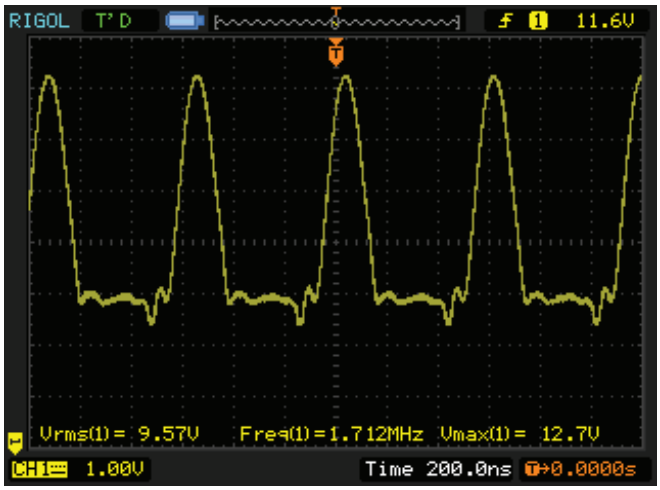

Figure 4.9. The transferred energy by the primary capacitive plate

The true RMS value of the signal is equal to 9.57 V at 1.7 MHz frequency. While the performance of the power amplifier circuit is computed, the transferred power is considered. While the RMS voltages of primary and secondary capacitive plates are considered, the power loss of wireless power transfer is quite low. The power performance of the copper plate coupling capacitor is computed by Equation 4.15.

$$\eta_1 = \frac{V_{out}}{V_{in}} = 94.75\% \tag{4.15}$$

This performance value is quite well when the other capacitive power and data transfer academic studies are considered. The drain-source signal characteristic of MOSFET is presented in Figure 4.10.

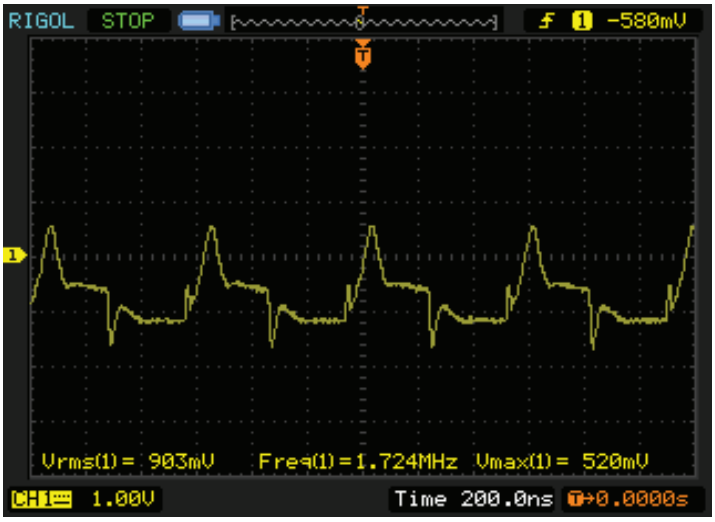

Figure 4.10. Drain-source signal form of MOSFET

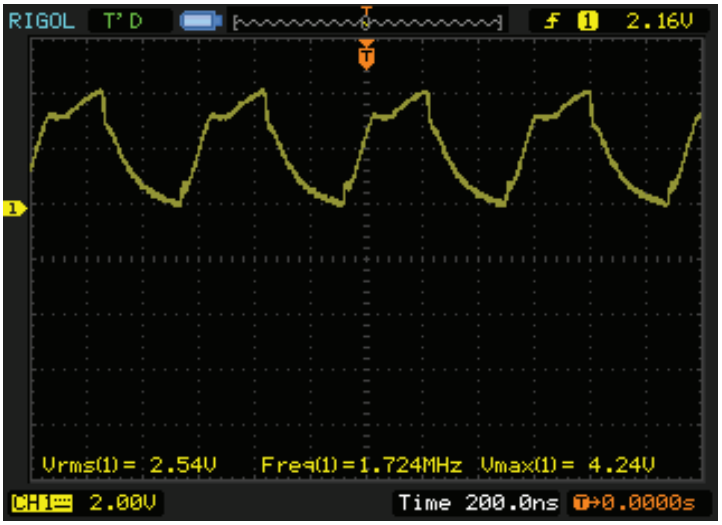

Figure 4.11. Gate-source signal form of IRF510 MOSFET in the oscilloscope screen

Besides, the gate-source signal form of MOSFET has been shown in Figure 4.11. After the power signal is transferred through the coupling capacitor, it is rectified by the full-wave rectifier circuit in order to power supply for the weight measurement system. The required potential difference for the measurement system is between 5 V and 5.5 V. The throughput of the full-bridge rectifier circuit converts the alternating current to direct current. Thus, the uninterrupted power is provided by the Class-E power amplifier circuit.

However, the throughput of the full-bridge rectifier circuit is more than the maximum operating voltage of the weight measurement system.

In order to resolve this problem, the LM7805 voltage regulator has been implemented in the capacitive data and power transfer system. The obtained voltage regulator output signal characteristic has been presented in Figure 4.12.

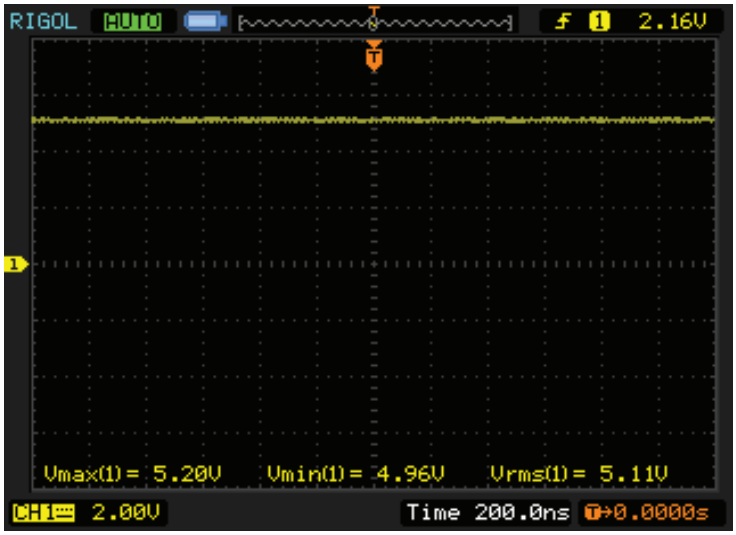

Figure 4.12. The rectified alternating current on the R1 resistor

5.1 RMS voltage value is obtained from the voltage regulator circuit. The voltage value is appropriate to supply the weight measurement system. The AC source and DC source information is tabulated on Table 4.3. V_{in} symbolizes the 12 V DC on the choke inductor. V_{supply} represents the required voltage to the MOSFET driver. I_{in} is drawn current by DC source. I_{supply} shows the drawn current by the MOSFET driver. V_{pwm} is the pulse that is implemented to activate the MOSFET with 50 % duty cycle.

Table 4.3. The magnitude of operating voltage, current and frequency

V_{in} (V)	V_{supply} (V)	I_{in} (A)	I_{supply} (A)	V_{pwm} (V_{pp})	F_{pwm} (MHz)
12	8	0.4	0.02	6	1.724

According to the 4.3 Table, the performance value is computed by the following equations.

First of all, the power consumption of the MOSFET driver and Class-E circuit have been evaluated. P_d is the consumed power by the Class-E circuit. P_{driver} is required power to activate MOSFET driver. P_{pulse} is the necessary energy to produce PWM pulse from the AC source.

The total consumed power is symbolized by P_{total}. The obtained energy is presented by P_{out}. The efficiency of the circuit is computed by Equation 4.21.

$$P_{dc} = 0.40 \times 12 = 4.8W \tag{4.16}$$

$$P_{driver} = 8V \times 0.02A = 0.16W \tag{4.17}$$

$$P_{pulse} = 3V \times 0.01A = 0.03W \tag{4.18}$$

$$P_{total} = P_{dc} + P_{driver} + P_{pulse} = 4.99W \tag{4.19}$$

$$P_{out} = \frac{V^2}{R1} = \frac{(9.57V)^2}{21.9\Omega} = 4.181W \tag{4.20}$$

$$\eta = \frac{P_{out}}{P_{total}} = \frac{4.181W}{4.99W} = 83.80\% \tag{4.21}$$

The 83.80 % performance is succeeded in capacitive power transfer experiment. The obtained energy is used to energize the weight measurement system. The data are transferred to the microcontroller by capacitive plates. The measurement system is energized by the Class-E power amplifier. In the next chapter, the sensor is calibrated and validation tests are carried out. The transferred data accuracy has been studied. Besides, the exact data and the transferred data are compared to obtain accuracy.

The experiments are applied to some materials that their weights are known. For obtaining the force (N), the data are converted from the mass to the weight. Therefore the capacitive power and data transfers are realized

CHAPTER 5

TESTS

After all the capacitive data and power experiments are realized, the prototype has been calibrated by the coding algorithm. The ATMEGA328P-PU is selected as microcontroller. First of all, some materials are measured, the mass of these materials are taken from their datasheet. The test results are discussed in chapter 6 and the calibration code algorithm is shared in the appendix part of the thesis. This prototype has been designed to measure the load which is applied to the axle of a vehicle. However, the mini prototype is not adequate for measuring this type of weight. Maximum weight measuring capacity is limited by the load cell. The chosen type of load cell is able to measure a maximum of 5 kg. In the near future, the designed capacitive data and power transfer system will reach the capacity to measure the load on the axle. The copper plates coupling capacitors are implemented to transfer data and power due to their high electrical conductive values. The sizes of the coupling capacitors are 100mm x 100mm. Thus, the surface area used by electric field lines are equal to the $1x10^{-4}$ m^2. The power and data are carried by electric fields.

The masses of coins are measured by a capacitive measuring system. The masses of 1 Turkish lira (TL) coin, 0.5 TL coin and 0.25 TL coin are monitoring by serial port screen. The real accurate values of coins are taken from the website of Treasury and Finance Ministries of the Republic of Turkey. Also, the masses of coins are measured by analytical balance. Firstly, the mass of 1 TL coin is measured. The error has been evaluated. Thus, the sensitivity of the system is tested. The signal characteristic of the sensor has been investigated and compared with the transferred signal from. The performance of the copper coupling capacitor is determined according to the result of the comparison process. While data are transmitted by the coupling capacitor, the synchronous communication process is used. The meaning of synchronous is that the sensor in the measurement system operates with the microcontroller synchronously or at the same frequency value.

This type of application is implemented in real-time experiments. The advantage of the synchronous communication process is that there are not date lose when data are transferred.

According to Treasury and Finance Ministries of the Republic of Turkey, the mass of 1 TL coin is 8.2 grams. The mass of the 1 TL coin is measured by a precision laboratory scale that has been shown in Figure 5.1.

Figure 5.1. The measured mass of 1 TL coin by precision laboratory scale

As can be seen in Figure 5.1, the mass of 1 TL coins is 8.16 grams. According to the sensor output, the average measured mass is 8.17 grams.

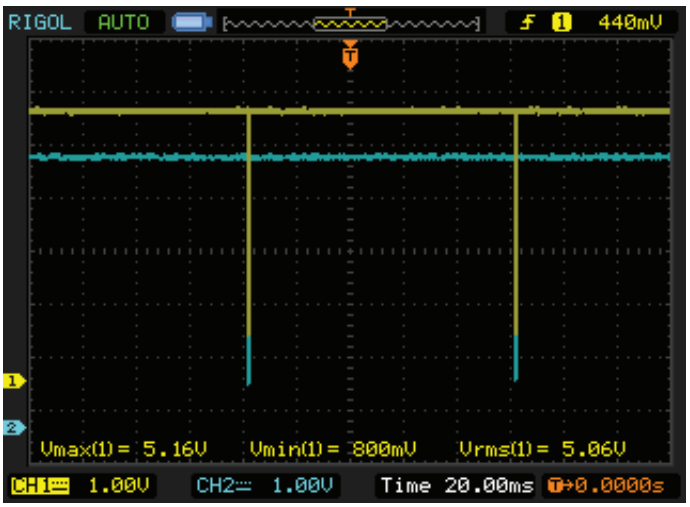

Figure 5.2. Signal forms of the obtained data and transferred data

The average of observed mass value is 8.193 grams in capacitive measurement system. The error of the capacitive measurement system is quite small as expected. Data losses in capacitive coupling plates are negligibly small. The operating system communication is provided as synchronous. The primary signal characteristic and the transferred signal are presented in Figure 5.2. In Figure 5.2, the yellow line shows the obtained data from the output of the sensor and the blue line represents the transferred data signal. It is very difficult to separate almost two data signals with each other. In order to see the resemblance of data signals, the signals are investigated at the same voltage scale. The weight of the 1 TL coin can be calculated as the following equations. The masses of coins are observed in 4 different ways. The weight taken from the Treasury and Finance Ministries of the Republic of Turkey is W_O. The weight read from the precision laboratory scale is W_P. The weight value observed from the sensor output is W_S. The weight value measured from the capacitive measurement system is W_C. The weight values of the 1 TL are calculated by the following equation

$$W_O = 0.0804N \tag{5.1}$$

$$W_P = 0.0800N \tag{5.2}$$

$$W_S = 0.0801N \tag{5.3}$$

$$W_C = 0.0803N \tag{5.4}$$

According to computed weights, the error calculations were applied to the same indexes. The sensor and capacitive measurement system errors are calculated with respect to the precision laboratory scale value. E_S and E_C represent the sensor and capacitive system errors, respectively.

$$E_S = 0.125\% \tag{5.5}$$

$$E_C = 0.375\% \tag{5.6}$$

The sensor error of the system is 0.125 %. The capacitive measurement system error is 0.375 %. It is a very small error value that can be neglected.

The small error value shows that the sub-kilowatt, efficient capacitive power and data transfer system is quite accurate. The next experiment is realized for the 0.5 TL coin.

The weight of 0.5 TL coin is 6.8 grams with respect to the Treasury and Finance Ministries of the Republic of Turkey. The mass of the 0.5 TL coin is measured by a precision laboratory scale that has been shown in Figure 5.3.

Figure 5.3. The measured mass of 0.5 TL coin by precision laboratory scale

As can be seen in Figure 5.3, the mass of 0.5 TL coins is 6.76 grams. According to the sensor output, the average measured mass is 6.70 grams. The average observed mass value is 6.696 grams in capacitive measurement system. The actual weight of the coin is computed by Equation 5.8. The errors of the system and sensor have been computed by the following Equation.

$$W_O = 0.0667N \tag{5.7}$$

$$W_P = 0.0663N \tag{5.8}$$

$$W_S = 0.0657N \tag{5.9}$$

$$W_C = 0.0656N \tag{5.10}$$

$$E_S = 0.904\% \tag{5.11}$$

$$E_C = 1.055\% \tag{5.12}$$

The error of the capacitive measurement system is found about 1.055 %. The error of the sensor is obtained at approximately 0.904 %. Those error values are acceptable. However, while the weight of coin decreases, the trueness of the system decreases. As mention, the beginning of this chapter the experiments are realized on different types of coins. The next sample to be measured is 0.25 TL coin. The mass of the 0.25 TL coin is measured by a precision laboratory scale that has been demonstrated in Figure 5.4.

Figure 5.4. The measured mass of 0.25 TL coin by precision laboratory scale

The mass of the 0.25 TL is measured 3.96 g by the precision laboratory scale. The average obtained mass value is 4.04 gram in the capacitive measurement system. The observed value from the sensor throughput is 4.03 g.

The weight values are calculated with respect to Treasury and Finance Ministries of the Republic of Turkey, precision laboratory scale, sensor output and capacitive measurement system, respectively.

At the end of the weight calculations, the sensor and the capacitive measurement system errors are observed.

$$W_O = 0.0392N \tag{5.13}$$

$$W_P = 0.0388N \tag{5.14}$$

$$W_S = 0.0395N \tag{5.15}$$

$$W_C = 0.0396N \tag{5.16}$$

$$E_S = 1.804\% \tag{5.17}$$

$$E_C = 2.061\% \tag{5.18}$$

The error of the capacitive measurement system is about 2.061%. The error value is higher than the previous one. The error of the sensor is approximately 1.804% However, it is bigger than 1% and this value is suitable for the wireless measurement system. According to these three errors, the average errors of the capacitive measurement system and sensor are computed by the following equations.

$$E_{avg\_S} = 0.94\% = \frac{1.804\% + 0.904\% + 0.125\%}{3} \tag{5.19}$$

$$E_{avg\_C} = 1.163\% = \frac{1.804\% + 0.904\% + 0.125\%}{3} \tag{5.20}$$

The average error of the capacitive measurement system is 1.163 % and it is smaller than 1 %. The average error of the sensor is 0.94 %.

The calculation process is proceeded according to mass values. The error values are not changed while the processes are realized with respect to weights.

The official mass data are taken from the Treasury and Finance Ministries of the Republic of Turkey. To observe the precise errors between experimental values and the trues, the computation process is realized in the kg unit.

CHAPTER 6

CONCLUSIONS

This thesis addresses the various facets of CPT technique. The aim of the thesis is to design a sub-kilowatt, efficient capacitive data and power transfer for monitoring the mechanical variables. The weight of the vehicle axle has been chosen as a mechanical variable. A small prototype is constructed which can measure the loads up to 5 kg. This limitation depends on the load cell. In order to realize the study in detail, the thesis is divided into two parts which are capacitive power transfer and capacitive data transfer.

Firstly, the efficient capacitive power transfer circuit is designed which is a Class-E power amplifier. The efficiency of the Class-E is theoretically 100%. Therefore, the Class-E amplifier is selected. The theoretical calculations are given in Chapter 2, the required equations are obtained. With these equations, the resonant circuit topology has been used in order to increase the performance of the capacitive power transfer. At the resonance frequency, the impedance of inductor or capacitor members cancel out each other, theoretically. According to the obtained equations, the magnitudes of circuit members are specified. However, the calculated exact values cannot be used. The theoretical values are optimized and the performance of capacitive power transfer is investigated.

Three types of circuits are tested which are LC parallel compensation, LC series compensation and fundamental Class-E circuit, respectively. The maximum efficiency value is obtained from a basic Class-E circuit topology of 83.80%. The copper plates are operated as coupling capacitors. The distance between the coupling capacitors is limited to millimetre scales. Otherwise, the energy or data cannot be transferred through the coupling capacitors. The electromagnetic interference is not observed on the embedded system. Thus, the stability of the embedded system is not affected. These carefully designed copper plates act like a capacitor. In the experiments, the capacitances of coupling capacitors were not stable. This characteristic deteriorated the performance of the circuit. Hence, the frequency scanning technique is carried out to find the maximum performance.

Although frequency scanning operation is implemented, the expected efficiency values are not obtained from the LC series and parallel resonance circuits. In order to design efficient power transfer circuit capacitively, the fundamental Class-E circuit is employed.

The maximum efficiency value is obtained at the 1.7 MHz operating frequency. The 4.99W power given to the circuit and the 4.181W power is obtained from the throughput of the Class-E power amplifier circuit. The IRF510 MOSFET cannot be operated at this high frequency. There is a small inherent capacitor at the gate of MOSFET. At the high frequency, the required charge cannot be pumped. For this reason, the TC4427 MOSFET driver is implemented. The MOSFET is activated by 6 V peak-to-peak PWM pulse at the 1.7 MHz operating frequency.

The output power is connected to the full-bridge rectifier circuit in order to convert alternating current to the direct current. The direct current is demanded by the weight measurement part. The 1N4007 diodes are used for this rectifying process. However, the rectified voltage is greater than the supply voltage range of the weight measurement system. Hence, the LM7805 voltage regulator has been attached to the circuit. In this way, the required voltage range which from 5 V to 5.5 V is provided.

The mechanical variable monitoring part consists of load cell, strain gauge, capacitive plates, 24 bit ADC HX711 chip with preamplifier and ATMEGA328P-PU microcontroller. In order to measure the weight, the load cell is used. The strain gauges are placed on it. With the help of the Wheatstone bridge logic, the voltage difference is generated between the branches. This potential difference is data that carry the weight measurement results. However, this potential difference is so small that cannot be sensed by the microcontroller.

In order to amplify the signal, the non-inverting amplifier circuit should be used. Non-inverting op-amps do not change the phase of the signal while the amplifying process is realized. Hence original the signal waveform is preserved. With by HX711 preamplifier chip, the voltage difference is amplified. Amplified data signals are sensed by the microcontroller, the weight of a material can be measured. The sensor is calibrated by measuring the weight of known objects.

In Chapter 5, the masses of materials are compared because the exact values of masses are known.

With the help of the equations, the weights are computed and error values are determined. Besides, the original weight measurement process is monitored by the serial port screen. The errors of the tests are so small that can be neglected.

The output power of the system is 4.181 W with 83.80 % efficiency. The average error of the capacitive measurement system is 1.1%. The SNRs of data signals are very high as can be seen in Figure 5.2. It shows that the capacitive weight measurement test performs with high accuracy. When the observed data from the sensor and transferred data are compared with each other, there are no major differences. These findings corroborated that the capacitive data and power transfer are executed properly.

Hence, the potentials of sub-kilowatt, efficient capacitive data and power transfer system have been presented. This methodology could well be deployed in defence, in medical, in automotive, in aerospace etc. The author believes that this technique promises new opportunities in the coming years.

REFERENCES

Abbas, S. M., Hannan, M. A., & Salina, A. S. (2012, February). Efficient class-E design for inductive powering wireless biotelemetry applications. In 2012 International Conference on Biomedical Engineering (ICoBE) (pp. 445-449). IEEE.

Anonymous (2015). Analog Multiplier [https://www.analog.com/media/en/technical-documentation/data-sheets/AD633.pdf], Last accessed in November 2019.

Anonymous (2014). Amplifier Classes [https://www.electronicstutorials.ws/amplifier/amplifier-classes.html], Last accessed in November 2019.

Bird, J. 1997. Wheatstone bridge. Electrical circuit theory and technology. Elsevier Science, pp. 98-100 Burlington USA

Beh, T. C., Kato, M., Imura, T., Oh, S., & Hori, Y. (2013). Automated impedance matching system for robust wireless power transfer via magnetic resonance coupling. IEEE Transactions on Industrial Electronics, 60(9), 3689-3698.

Brown, W. C. (1973, June). Adapting microwave techniques to help solve future energy problems. In 1973 IEEE G-MTT International Microwave Symposium (pp. 189-191). IEEE.

Brown, W. C. (1984). The history of power transmission by radio waves. IEEE Transactions on microwave theory and techniques, 32(9), 1230-1242

Brown, W. C. “The history of the development of the rectenna,” in Proc. SPS Microwave Systems Workshop at JSC-NASA, 1980, pp. 271–280.

Chabrol, J. Power Transfer Circuit. Regie Nationaledes Usines Renaults,Boulogne Billancourt,France,1980.

Chang, C. K., Da Silva, G. G., Kumar, A., Pervaiz, S., & Afridi, K. K. (2015, May). 30 W capacitive wireless power transfer system with 5.8 pF coupling capacitance. In 2015 IEEE Wireless Power Transfer Conference (WPTC) (pp. 1-4). IEEE.

Covic, G. A., & Boys, J. T. (2013). Inductive power transfer. Proceedings of the IEEE, 101(6), 1276-1289

Culurciello, E., & Andreou, A. G. (2006). Capacitive inter-chip data and power transfer for 3-D VLSI. IEEE Transactions on Circuits and Systems II: Express Briefs, 53(12), 1348-1352.

Cripps, Steve C. (2006). Efficiency Enhancement Techniques. RF Power Amplifiers forWireless Communications, pp. 285-335 BOSTON LONDON

Dai, J., & Ludois, D. C. (2014). Single active switch power electronics for kilowatt scale capacitive power transfer. IEEE journal of emerging and selected topics in power electronics, 3(1), 315-323.

Dai, J., & Ludois, D. C. (2015). Capacitive power transfer through a conformal bumper for electric vehicle charging. IEEE Journal of Emerging and Selected Topics in Power Electronics, 4(3), 1015-1025.

Dickinson, R. M. (1976, June). Performance of a high-power, 2.388-GHz receiving array in wireless power transmission over 1.54 km. In 1976 IEEE-MTT-S International Microwave Symposium (pp. 139-141). IEEE.

Duong, T. P., & Lee, J. W. (2011). Experimental results of high-efficiency resonant coupling wireless power transfer using a variable coupling method. IEEE Microwave and Wireless Components Letters, 21(8), 442-444.

Fan, Q., Huijsing, J., & Makinwa, K. A. (2013, February). A multi-path chopper-stabilized capacitively coupled operational amplifier with 20V-input-common-mode range and 3μV offset. In 2013 IEEE International Solid-State Circuits Conference Digest of Technical Papers (pp. 176-177). IEEE.

Fnato, H., Chiku, Y., & Harakawa, K. (2010, October). Wireless power distribution with capacitive coupling excited by switched mode active negative capacitor. In Electrical Machines and Systems (ICEMS), 2010 International Conference on (pp. 117-122). IEEE

Fujino, Y. Itoh, T. Fujita, M. Kaya, N. Matsumoto, H. Kawabata, K. Sawada, H. and Onodera, T. "A rectenna for MILAX," in Proc. Wireless Power Transmission Conf., 1993, pp. 273–277.

Green, A. W., & Boys, J. T. (1994). 10 kHz inductively coupled power transfer-concept and control.

Hu, A. P., Liu, C., & Li, H. L. (2008, December). A novel contactless battery charging system for soccer playing robot. In Mechatronics and Machine Vision in Practice, 2008. M2VIP 2008. 15th International Conference on (pp. 646-650). IEEE

Huh, J., Lee, S. W., Lee, W. Y., Cho, G. H., & Rim, C. T. (2011). Narrow-width inductive power transfer system for online electrical vehicles. IEEE Transactions on Power Electronics, 26(12), 3666-3679.

Huh, J., Lee, S. W., Lee, W. Y., Cho, G. H., & Rim, C. T. (2011). Narrow-width inductive power transfer system for online electrical vehicles. IEEE Transactions on Power Electronics, 26(12), 3666-3679.

Imura, T., & Hori, Y. (2011). Maximizing air gap and efficiency of magnetic resonant coupling for wireless power transfer using equivalent circuit and Neumann formula. IEEE Transactions on industrial electronics, 58(10), 4746-4752.

Kawamura, A., Ishioka, K., & Hirai, J. (1996). Wireless transmission of power and information through one high-frequency resonant AC link inverter for robot manipulator applications. IEEE Transactions on Industry Applications, 32(3), 503-508.

Kim, J., & Bien, F. (2013, April). Electric field coupling technique of wireless power transfer for electric vehicles. In IEEE 2013 Tencon-Spring (pp. 267-271). IEEE.

Kim, J., Son, H. C., Kim, K. H., & Park, Y. J. (2011). Efficiency analysis of magnetic resonance wireless power transfer with intermediate resonant coil. IEEE Antennas and Wireless Propagation Letters, 10, 389-392.

Liu, C., & Hu, A. P. (2009, September). Steady state analysis of a capacitively coupled contactless power transfer system. In Energy Conversion Congress and Exposition, 2009. ECCE 2009. IEEE (pp. 3233-3238). IEEE.

Liu, C., Hu, A. P., & Nair, N. K. C. (2009, February). Coupling study of a rotary capacitive power transfer system. In 2009 IEEE International Conference on Industrial Technology (pp. 1-6). IEEE.

Martin, N. T.C. “The inventions, researches and writings of nikola tesla, with special reference to his work in polyphase currents and high potential lighting,” in New York: The Electrical Engineer, 1894.

Maruyama, T., Makikawa, M., Shiozawa, N., & Fujiwara, Y. (2007, May). ECG measurement using capacitive coupling electrodes for man-machine emotional communication. In 2007 IEEE/ICME International Conference on Complex Medical Engineering (pp. 378-383). IEEE.

Matsumoto, H. (2002). Research on solar power satellites and microwave power transmission in Japan. IEEE microwave magazine, 3(4), 36-45

Matsumoto, H., Kaya, N., Fujita, M., Fujino, Y., Fujiwara, T., & Sato, T. (1993, March). MILAX airplane experiment and model airplane. In 12th ISAS Space Energy Symposium, Tokyo, Japan.

McKinstrie, C. J., Li, J. S., Giacone, R. E., & Vu, H. X. (1996). Two-dimensional analysis of the power transfer between crossed laser beams. Physics of Plasmas, 3(7), 2686-2692.

Piipponen, K. V. T., Sepponen, R., & Eskelinen, P. (2007). A biosignal instrumentation system using capacitive coupling for power and signal isolation. IEEE Transactions on Biomedical Engineering, 54(10), 1822-1828.

Serway A. R. & Jr. J. W. J. (2010). Gauss's Law. Physics for scientists and engineers with modern physics Michelle Julet USA, 692, Belmont USA.

Schlesak, J. J., Alden, A., & Ohno, T. (1988, May). A microwave powered high altitude platform. In 1988., IEEE MTT-S International Microwave Symposium Digest (pp. 283-286). IEEE.

Shimokura, N., Kaya, N., Shinohara, M., & Matsumoto, H. (1997). Point-to-point microwave power transmission experiment. Electrical engineering in Japan, 120(1), 33-39.

Shinohara, N. (2007). Wireless charging system by microwave power transmission for electric motor vehicles. IEICE Technical Report, SPS2006-18.

Shinohara, N. (2011). Power without wires. IEEE Microwave Magazine, 12(7), S64-S73.

Shinohara, N., Kojima, J. I., Mitani, T., Hashimoto, T., Kishi, N., Fujita, S. & Nishikawa, S. (2007). Assessment study of electric vehicle charging system with microwave power transmission II. Tee. Report of IEICE, SPS2006-18 (2007-02), 21-24.

Slade, B. (2010). Notes on designing class-E RF power amplifiers. no. May, 1-11.

Sokal, N. O., & Sokal, A. D. (1975). Class EA new class of high-efficiency tuned single-ended switching power amplifiers. IEEE Journal of solid-state circuits, 10(3), 168-176.

Sodagar, A. M., & Amiri, P. (2009, April). Capacitive coupling for power and data telemetry to implantable biomedical microsystems. In 2009 4th International IEEE/EMBS Conference on Neural Engineering (pp. 411-414). IEEE.

.

Tesla, N. (1891). Experiments with alternate currents of very high frequency and their application to methods of artificial illumination. Transactions of the American Institute of Electrical Engineers, 8(1), 266-319.

Tesla, N. (1914). U.S. Patent No. 1,119,732. Washington, DC: U.S. Patent and Trademark Office.

Tsakiris, V., Kappel, W., & Alecu, G. (2011). Solid state diffusion welding of Cu-Fe/Al/Ag and Al-Ni dissimilar metals. Journal of Optoelectronics and Advanced Materials, 13(9), 1176

Vidkjær, J. 2012. Basic Modulation Types and Concepts. Modulation, Transmission, And Demodulation Massachusetts, pp.1-5 Massachusetts USA

Xie, L., Shi, Y., Hou, Y. T., & Lou, A. (2013). Wireless power transfer and applications to sensor networks. IEEE Wireless Communications, 20(4), 140-145.

Zhang, H., Lu, F., Hofmann, H., Liu, W., & Mi, C. C. (2016). A Four-Plate Compact Capacitive Coupler Design andLCL-Compensated Topology for Capacitive Power Transfer in Electric Vehicle Charging Application. IEEE Transactions on Power Electronics, 31(12), 8541-8551.

APPENDIX A

THE CODE ALGORITHM

```
#include "HX711.h"  //You must have this library in your Arduino library folder


#define DOUT  4
#define CLK  5


HX711 scale(DOUT, CLK);
#include <LiquidCrystal.h>
 LiquidCrystal lcd(12, 11, 7, 6, 3, 2);
//Change this calibration factor as per your load cell once it is found you many need to vary it in thousands
float calibration_factor = -419650; //-106600 worked for my 40Kg max scale setup


//====================================================================================
//                    SETUP
//====================================================================================
void setup() {
  Serial.begin(9600);
  Serial.println("Press T to tare");
  scale.set_scale(-419650);  //Calibration Factor obtained from first sketch
  scale.tare();             //Reset the scale to 0
  lcd.begin(16, 2);
```

```
lcd.print(“Capacitive weight measurement system");
delay(500);
lcd.clear();
}

//=============================================================
=====================================
//                    LOOP
//=============================================================
=====================================
void loop() {
  Serial.print("Weight: ");
float abc = scale.get_units()*9.81;
  Serial.print(abc, 4);  //Up to 4 decimal points
  Serial.println(" N"); //

  if(Serial.available())
  {
    char temp = Serial.read();
    if(temp == 't' || temp == 'T')
      scale.tare();  //Reset the scale to zero
  }

}
```